

ISTANBUL TECHNICAL UNIVERSITY ★ GRADUATE SCHOOL OF SCIENCE
ENGINEERING AND TECHNOLOGY

DESIGN OF A PIEZOELECTRIC TACTILE SENSOR

M.Sc. THESIS

Emre AKÇA

Department of Mechanical Engineering
System Dynamics and Control Programme

FEBRUARY 2012

ISTANBUL TECHNICAL UNIVERSITY ★ GRADUATE SCHOOL OF SCIENCE
ENGINEERING AND TECHNOLOGY

DESIGN OF A PIEZOELECTRIC TACTILE SENSOR

M.Sc. THESIS

Emre AKÇA
(503081620)

Department of Mechanical Engineering
System Dynamics and Control Programme

Thesis Advisor: Assist. Prof. Dr. İlker Murat KOÇ

FEBRUARY 2012

İSTANBUL TEKNİK ÜNİVERSİTESİ ★ FEN BİLİMLERİ ENSTİTÜSÜ

PIEZOELEKTRİK TABANLI DOKUNSAAL ALGILAYICI TASARIMI

YÜKSEK LİSANS TEZİ

Emre AKÇA

Makina Mühendisliği Anabilim Dalı

Sistem Dinamiği ve Kontrol Programı

Tez Danışmanı: Yrd. Doç. Dr. İlker Murat KOÇ

ŞUBAT 2012

Emre AKÇA, a M.Sc. student of ITU Graduate School of Science Engineering and Technology student ID 503081620, successfully defended the thesis entitled “Design of a Piezoelectric Tactile Sensor”, which he prepared after fulfilling the requirements specified in the associated legislations, before the jury whose signatures are below.

Thesis Advisor : **Assist. Prof. Dr. İlker Murat KOÇ**
İstanbul Technical University

Jury Members : **Prof. Dr. Ata MUĞAN**
İstanbul Technical University

Assist. Prof. Dr. İlker Murat KOÇ
İstanbul Technical University

Assist. Prof. Dr. Ali Fuat ERGENÇ
İstanbul Technical University

Date of Submission : 20 February 2012

Date of Defense : 21 February 2012

To my family,

FOREWORD

I would like to express my deep appreciation to my family and my advisor İlker Murat Koç. I would also like to thank to Dr. Bilsay Sümer from Hacettepe University for his valuable contributions to make this research possible. This work was supported by the Mechatronics Education and Research Center and I am also grateful to my professors Ata Muğan and Pınar Boyraz. I would also like to thank to my colleagues Okan Türkmen, Ayşegül Güvenç, Mehmet Akif Ceylan, Ahmet Hamdi Güzel, Hasan Heceoğlu, Çağrı Dikilitaş, Eray Çakıray and Ziya Ercan for their support throughout this study.

February 2012

Emre AKÇA
Mechanical Engineer

TABLE OF CONTENTS

	<u>Page</u>
FOREWORD	ix
TABLE OF CONTENTS.....	xi
ABBREVIATION.....	xiii
LIST OF TABLES.....	xv
LIST OF FIGURES.....	xvii
SUMMARY	xix
ÖZET	xxi
1. INTRODUCTION	1
1.1 Purpose of the Thesis	1
1.2 Literature Review	2
1.3 Hypothesis.....	2
2. TACTILE SENSING.....	5
2.1 Basics of Tactile Sensing	5
2.2 Human Tactile Sensing	5
2.3 Definition of Tactile Sensors.....	7
2.4 Types of Tactile Sensors.....	8
2.4.1 Mechanically based sensors	9
2.4.2 Resistive based sensors	9
2.4.3 Force sensing resistor.....	11
2.4.4 Capacitive based sensors.....	11
2.4.5 Magnetic based sensor	12
2.4.6 Optical sensors	12
2.4.6.1 Modulating the intensity of light by moving an obstruction into the light path	13
2.4.6.2 Photoelasticity.....	13
2.4.7 Optical fibre based sensors.....	13
2.4.8 Piezoelectric sensors	14
2.4.9 Smart sensors.....	14
2.4.10 Multi-stimuli touch sensors.....	15
3. PIEZOELECTRICITY	17
3.1 Basics of Piezoelectricity	17
3.1.1 Mathematical description	18
3.1.2 Manufacturing process of piezoelectric polymer	19
3.2 Conversion of Energy between Mechanical & Electrical	20
3.2.1 Mechanical to electrical	20
3.2.2 Electrical to mechanical	22
3.3 History of Piezoelectricity.....	22
3.4 Application Areas	26
4. MODELING AND DESIGN CRITERIA	31
4.1 Modeling of the Tactile Sensor	31

4.1.1	Buckling of fibers.....	36
4.1.2	Matting condition.....	39
4.1.3	Flaw-insensitive condition.....	40
5.	STATIC ANALYSIS OF THE PIEZOELECTRIC TACTILE SENSOR..	45
5.1	Static Single Pillar Analysis.....	45
5.1.1	Sensor mode analysis	45
5.1.1.1	Force-voltage.....	46
5.1.1.2	Thickness-voltage.....	47
5.1.1.3	Diameter-voltage	48
5.1.2	Actuator mode analysis	49
5.2	Static Fiber Array Analysis.....	51
5.2.1	Thickness of piezo film & coupling	52
5.2.2	Spacing of fibers & coupling	56
6.	VISCOELASTICITY OF PDMS	61
6.1	Viscoelastic Material Models	61
6.1.1	Mathematical models of viscoelastic behavior	61
6.1.1.1	Maxwell model.....	62
6.1.1.2	Kelvin–Voigt model	65
6.1.1.3	Standard linear solid model.....	67
6.1.1.4	Generalized Maxwell model	68
6.2	Experimental Work	69
7.	DYNAMIC ANALYSIS OF THE PIEZOELECTRIC TACTILE SENSOR	75
7.1	Single Pillar Frequency Analysis	75
7.1.1	Contribution of viscoelasticity to FEM analysis.....	75
7.1.2	Single pillar modal analysis.....	78
7.1.3	Single pillar harmonic response analysis.....	79
7.1.4	Single pillar transient response analysis.....	83
7.2	Fiber Array Frequency Analysis	87
7.2.1	Fiber array modal analysis.....	87
7.2.2	Fiber array harmonic response analysis	88
7.2.3	Fiber array impulsive response analysis	89
8.	TACTILE SENSING SIMULATION TESTS	93
8.1	Hemispheric Tip Indentation	93
8.2	Shear Force Sensing Capability & Quadrant Method.....	95
8.3	Rough Surface Adaptation.....	98
9.	CONCLUSION AND RECOMMENDATIONS	101
	REFERENCES.....	103
	APPENDICES	107
9.1	APPENDIX A.1:	108
	CURRICULUM VITAE	111

ABBREVIATION

FA	: Fast Adapting Receptor
FEM	: Finite Element Method
FFT	: Fast Fourier Transform
MEMS	: Micro-Electro-Mechanical Systems
PDMS	: Polydimethylsiloxane
PVDF	: Polyvinylidene Fluoride
PVDF-TrFE	: Polyvinylidene Fluoride-trifluoroethylene
PZT	: Lead Zirconate Titanate
SA	: Slow Adapting Receptor

LIST OF TABLES

	<u>Page</u>
Table 2.1 : Receptor types related to frequency range	6
Table 4.1 : Simulation parameters of materials of PVDF piezoelectric film and PDMS as polymer fiber used in the finite element analysis	35
Table 4.2 : Buckling Formula Abbreviations.....	36
Table 6.1 : Prony Series Coefficients	72
Table 7.1 : Natural Frequency Distribution for Single Pillar	79
Table 7.2 : Natural Frequency Distribution of the Fiber Array	88

LIST OF FIGURES

	<u>Page</u>
Figure 2.1 : Change in resistance by deformation.....	9
Figure 2.2 : Dot-and-ring arrangement for single surface tactile data measurement [20]	10
Figure 2.3 : A single compact optical sensor components	13
Figure 3.1 : Directional numbers given for applied force and voltage output	21
Figure 4.1: (a) PVDF with Bulk PDMS, (b) Patterned PVDF with PDMS Fibers	32
Figure 4.2: Relative Sensitivity Comparison	34
Figure 4.3: Basic Geometry of a Single Pillar	35
Figure 4.4: Illustration of the Proposed Sensor.....	36
Figure 4.5: Stress Applied versus Aspect Ratio	38
Figure 4.6: Stress Saturation Limit on PDMS Upper Surface	39
Figure 4.7: Dimensional Constraints for Design Criteria	41
Figure 4.8: Buckling Limit and Matting Condition Inequality for Dimensions	42
Figure 4.9: a) Two Dimensional Design Criteria for a Diameter of 40 μm b) Design Criteria for Aspect Ratio (l/d)	43
Figure 5.1: a) Deformation of a Single Pillar b) Potential Difference across the Piezoelectric Film.....	45
Figure 5.2: Applied Force-Voltage Graph for Single Pillar	46
Figure 5.3: Thickness of Piezoelectric Film versus Voltage Graph for 1 kPa Upper Surface Pressure	47
Figure 5.4: Percent Error for Different Meshing Sizes	48
Figure 5.5: Fiber Diameter versus Voltage Graph for Single Pillar of 25 μm Piezoelectric Film Thickness	49
Figure 5.6: Sensor Mode Comparison of Piezoelectric Materials	50
Figure 5.7: Actuator Mode Comparison of Piezoelectric Materials	50
Figure 5.8: Stiffness Change of Piezoelectric Materials	51
Figure 5.9: Geometry of the Fiber Array.....	51
Figure 5.10: Deformation of the Fiber Array.....	52
Figure 5.11: Voltage Distribution for (a) 5, (b) 25, (c) 40, (d) 75, (e) 100 μm Film Thickness	53
Figure 5.12: Effect of Piezoelectric Film Thickness on Voltage Output	54
Figure 5.13: Illustration of Fiber Array for Coupling of Fibers.....	55
Figure 5.14: Percent Coupling of Fibers for Different Piezoelectric Film Thicknesses	55
Figure 5.15: Voltage Distribution for 20, 40, 60, 80 μm Spacing	57
Figure 5.16: Coupling Effect Limit for Spacing Between the Fibers	57
Figure 5.17: Percent Coupling for Spacing Change Between the Fibers	58
Figure 5.18: Voltage Coupling Limit for Fiber Diameter and Fiber Spacing	58
Figure 5.19 : Two Dimensional Coupling Limit Curve	59
Figure 6.1: Typical Creep and Recovery [37].....	62

Figure 6.2: Maxwell Viscoelastic Model [39]	63
Figure 6.3 : Creep and Recovery for Maxwell Model [39]	65
Figure 6.4: Kelvin–Voigt Viscoelastic Model [38]	65
Figure 6.5 : Creep and Recovery for Kelvin–Voigt model [39]	67
Figure 6.6 : Creep and Recovery for standard linear solid model [39]	68
Figure 6.7 : Generalized Maxwell Model [36]	69
Figure 6.8 : Indentation Test Set-up.....	70
Figure 6.9 : Illustration of Indentation into PDMS Polymer	71
Figure 6.10 : Force Data of Indentation Experiments	71
Figure 6.11: Relaxation Curves for 1:10, 1:13, 1:20 Mixing Ratios	73
Figure 7.1 : Demonstration of the parameters for Viscoelastic PDMS Pillar	75
Figure 7.2 : Vertical Displacement of Polymer Fiber Upper Surface	76
Figure 7.3 : Displacement Response in Frequency Domain	77
Figure 7.4 : Stress Exerted to Piezoelectric Film by Polymer Fiber	77
Figure 7.5 : Stress Developed Response to Impulse in Frequency Domain	78
Figure 7.6 : Natural Frequencies for Single Fiber	80
Figure 7.7 : Harmonic Input for Single Fiber Analysis	80
Figure 7.8 : Frequency Sweep up to 300 Hz vs. Voltage Output	81
Figure 7.9 : Natural Frequency Harmonic Input Sweep	82
Figure 7.10 : Frequency Sweep of Z-Displacement for FZ	82
Figure 7.11 : Frequency Sweep of Voltage Output for FZ	83
Figure 7.12 : Displacement on the Upper Surface of the PDMS.....	84
Figure 7.13 : FFT of Displacement on the Upper Surface of the PDMS	85
Figure 7.14 : Voltage Output from the PVDF Film.....	86
Figure 7.15 : FFT of Voltage Output from the PVDF Film	86
Figure 7.16 : Fiber Array Dynamic Analysis Model	87
Figure 7.17 : Demonstration for the natural frequency values	88
Figure 7.18 : Frequency Sweep of Voltage Output for Applied Pressure on the Upper Surface of PDMS	89
Figure 7.19 : Y-Displacement on the Upper Surface for Upper Surface Pressure .	90
Figure 7.20 : FFT of Y-Displacement on the Upper Surface for Upper Surface Pressure	91
Figure 7.21 : Voltage Output on PVDF Film for Upper Surface Pressure	91
Figure 7.22 : FFT of Voltage Output on the Upper Surface for Upper Surface Pressure	92
Figure 8.1 : Piezoelectric film with unpatterned PDMS bulk	93
Figure 8.2 : Piezoelectric film with patterned structure: PDMS pillars	94
Figure 8.3 : Comparison of voltage output in response to pressure distribution between patterned and unpatterned PDMS samples	95
Figure 8.4 : Model of the Quadrant Electrode Pillar.....	96
Figure 8.5 : Voltage Graph for Shear Stress.....	97
Figure 8.6 : Bottom Voltage Output for Shear Stress on PDMS Upper Surface....	98
Figure 8.7 : a) Rough surface on bulk PDMS, b) Rough surface on patterned pillars 99	
Figure 8.8 : Rough surface adaptation for patterned and flat case.....	100

DESIGN OF A PIEZOELECTRIC TACTILE SENSOR

SUMMARY

The sensing of the surrounding is made by hair cell receptors that are specialized in order to achieve the sense of hearing, balance in mammals and water motion and predator detection in many other animals. In humans, tactile sensing gives the ability to understand and interact with the surrounding. The sensing is crucial at the fingertips of the human hand. The human sense of touch is the main inspiration to tactile sensing. The aim of this thesis is to design and manufacture a novel synthetic polymer fiber array with sensing capability of the pressure distribution. The polymer fiber array has both bio-inspired fibrillar structures that can adapt to the surface roughness and polymer piezoelectric film that can generate potential difference proportional to the pressure generated by the contact with the surrounding.

In this work, the sensing capability of polyvinylidene fluoride (PVDF) piezoelectric film integrated with PDMS (Polydimethylsiloxane) polymer vertical fiber array has been analyzed using finite element method (FEM). The fiber structure on the foot of the gecko, spiders and other insects gives inspiration for production of synthetic fibrillar structures which have superior adhesion property on various surfaces. Unlike the passive mode operation of the synthetic fibrillar structures, sensing property integrated synthetic polymer fiber array has the capability of easy adaptation to the roughness of the surface and it is expected to increase the adhesion with respect to passive synthetic polymers and thin film polymers.

Piezoelectric polymer generates electric potential difference with the applied force, which can be decoupled by the micro/nano polymer pillars, results in the mapping of the pressure distribution among the polymer film. The contribution of the pillars, made out of PDMS (Polydimethylsiloxane), to the output voltage and the dimensional parameters are examined for a satisfactory design that can meet the spatial resolution of the human hand. In order to meet all design requirements, the sensor design should include the static and dynamic analysis and understanding of neurophysiology of touch. Therefore, the interaction with the objects is examined

which give information about the proposed sensor for both static and dynamic environments.

The human hand contains a complex array of specialized receptors that can sense impacts as well as detecting vibrations and soft touch simultaneously. Therefore, design of artificial touch sense of the human hand is a hard but promising challenge including the quasi-dynamic, dynamic and impact analyses. The human hand is such sensitive that it can sense even the slightest vibrations ranging from 0.1-100 Hz. The complexity of the human skin should be reduced due to the requirements of the application area.

The design parameters such as the fiber diameter, spacing ratio and aspect ratio will be analyzed by performing static analysis. Furthermore, the rough surface adaptation and use of the sensor as a shear sensor will be discussed. In the dynamic analysis, the vibration characteristics as well as viscoelastic nature of the fibers will be discussed. The outcome of this work is expected to give clues for the optimal manufacturing conditions of active fibrillar structures.

PIEZOELEKTRİK TABANLI DOKUNSAL ALGILAYICI TASARIMI

ÖZET

Çevreyi algılama, saç hücresi reseptörleri tarafından yapılır. Bu reseptörler, duyma hissine ulaşma, memeli hayvanlarda denge ve birçok diğer hayvanda su ve hava hareketlerinin ve çevredeki yırtıcıların tespit edilmesi gibi amaçlar için uzmanlaşmıştır. İnsanlarda ise dokunsal algılama çevreyi anlama ve onunla etkileşim olanağı sağlar. Algılama, insan elinin parmaklarının ucunda çok önemlidir. İnsanlardaki dokunma duyusu, dokunsal algılayıcıların ana ilham kaynağı olmuştur. Bu çalışmadaki amaç ise dokunma duyusuna yakınsayacak yeni nesil sentetik polimer fiber dizisinin tasarımı ve üretimidir. Bu fiber dizisinin üzerindeki basınç dağılımını algılaması amaçlanmaktadır. Tasarlanan fiber dizisinin hem yüzey pürüzlülüğüne adapte olabilen biyolojiden esinlenilmiş fiber yapısının bulunması, hem de oluşan temas ile ortaya çıkan basıncı elektriksel potansiyel farka çevirebilecek piezoelektrik ince tabakaya sahip olması gerekmektedir.

Yapılan çalışmada basıncı algılama kabiliyetine sahip PVDF piezoelektrik tabakaya ilave edilmiş PDMS polimer düşey fiber dizisini sonlu eleman metodu kullanılarak analizi yapılmıştır. Gecko, örümcekler ve diğer böceklerin ayaklarında bulunan fiber yapı, çeşitli yüzeylerde üstün yapışma özelliğine sahip sentetik fibriler yapıların üretimi için ilham vermektedir. Bu hayvanların ayaklarındaki yapılar, kuru ve yaş ortamlarda vakumlu ortam dahil çok değişik yüzeylere kontrollü bir biçimde yapışmalarını sağlar. Ayrıca, bu mikro-nano yapıların yapışmalarında kendi kendine temizleme özellikleri dolayısıyla uzun süre kullanım, tekrarlanabilir yapışma ve yüzeyde herhangi bir kalıntı bırakmama gibi özellikler barındırırlar. Pasif çalışma biçiminin aksine, sentetik fiberlerle birleştirilmiş piezoelektrik algılayıcı yüzey pürüzlülüğüne çok daha kolay adapte olma kabiliyetine sahip olmakla birlikte yüzeye yapışma konusunda da daha iyi olması beklenmektedir.

Piezoelektrik polimer uygulanan kuvvet sonucunda elektriksel potansiyel farkı yaratmaktadır. Bu potansiyel fark mikro/nano polimer fiberler sayesinde ayrıştırılabilir ve bu ayrıştırma polimer tabaka üzerindeki basıncın

haritalandırılmasına yarar. Tasarlanan algılayıcıda PDMS polimerden üretilmiş fiberlerin çıkış voltajına ve insan elinin uzamsal çözünürlüğe yakınsamasındaki boyutsal değişkenlere etkisi araştırılmıştır. Tüm bu tasarım ölçütlerinin sağlanabilmesi statik ve dinamik çalışma koşullarının incelenmesi ve dokunma algısının altında yatan nörofizyolojinin özümsemesini içermektedir. Bu nedenle tasarlanan algılayıcı hakkındaki bilgilerin edinilebilmesi için tüm çevre koşulları irdelenmiştir.

İnsan eli ani darbeler, titreşimler ve yumuşak dokunuş gibi birçok etkiyi eşzamanlı olarak hissedebilen karmaşık bir özelleşmiş reseptörler dizisi içerir. Bu nedenle yapay insan eli dokunma hissi tasarımı oldukça zor fakat gelecek vadeden bir sorun oluşturmaktadır. İnsan eli çok düşük 0.1- 100 Hz arasında değişen titreşimleri bile algılayabilecek kadar hassastır. Bu nedenle yapılacak tasarımın amacı belirlenip buna bağlı olarak insan elinin karmaşıklığı daha basit bir seviyeye indirgenmelidir. Ancak bu sayede istenilen seviyede insan derisini taklit edebilecek algılayıcı ve eyleyici tasarımları gerçekleştirilebilir. Bu algılayıcılar mikro/nano boyutta kuvvet algılayıcılar, minimal ilerleme gerektiren cerrahi operasyonlar, hava akış algılayıcıları gibi uygulamalarda kullanılabilir. İnsanlardaki dokunsal algılama diğer duyularla etkileşim halindedir ve görüntü geri beslemesi olmadan yeteri kadar hassas değildir. Buna ek olarak 20-30 ms gecikmesi bulunmaktadır. Bu nedenle dokunsal algılayıcılar bu noktalarda geliştirilmelidir. Dokunsal algılayıcı teknolojisi uzamsal çözünürlük, esneklik, yüzey pürüzlülüğüne adapte olma ve dokunma algısının geniş bir alana yayılması konularında yetersiz kalmaktadır. Son dönemlerde ise geckonun ayaklarındaki üstün yapışabilme yetisi insan yapımı sentetik mikro fiber yapılarının oluşturulmasına öncü olmuştur.

Mikro fiberlerin birbirlerini etkilemeyecek şekilde tasarlanmasından dolayı, algılayıcı tabaka halindeki piezoelektrik algılayıcıya oranla daha iyi yüzeye adapte olabilme ve daha iyi yapışma özelliğine sahiptir. Piezoelektrik polimerin elektrotlanması sayesinde gecko ayaklarının yapışma ve yüzeyi tanıma özelliği taklit edilmeye çalışılmıştır. Fiberlerin geometrileri sayesinde basıncın belli bir alana yoğunlaştırılması sağlanmış bu sayede birim kuvvete elde edilecek potansiyel farkın artırılması ve algılayıcının hassasiyetinin artırımı sağlanmıştır. Fakat piezoelektrik PVDF polimerin yüzey enerjisinin diğer polimerlere oranla daha düşük kalmasından dolayı yapışma özelliği yetersiz kalmaktadır. Bu ise üzerine yerleştirilmiş PDMS ya

da PMMA gidi sık kullanılan polimerler sayesinde telafi edilmiştir. Ayrıca piezoelektrik polimerin yüksek olan elastisite modülü üzerindeki polimer sayesinde düşürülmüş ve daha esnek bir yapıya dönüştürülmüştür.

Fiberlerin çapı ve boyu, fiberlerin arasındaki uzaklık gibi tasarımsal değişkenlerin belirlenmesi statik analizlerin yapılması ile gerçekleştirilmiştir. Burada mekanik ve elektriksel olarak fiberlerin dayanabileceği kuvvetler, birbirlerinden etkilenmesi ve temas edeceği yüzeye yapışması gibi özellikler düşünülerek fiberlerin boyutları için tasarım limitleri belirlenmiştir. Piezoelektrik filmin boyutları da bu fiberlerin birbirleri ile etkileşimini en az seviyeye indirecek kadar az, en üst düzeyde potansiyel fark yaratıp bu potansiyel farkın non-lineer seviyede olmamasını sağlayacak kadar da büyük olmalıdır.

Polimer fiberlerin viskoelastik özellikleri fazla olduğundan dinamik yapıda sistem modelinde büyük farklılıklar yaratmaktadır. Buna uygun olarak tasarlanan fiber dizisine uygun viskoelastik model seçilip parametreleri bulunmuştur. Buna bağlı olarak sistem modelinin elastik modele olan farkları araştırılmıştır.

Boyutları ve modeli belirlenen algılayıcı daha sonrasında dinamik koşullarda irdelenmiştir. Dinamik analizler öncelikle yapının doğal frekanslarının bulunması, daha sonrasında frekans taraması ve en son olarak darbeye karşı verdiği tepkiler simule edilmiştir. Bu sayede algılayıcının dinamik, harmonik girişlere karşı nasıl tepki vereceği gözlemlenmiştir. Bu dinamik yapının incelenmesi hem tek fiber hem de fiber dizisi için yapılmıştır. Bu sayede fiberlerin yan yana dizilmesinin her bir fibere etkisi görülmüştür.

Fiber yapısının hem statik hem de dinamik olarak irdelenmesinde sonra, simülasyon testleri yapılmıştır. Öncelikle cam küresel bir yüzeyin algılayıcı üzerindeki performansı araştırılmıştır. Fiberlerin birbirlerinden ayrılmasının etkisi potansiyel fark yaratımı olarak incelenmiştir. Buna ek olarak tasarımın pürüzlü yüzeye adapte olması yanal kuvvetleri algılayabilme özellikleri tartışılmıştır. Bu çalışmanın sonucu olarak üretilecek olan algılayıcının en uygun yapının oluşturulmasına katkı sağlanması istenmektedir.

1. INTRODUCTION

The human hand contains a complex array of specialized receptors that can sense impacts as well as detecting vibrations and soft touch simultaneously [1]. Therefore, design of artificial touch sense of the human hand is a hard but promising challenge. The human hand is such sensitive that it can sense even the slightest vibrations ranging from 10-100 Hz. In order to meet these design requirements, the sensor design should include the static and dynamic analysis and understanding of neurophysiology of touch.

The complexity of the human skin should be reduced due to the requirements of the application area. Thus, reasonable sensors and actuators that can mimic the abilities of the human skin can be manufactured [2]. Such sensors that mimic the human touch could be used as micro/nano force sensors, restore the loss of sense of touch occurred due to shift from traditional to minimally invasive surgeries (MIS), air flow sensors as well as acoustic sensors [3-5]. Since the human tactile sensing is dim without visual feedback and it has a latency of 20-30 ms in response, the tactile sensors provide advantageous that should be exploited [6].

1.1 Purpose of the Thesis

The sensing of the surrounding is made by hair cell receptors by a wide class of mechano-receptive organs that are specialized in order to achieve the sense of hearing, balance in mammals and water motion and predator detection in many other animals [7]. In humans, tactile sensing gives the ability to understand and interact with the surrounding. The sensing is crucial at the fingertips of the human hand. The interaction with the objects and surfaces are examined by the hands which give information about the pressure distribution, friction with the object and adhesion of the object.

Measuring the pressure distribution among a surface or an object is crucial and has many application areas. The purpose of this thesis is to generate a tactile sensor array

that has both resolution and sensing range close to the human hand. Therefore, the pressure distribution that is related to the sense of touch of human can be simulated. This can lead to accurate positioning of grabbed objects like surgery operations or lead to optimization of the adaptation to the surface, increasing the adhesion between the surfaces.

The optimization process enables the capability of easy adaptation to the surface roughness. Gecko uses this adaptation in order to increase the adhesion such that the animal can carry its own weight by just sticking to any surface.

1.2 Literature Review

Many efforts have been devoted to design piezoelectric based tactile sensors. In designing piezoelectric tactile sensors, the fibrillar structure is more likely to be proposed since it can distribute the surface roughness more evenly. The literature contains works about piezoelectric sensors with piezoelectric fibers in different shapes, spacing and tilted angles. However, since the piezoelectric fibers are stiff, the adaptation is limited. For higher adaptation, polymers have been proposed with lower stiffness so that the contacting surface is like submerged into the polymer layer which leads to better understanding of the topography. Moreover, the shear sensing capability is also considered with floating electrodes on piezoelectric film which is manufactured in flexible printed circuit boards.

The lower in stiffness and bio-compatible, polymers like PDMS and PMMA are used as the fiber material in piezoelectric tactile sensors. These polymers are molded and integrated on piezoelectric films resulting in stress amplification units with superior compatibility. But the molding of polymers leads to connection of fibers which makes them depend on each other. Unlike the traditional methods, MEMS techniques like soft lithography results in manufacturing of fibers eliminating the coupling between them.

1.3 Hypothesis

In this thesis, it is aimed to search for the best design by understanding the basics of the tactile sensing and the surface adaptation. The pressure among a surface is examined in order to observe the surface roughness and generate the best adaptation

geometry. The fiber arrays which are the pillars are generated from PDMS which is a highly bio-compatible polymer. The pressures among those pillars are transmitted to the piezoelectric film in order to generate electric potential difference. Since the voltage output is linearly proportional to the pressure applied, the data obtained from the piezoelectric film will result in the mapping of the pressure exerted by the rough surface in contact with the sensor. Therefore, using the piezoelectric polymer PVDF will be appropriate for the tactile sensor application.

Piezoelectric polymers can be used to mimic the tactile sensing of Gecko as being able to adapt to many surfaces and produce electric potential with the applied force. Since the piezoelectric materials generate charge collected at the electrodes, the distribution of electrodes, which are below the PDMS polymer fiber arrays, will result in the mapping of the pressure distribution among the piezoelectric film.

Considering the constraints obtained from the laws of physics and the manufacturing capabilities, it is desired to design a tactile sensor converging the resolution and measurement limits of the human hand.

2. TACTILE SENSING

2.1 Basics of Tactile Sensing

Human dexterity is such an important aspect that it provides the recognition and grasp of the various shapes and sizes perform complex tasks and switch between the responses by the change in these tasks. These tasks can be accomplished since the structure of the fingers has many degrees of freedom and there exists a closed-loop control mechanism by the skin especially at the tip of the fingers. This control capability is founded on tactile and force sensing at the contact between the finger and the object.

For the past few decades, researchers have worked to mimic the manipulation capabilities that humans possess. Although vision has received the most attention, the sense of touch is essential in many applications. Dexterous manipulations require the closed loop control mechanism of force and the motion at the fingertip and the environment which can only be achieved by the sense of touch. Tactile sensing of the objects may provide information about the mechanical properties such as mass, adhesion, friction, viscoelasticity and the compliance.

Despite the importance of touch sensing on the dexterous manipulation, much work has been devoted to the creation of sensor devices and object recognition algorithms. Particular attention has been devoted to sense of touch by a simple experiment of exploring the objects after putting hands on icy blocks for a while. The experiment which is performed by cooling the skin, showed the instability in maintaining the grasp of the objects [8]. The movements become inaccurate and unstable when the sense of touch is lost.

2.2 Human Tactile Sensing

The human sense of touch is the main inspiration to tactile sensing. Many studies have been carried out in understanding the mechanisms underlying the human taction [9,10]. There are two different components of contact sensing in humans: kinesthetic

sensing refers to perception of limb motion and forces with internal receptors and cutaneous sensing refers to contact information with receptors in the skin. The receptors included in the human skin are given in Table 2.1. The kinesthetic receptors include muscle spindles and tendon organs which sense the change in muscles. There are also receptors in the joints which sense the joint angles and forces in addition to the deformation in the skin near the joints which reports the deformation on the joints.

The fingers of the human body are actuated by the muscles located in the forearm transmitted by the tendons passing through the wrist. The accurate sensing and control of the fingertip in robotics are difficult to achieve since there exist some factors such as friction, backlash and inertia [11]. Therefore, considering small motions and light forces those transmission dynamics elements become dominant and kinesthetic information from the muscles becomes insufficient for good control of the contact. This makes tactile sensors crucial in determining the environment at the contact location.

Table 2.1 : Receptor types related to frequency range

Receptor Type	Frequency Range	Postulated Sensed Parameter
FA I	10-60 Hz	Skin stretch
SA I	DC-30 Hz	Compressive stress
FA II	50-1000 Hz	Vibration
SA II	DC-15 Hz	Directional skin stretch

There are four types of specialized mechanoreceptor nerve endings in the smooth skin of the human hand. They are categorized by their size of active area and response to static stimuli. Nerve endings with small receptive fields are called Type I whereas endings with large fields are called Type II. Units that respond to static stimuli are denoted as SA (slow adapting) while units with no static response are called FA (fast adapting). There are about 17,000 mechanoreceptors in human hand. In addition to these specialized mechanoreceptors, there are free nerve endings in order to sense the mechanical deformation, temperature and pain [12]. Therefore, tactile sensing needs many sensors specialized for different purposes in order to fully mimic the human skin.

2.3 Definition of Tactile Sensors

Tactile and touch sensor are transducers that measure the parameters such as touch, force, pressure of a contact between an object and the sensor. On the contrary to force and torque sensor which measure the total force or torque acting on an object, the interaction between the object and the tactile sensor is limited to a small specific region. Tactile sensor technology suffers from the spatial resolution, flexibility, degree of adaptation to rough surfaces and touch sensation over a large area [13]. Recently, the amazing adhesion capability of gecko foot to any kind of surface gives inspiration of human-made synthetic micro-fibrillar structures [14-18].

A simple form of tactile sensing is touch sensing. It is the detection and measurement of a contact force at a specific point of contact. It can also be reduced to sensor of giving binary information. In that case there are two options which are there is contact or no contact between the object and the sensor at the predefined point.

An array of touch sensors leads to tactile sensors. Tactile sensors detect and measure the spatial distribution of a force perpendicular to the sensor area. Over a predefined area tactile sensors interpret the spatial information and the touching information of every tactel (short form of tactile element) gives the pressure distribution among the tactile sensing element.

The measurement and the detection of the movement of an object are called the slip. The slip data of an object can either be gathered by sensors that are specially designed for slip detection or by the interpretation of the data of a tactile array.

Tactile sensors can be used to sense a diverse range of stimulus ranging from detecting the presence or absence of a grasped object to discovering a complete tactile image of the environment of the tactile sensor. In everyday life, tactile sensors are used as elevator buttons or lamps which dim or brighten by touching the base. Tactile sensors are noted to be used in manufacturing of automobiles to battery laminations, bolted joints and fuel cells [19]. For further technology, tactile sensors are used in surface pressure calculations and also many researches has been made on integration of tactile sensing to industrial robotics which will increase the manufacturing performance in mass production areas. The principle unit of a tactile sensor array is touch sensitive sites which are capable of measuring more than one property. Texture, impact, slip and

other contact conditions generate specific force and position patterns which can be used to identify the state of manipulation.

There is no complete theory that defines the sensing requirements of a robotic system. Therefore, the knowledge is drawn from the investigation of the human sensing and the desired characteristics of a tactile sensor are based on this data which is also given below.

- An ideal touch sensor is a single point contact but a sensory area of 1-2 mm² is also considered to be ideal. This assumption is made considering the compromise between the limitations of manufacturing and the spatial resolution of the sensing element.
- For most of the applications a sensitivity within the range of 0.4 to 10 N is considered to be satisfactory including the allowance for accidental mechanical overload.
- A minimum sensor bandwidth of 100 Hz.
- The sensor characteristics should be stable and repeatable with low hysteresis. Ideally a linear output is desired but the little hysteresis can be eliminated by the data processing techniques. Therefore any nonlinearity can be compensated in order to work in the linear region of the tactile sensing element.
- The sensor should be robust that is it shouldn't be effected from the surrounding and also it should be protected from that surrounding in order not to get any damage.

2.4 Types of Tactile Sensors

Many physical principles have been exploited in the development of the tactile sensors. Since there is diversity in the technology beyond these developments, there have been many different designs created. The development criteria is mostly application dependent and therefore the operation of the tactile sensor is very crucial. In most of the cases, the materials handled are rigid objects and the designs are made according to this assumption. However, non-rigid materials are considered, conventional sensors should be modified to operate with those non-rigid materials.

2.4.1 Mechanically based sensors

The most basic form of touch sensor is a mechanical micro-switch which is activated by the applied force and forms a binary touch sensor. The switch is either on or off depending on the force applied is above than a certain value. This certain force value to activate the switch will be determined by the actuating characteristics of the switch and by any external constraints. Some more complicated mechanically based sensors contain a secondary device such as a potentiometer or displacement transducer which gives more information than just a simple on-off signal. The secondary device will determine the magnitude of the force applied which will enable to handle more complicated applications.

2.4.2 Resistive based sensors

Materials that have well defined force-resistance characteristics are widely utilized in touch and tactile sensor applications. The operating principle of such tactile sensor is the measurement of the resistance of a conductive elastomer between two points which is demonstrated in Figure 2.1. The resistance of the sensor changes as the elastomer is deformed and the particle density alters.

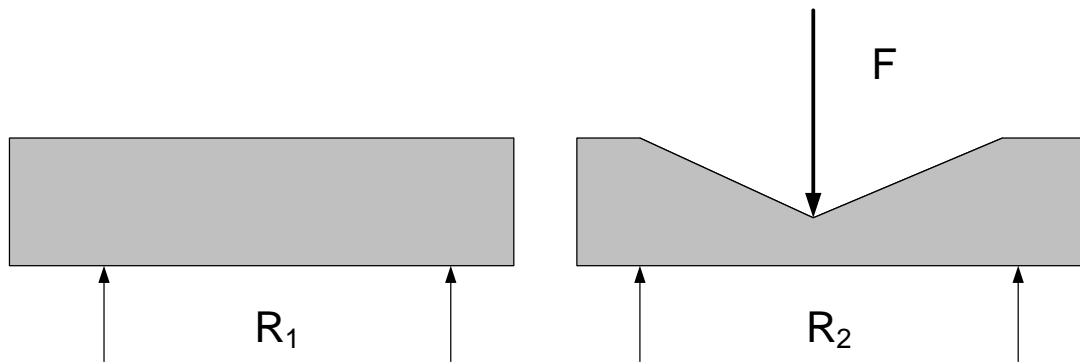


Figure 2.1 : Change in resistance by deformation

The resistance measurement should be made allowing the movement of the conductive elastomer so that it will deform and change shape. Therefore, if the measurement is to be taken on the opposing surfaces, the upper surface where the force is to be applied should be made using a flexible printed circuit. This will allow the movement on the upper surface. If the measurement is to be taken from a single surface, the dot-and-ring arrangement is used which is given in Figure 2.2. This eliminates the direct contact between the two points of contact where the measurement is taken and the circuit is

drawn with the conductive elastomer as the resistive element. The change in resistance gives the magnitude of the deformation.

Elastomer cords laid in a grid pattern can be used to develop resistive sensors where the resistance measurement is taken at the point of contact. Making use of this utility, array can be generated with 256 elements which is satisfactory enough to get a tactile image of good resolution.

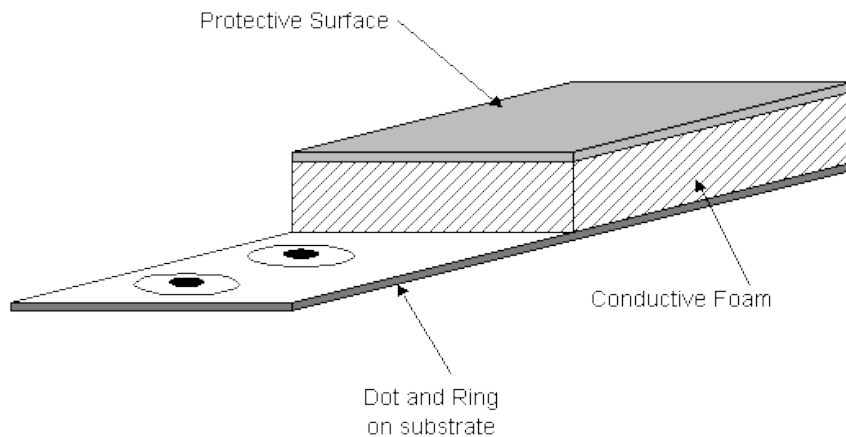


Figure 2.2 : Dot-and-ring arrangement for single surface tactile data measurement [20]

Despite the simplicity of conductive elastomer based resistive sensors, they do have some significant disadvantages.

- An elastomer is a viscoelastic material with a high nonlinear time constant. Moreover, this time constant differs whether the applied force is still acting or removed. This difference generates some significant deviation from the actual values.
- The force-resistance characteristic of conductive elastomer is highly nonlinear which requires the further processing of the data acquired.
- For the long term and cyclic application of forces, elastomer will migrate over a period of time. Furthermore, due to the cyclic loading fatigue will occur, leading to permanent deformation of the sensor. This will lead to poor long-term stability and will require replacement after some period of time.

In spite of these disadvantages of conductive elastomer resistive sensors, in most of the industrial analogue touch and tactile sensors the principle of resistive sensing is used. This is due to the simplicity and the ease of integration to the robotics systems.

2.4.3 Force sensing resistor

A force sensing resistor is a piezoresistive polymer which changes its resistance with the applied force on its surface. It is generally a polymer sheet which consists of both electrically conductive and non-conductive particles. Those particles are in the order of microns and are formulated to reduce the temperature effects, improve mechanical properties and increase surface durability. Application of a force results in the touch of the conducting electrodes changing the resistance of the film. As with all the resistive based sensors, it contains the same disadvantages and needs a simple interface and can operate satisfactorily in moderately hostile environments.

2.4.4 Capacitive based sensors

The capacitance between two parallel plates is given by the Equation 2.1.

$$C = \frac{\epsilon A}{d} \quad (2.1)$$

where C is the capacitance, ϵ is the permittivity of the dielectric medium between the plates, A is the effective plate surface area and d is the distance between the plates. The main principle that a capacitive based sensor works is that it changes capacitance as a force is applied by changing the distance between the plates or by changing the effective surface area of the plates. In capacitive based sensors, the plates are separated by a dielectric medium which is an elastomer so as to give certain force to capacitance characteristic.

The maximum change in capacitance can be achieved by using a high permittivity, dielectric in a coaxial design. In capacitive based sensors, as the size of the sensor reduced in order to increase the resolution, the sensors capacitance will decrease. Therefore, this sets a limit on the resolution by the sensitive measurement of the change of the capacitance. The use of highly dielectric polymer such as PVDF (polyvinylidene fluoride) increases the capacitance, increasing the limit for spatial resolution. Also, for the same area the coaxial design will produce more capacitance change compared to parallel plate design.

2.4.5 Magnetic based sensor

Considering the magnetic based sensors, two principle approaches have been used. Firstly, the magnetic flux density has been measured and by changing the position of a small magnet this flux density changes. Using a Hall effect or magnetoresistive device the flux can be measured and any change related to the movement of the small magnet can be detected. Secondly, the core of a transformer or inductor is manufactured from a magnetoelastic material which deforms by an applied external force. This will cause the coils inductance to change and therefore detection of the applied force. Magnetoelastic materials change their magnetic characteristics with the applied force. The use of magnetoelastic materials has some advantages such as high sensitivity, high dynamic range, no mechanical hysteresis, linear response and physical robustness.

2.4.6 Optical sensors

Optical based sensors can also be utilized as touch and tactile sensors. There are two main operating principles for optical based sensors:

- *Intrinsic*, where the optical phase, intensity, or polarization of transmitted light are modulated without interrupting the optical path
- *Extrinsic*, where the physical stimulus interacts with the light external to the primary light path.

Both optical sensors can be used for touch, torque and force sensing. Both methods can be used but the most suitable will be that which requires the least optical processing. For robotic touch and force sensing applications, the extrinsic sensor based on intensity measurement is the most widely used due to the simplicity of construction. The benefits of using an optical sensor are given as:

- Intrinsically safe
- The sensor can be located some distance away from the optical source and the receiver.
- Lightweight and small in volume

Touch and tactile optical sensors have been developed using a range of optical technologies:

2.4.6.1 Modulating the intensity of light by moving an obstruction into the light path

In this type of design, the force sensitivity is determined by the spring constant of the steel. Since the sensor has been constructed such that it is surrounded by a deformable tube, it is very compact as well as being able to prevent the cross-talk between the adjacent sensors in the array.

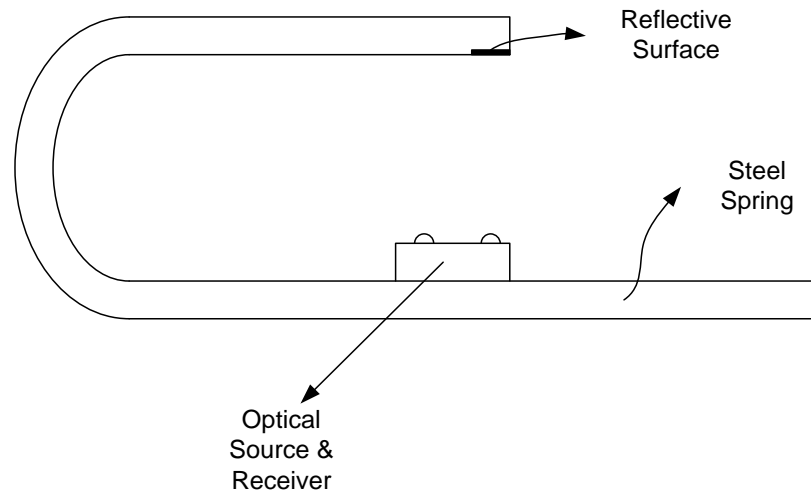


Figure 2.3 : A single compact optical sensor components

In Figure 2.3, the distance between the reflective surface and the optical source & receiver is variable. Therefore, since the intensity of light is related to this distance, it is also a function of the force applied which is the cause of the change in the distance.

2.4.6.2 Photoelasticity

Photoelasticity is the experimental method where stress or strain causes birefringence, which is a property by virtue of which a ray of light passing through a birefringent material experiences two refractive indices, in an optically transparent material [21]. Light passes through the photoelastic medium which rotates the plane of polarization when stressed. This type of optical sensor is important in the measurement of the slip.

2.4.7 Optical fibre based sensors

In optical based sensors, the main principle is the transmission of light to and from the sensor. However, tactile sensors can also be constructed from the fibre itself which will simplify the model so that the structure will be much smaller and the working principle gets easier. In this type of sensor, design is based on internal state micro

bending, which is the process of light attenuation in the core of the fiber when a mechanical load is applied on the outer surface of the fibre, of optical fibres.

2.4.8 Piezoelectric sensors

Piezoelectricity can be utilized as a touch or tactile sensor. While quarts and some other ceramic materials exhibit strong piezoelectricity, polymeric materials such as polyvinylidene fluoride (PVDF) are generally used in tactile sensing. Since such materials are polymers, they can suit to surfaces much better than ceramics so that they can give much better information about the changes at the contact surface.

Polyvinylidene fluoride has the piezoelectricity but in its raw state the piezoelectric effect should be given by poling the film. From the raw state the PVDF film is heated and after that a strong electric field is applied on the two surfaces where the electric potential is to be gathered. These film sheets can be from 5 microns to 2 mm thick and it has good mechanical properties. After the poling process, the two surfaces where the electric field is applied are metalized in order to collect the charge generated by the application of force. Another advantage of using piezoelectric sensors is that they can be molded so that it can take every shape enabling the integration of the film to many surfaces and mimic the human skin.

2.4.9 Smart sensors

In many types of the tactile sensors, the main problem is the signal processing. Every individual sensor develops a signal and as the number of the sensors increase it becomes almost impossible to process the data. Therefore, it is more convenient to develop a complete sensor system rather than individual sensors. This way, the signal processing can be brought closer to the sensor or the electronic unit can be integrated into the sensor. As the silicon fabrication techniques improve, the smart sensor designs develop. Since silicon can be machined to form parts such as diaphragm and beams, a tactile sensor can be manufactured from a single silicon layer. However, there are problems in integrating the technology produced in laboratory to industry.

In all tactile sensors, the major problem is the data processing and the interconnections of this information. Therefore, it is desired to reduce the wires and interconnections due to the ease of construction and reliability. For this purpose, each sensing element

not only measures but also processes the data. But, the main difficulty with this approach was the poor discrimination, and susceptibility to physical damage.

2.4.10 Multi-stimuli touch sensors

Touch sensors are usually designed to respond only to force. However, human skin also responds to other external stimuli, in particular, temperature. PVDF film has also pyroelectric effect which is the production of voltage as the temperature changes. Therefore, there is another PVDF film which is unstressed in order to compensate the temperature effects. It is possible for a sensor to respond both to force and temperature changes. This has a particular use for object recognition between materials that have different thermal conductivity, between a metal and a polymer. If the processing of the data is very complex, a touch sensor can be constructed such that it utilizes a resistive elastomer for force and thermistor for temperature measurements. As the number of the force sensing layers is increased with different characteristics, the dermal and epidermal layers of the human skin can be simulated.

3. PIEZOELECTRICITY

3.1 Basics of Piezoelectricity

All crystal structures can be classified into one of the 32 possible forms of crystal symmetry. 21 of those crystal structures are said to be non-centrosymmetric where 20 of them exhibit piezoelectricity. In 10 of these crystal groups there is a permanent electric dipole, and the equilibrium of the electrostatic potential caused by this dipole is distorted by mechanical stress (piezoelectricity) or temperature change (pyroelectricity).

Piezoelectricity is the form of electricity created in 20 of the non-centrosymmetric crystal structures when they are bent or deformed. The word is derived from the Greek piezo which means to press and is the electricity resulting from pressure. Piezoelectricity is the direct result of the piezoelectric effect which is the electromechanical interaction between the mechanical and electrical state in crystalline materials with no inversion symmetry. Piezoelectric effect is reversible such that when a small current is run through, the crystalline structure changes shape slightly which can be a change up to 4% volume change.

The nature of the piezoelectric effect is closely related to the occurrence of electric dipole moments in solids. The dipole density or the polarization for crystals is the vectorial sum of the dipole moments of the crystallographic unit cells. The groups of unit cells with the same orientation are called Weiss domains. These Weiss domains are randomly oriented but being ferroelectric, the orientation of these domains can be aligned using the process of poling which is the application of a strong electrical field across the material at elevated temperature values. The poling process is not valid for all piezoelectric materials.

Rochelle salt is the earliest reported piezoelectric material which was first produced by pharmacist Elie Seignette in 1665 in France for medical purposes. In 1880, pioneering work was done by Jacques and Pierre Curie who have discovered that electric potential can be generated by applying pressure to this material. This phenomenon was

named as the “piezo effect”. Later Curie brothers ascertained that piezoelectric materials when exposed to electric potential change shape. This was also named as the “inverse piezo effect”.

3.1.1 Mathematical description

Piezoelectricity is the combination of the mechanical structure and the electrical behavior of the system. Therefore, the constitutive equations are given as coupled equations of both fields.

$$D = \varepsilon . E \quad (3.1)$$

where D is the electric charge density displacement, ε is the permittivity and E is the electric field strength.

From the Hooke’s Law,

$$S = s . T \quad (3.2)$$

where S is the strain, s is the compliance and T is stress.

The coupled equations, which are formed by adding the piezoelectric effect terms to the Equations 3.1 and 3.2, are given as:

$$\{S\} = [s^E]\{T\} + [d^t]\{E\} \quad (3.3)$$

$$\{D\} = [d]\{T\} + [\varepsilon^T]\{E\} \quad (3.4)$$

where $[d]$ is the matrix for the direct piezoelectric effect, $[d^t]$ is the matrix for the converse piezoelectric effect. The superscript E is for constant or zero electric field.

The former equation is for the converse piezoelectric effect and can be expanded as:

$$\begin{bmatrix} S_1 \\ S_2 \\ S_3 \\ S_4 \\ S_5 \\ S_6 \end{bmatrix} = \begin{bmatrix} s_{11}^E & s_{12}^E & s_{13}^E & 0 & 0 & 0 \\ s_{21}^E & s_{22}^E & s_{23}^E & 0 & 0 & 0 \\ s_{31}^E & s_{32}^E & s_{33}^E & 0 & 0 & 0 \\ 0 & 0 & 0 & s_{44}^E & 0 & 0 \\ 0 & 0 & 0 & 0 & s_{55}^E & 0 \\ 0 & 0 & 0 & 0 & 0 & s_{66}^E \end{bmatrix} \begin{bmatrix} T_1 \\ T_2 \\ T_3 \\ T_4 \\ T_5 \\ T_6 \end{bmatrix} + \begin{bmatrix} 0 & 0 & d_{31} \\ 0 & 0 & d_{32} \\ 0 & 0 & d_{33} \\ 0 & d_{24} & 0 \\ d_{15} & 0 & 0 \\ 0 & 0 & 0 \end{bmatrix} \begin{bmatrix} E_1 \\ E_2 \\ E_3 \end{bmatrix} \quad (3.5)$$

The latter equation stands for the direct piezoelectric effect and can be expanded as:

$$\begin{bmatrix} D_1 \\ D_2 \\ D_3 \end{bmatrix} = \begin{bmatrix} 0 & 0 & 0 & 0 & d_{15} & 0 \\ 0 & 0 & 0 & d_{24} & 0 & 0 \\ d_{31} & d_{32} & d_{33} & 0 & 0 & 0 \end{bmatrix} \begin{bmatrix} T_1 \\ T_2 \\ T_3 \\ T_4 \\ T_5 \\ T_6 \end{bmatrix} + \begin{bmatrix} \varepsilon_{11} & 0 & 0 \\ 0 & \varepsilon_{22} & 0 \\ 0 & 0 & \varepsilon_{33} \end{bmatrix} \begin{bmatrix} E_1 \\ E_2 \\ E_3 \end{bmatrix} \quad (3.6)$$

In the Equations 3.5 and 3.6, double subscripts are used to describe the relationship between mechanical and electrical parameters. The first one stands for the direction of stimulus while the second subscript gives the direction of the reaction of the system. The subscripts 1, 2 and 3 are used for directions of x, y and z respectively. The subscripts of 4, 5 and 6 are for rotations and stand for θ_x , θ_y and θ_z respectively.

3.1.2 Manufacturing process of piezoelectric polymer

Poly(vinylidene fluoride) (PVDF) is a prototypical ferroelectric polymer and due to its attractive ferroelectric properties, so much research have been conducted on PVDF and its copolymers. PVDF is a linear fluorinated hydrocarbon with a repeat unit ($\text{CH}_2\text{--CF}_2$), which is semi-crystalline and exhibits α , β , γ and δ crystalline phases. The α phase is non-piezoelectric. The γ and δ phases are not common. The α -form, which is the more stable form, is formed during simple crystallization upon cooling from the melt in quiescent conditions whereas the β -form provides the best ferroelectric and piezoelectric properties.

Therefore, in order to utilize the PVDF as piezoelectric sensors, it is needed to prepare the β -phase. The preparation of piezoelectric PVDF consists of two processes, the stretching process and the poling process. The stretching process also called as the α to β transformation is the stretching of the electrically inactive material called the α -phase with a stretching ratio of 4:1. The stretching process alone can not achieve a full transformation even at the highest stretching ratio of 7:1. Therefore, a second process called the poling is needed where the sample is subjected to large and enduring electric fields in order to achieve the realignment of the dipolar moments. After the application of the poling process, these dipolar moments are aligned along the direction of the applied electric field. Thus, the β -PVDF chains have a net dipole moment, pointing from the electronegative fluorine to the electropositive hydrogen, producing a net dipole moment nearly perpendicular to the polymer chain [22].

Moreover, the copolymer of PVDF-TrFE crystallizes directly into the beta phase when cooled eliminating the need for mechanical drawing and hence eliminating the artifacts such as voids and defects [23]. In addition to simplicity in the fabrication processes and advantages of being a more structurally uniform, when exposed to high electron irradiation, the P(VDF-TrFE) exhibits strong electro-strictive response, little polarization hysteresis and high operational frequency as well [24].

3.2 Conversion of Energy between Mechanical & Electrical

3.2.1 Mechanical to electrical

Materials having the piezoelectric effect generate charge with an applied load on it. The amplitude and the frequency of the generated signal is proportional to the mechanical deformation and the rate of change of the mechanical deformation respectively. The deformation causes a change in the surface charge density of the material resulting in a voltage difference between the electroded surfaces. The direction of the force is important so reversing the force results in opposite polarity and the replication of the reversal of the force generates an alternating output voltage.

Piezoelectric films are dynamic materials that develop electric charge proportional to the change in the mechanical stress applied. Therefore, they are not suitable for static measurements since they have high internal resistances and the decay of the electric charge has a time constant which is determined by the property named as the dielectric constant and the internal resistance of the piezo film. There exist some methods to achieve a dc voltage from the piezo film which requires the use of it both as actuator and sensor but in practice the lowest frequency value that can be achieved by the piezo film is in the order of 0.001 Hz.

Under conditions approaching a short circuit, the charge density is given by:

$$D = \frac{Q}{A} = d_{3n}X_n \quad (3.7)$$

where, D is the charge density developed, Q is the charge developed, A is the area of the electroded surface, d is the appropriate piezoelectric coefficient for the axis of applied stress, n is the axis of the applied stress and X is the magnitude of the applied stress on the relevant direction.

The open-circuit output voltage is given by:

$$V_0 = g_{3n} X_n t \quad (3.8)$$

where, addition to the notations above g is the appropriate piezoelectric coefficient for the axis of the applied stress and t is the film thickness.

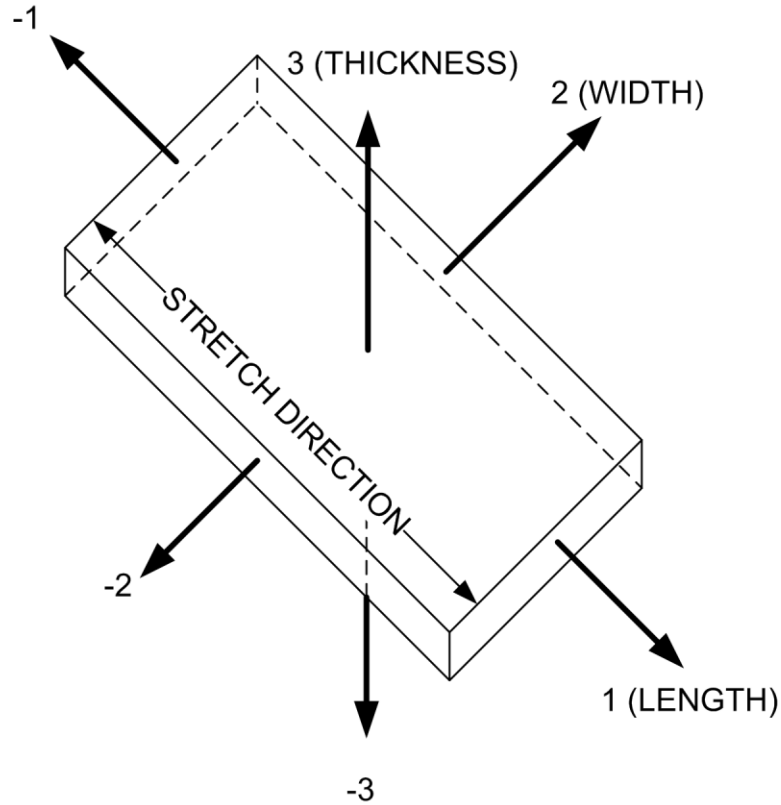


Figure 3.1 : Directional numbers given for applied force and voltage output

The direction of the applied force and the voltage output is given in Figure 3.1 and also by the convention:

1 = length (or stretch) direction

2 = width (or transverse) direction

3 = thickness direction

The d_{3n} and g_{3n} which are the charge mode and voltage mode piezoelectric coefficients have two subscripts. The first one stands for the electrical axis and the second one stands for the mechanical axis. Since the piezo films are thin, their electroded surfaces are along the thickness direction.

Typically, for low frequency applications the piezo film is used in the mechanical 1 direction whereas for high frequency applications the mechanical direction is 3.

3.2.2 Electrical to mechanical

The piezo film can also be used as an actuator since for a given electrical voltage the film changes its dimensions. For one polarity of the voltage, the piezo film becomes thinner but longer and wider. For the opposite polarity, the film contracts and becomes thicker. If an alternating current is applied, the film starts to vibrate.

The length change of the piezo film is related to the piezoelectric constant “ d_{3n} ”.

For length change,

$$\Delta l = l d_{31} V / t \quad (3.9)$$

For width change,

$$\Delta w = w d_{32} V / t \quad (3.10)$$

For thickness change,

$$\Delta t = \frac{t d_{33} V}{t} = d_{33} V \quad (3.11)$$

where, Δl is the change in film length, l is the original film length, d_{3n} is the related piezoelectric coefficient for length, V is the applied voltage across the thickness and t is the film thickness.

3.3 History of Piezoelectricity

The first experiments that demonstrate the connection between the macroscopic piezoelectric phenomena and the crystallographic structure were carried out by Pierre and Jacques Curie brothers in 1880. The experiments were based on the measurement of the surface charges appearing in some specially prepared crystals such as tourmaline, quartz and Rochelle salt which were subjected to mechanical stress. The results showed a deviation in the surface charge and this effect was called as the “*piezoelectricity*” in order to distinguish it from other phenomena like “*contact electricity*” which is the static electricity generated by friction and “*pyroelectricity*” which is the electricity generated by the temperature change.

The Curie brothers didn't predict that the crystals which exhibit the direct piezoelectric effect (generation of electricity by the application of mechanical stress) could also exhibit the converse piezoelectric effect (generation of mechanical stress or displacement in response to an applied electric field). The converse piezoelectric effect was mathematically deduced from the fundamental thermodynamic principles by Lippmann in 1881 [25]. The Curie brothers immediately worked on this effect and experimentally confirmed the existence of the converse piezoelectric effect and obtained quantitative proof of the reversibility of electro-elasto-mechanical deformations in piezoelectric crystals.

In the following two years, the interactive work within the European scientific community led to the establishment of the core of the piezoelectric applications. Those scientific studies were based on the identification of the piezoelectric crystals on the basis of asymmetric crystal structure, reversible exchange of electrical and mechanical energy and integration of the principles of thermodynamics to the relationships between mechanical, electrical and thermal variables. Leading up to 1910, much more laboratory work was done in order to explore and define the crystal structures that exhibit piezoelectricity. In 1910 the publication of "*Lerbuch der Kristallphysik*" (textbook on crystal physics) by Woldemar Voigt became a standard reference work which described the 20 natural crystal classes capable of piezoelectricity and defined the piezoelectric constants using tensor analysis [26].

The first serious application of piezoelectric devices was sonar which took place during World War I. In 1917 in France, Paul Langevin and his coworkers developed an ultrasonic submarine detector. The detector consisted of a transducer which was a mosaic of thin quartz crystals glued between two steel plates and a hydrophone to detect the returned echo. By emitting a high-frequency chirp from the transducer, and measuring the amount of time it takes to hear an echo from the sound waves bouncing off an object, one can calculate the depth to that object.

The success of using piezoelectricity in sonar created intense development interest in piezoelectric devices. Over the next few decades, new piezoelectric materials and new applications for those materials were explored and developed. Some examples of this activity include:

- Megacycle quartz resonators were developed as frequency stabilizers for vacuum-tube oscillators.
- A new class of materials testing methods was developed based on the propagation of ultrasonic waves. For the first time, elastic and viscous properties of liquids and gases could be determined with comparative ease, and previously invisible flaws in solid metal structural members could be detected. Ultrasonic time domain reflectometers could find flaws inside casted metals which lead to improvements in structural safety.
- Also, new ranges of transient pressure measurement were opened up permitting the study of explosives and internal combustion engines, along with a host of other previously immeasurable vibrations, accelerations, and impacts.

In fact, during the revival following the World War I, most of the applications which are now considered to be classical were conceived in an increasing manner despite the limited device performance and limitations of commercial exploitations.

During World War II, in the United States, the Soviet Union and Japan, isolated research groups working on improved capacitor materials discovered a new class of man-made materials, called ferroelectrics, which exhibited dielectric constants up to 100 times higher than natural materials. Furthermore certain ceramic materials (prepared by sintering metallic oxide powders) were made to exhibit similar improvements in piezoelectric properties. This discovery of easily manufactured piezoelectric ceramics with astonishing performance characteristics had started an intense research and development into piezoelectric devices.

The advances in materials science that were made during this phase fall into three categories:

1. Development of barium titanate and later lead zirconate titanate materials with specific properties for particular applications.
2. Development of an understanding of the correspondence of the perovskite crystal structure to electro-mechanical activity.
3. Development of a rationale for doping both of these families with metallic impurities in order to achieve desired properties such as dielectric constant, stiffness, piezoelectric coupling coefficients, ease of poling, etc.

The piezoelectric device development was dominated by industrial groups in the United States in the interest of securing profitable patents. Despite the development of new materials and the maturation of the manufacturing processes, the United States market had not grown as quickly and without new application areas the growth of piezoelectric industry suffered.

On the contrary, the Japanese manufacturers did not embrace the “*secrecy policy*” practiced among the United States piezoceramic manufacturers and shared their information. Several Japanese companies and universities formed a competitively cooperative association and established the Barium Titanate Application Research Committee in 1951. This association set an organizational precedent for quickly overcoming the technical and manufacturing challenges and creating new markets.

In 1965 Japanese commercial enterprises began to reap the benefits of steady applications and the work on new material development. From the perspective of international business they were leading the technology developing new knowledge, new applications, new processes and new commercial market areas in a coherent and profitable way. Persistent efforts of Japanese manufacturers in material development had created new piezoceramic families with free of patent restrictions. Using these materials manufacturers quickly developed several types of piezoceramic signal filters which were used in communication equipment markets and piezoelectric igniters which generates sparks for small engine ignition systems. As time passed by, the markets for these products continued to grow and some valuable markets were created. The number of applications worked on was staggering, including the following highlights and curiosities:

- New powerful sonar based on new transducer geometries and sizes achieved by ceramic casting.
- Piezo ignition systems which generate spark voltages by compression
- Sonobuoy which is the sensitive hydrophone listening or radio transmitting buoys for monitoring ocean vessel movements.
- Small and sensitive microphones
- Relays

In the revival period of the piezo development, especially in United States, piezo material developing individual companies were established. As a matter of “secrecy

policy” those companies did not communicate. The reason was threefold: first during the wartime the experienced workers on improved materials were working in a classified atmosphere; second, after the war the entrepreneurs saw the promising profits secured by patents and secret processes; and finally the piezoceramic materials were extremely difficult to develop but once the process has been fully understood it was easy to replicate.

In the business perspective, the market development for piezoelectric devices lagged behind the technology developed for the devices. All the materials still commonly used today were developed by 1970 but at that time there were only a few high volumes commercial applications had evolved. On the other hand, the commercial success of the Japanese efforts has attracted the attention of the industry in many other nations to develop successful piezoceramic products. There has been an increase in the number of the piezo patents granted by the United States Patent Office. Moreover, there has been a large increase in the number of the publications in Russia, China and India [27].

Nowadays, the technical goals of the leading companies are to obtain useful and reasonably priced actuators which are low in power and energy consumption as well as being high in reliability and robustness. The search for perfect piezo product opportunities is now in progress. As observed, since there is an increase in worldwide activity and the success encountered in the last quarter of the 20th century, investment in order to have important economic and technical development seem certain.

3.4 Application Areas

Piezoelectricity can be utilized in many application areas both as sensors using the direct piezoelectric effect and as actuator using the converse piezoelectric effect. Moreover, the material of the sensor or actuator can be piezoceramic or polymer depending on the application parameters. The space limitations or the force range to be measured may have influence on the material used.

Since the piezoelectric charge on the electroded surfaces occurs during mechanical deformation, the piezoelectric property can be used for force, pressure and acceleration sensors. As the amplitude of the charge is increased by a charge amplifier, the occurrence can be converted into a measurable electric field. However,

piezoelectric elements are suitable for the assessment of the dynamic processes. In static application, there exists a problem of detecting the low charge generation.

The advantage of piezoelectric sensor over other types is that the piezoelectricity is an active measurement method. Therefore, the sensor produces its own signal in response to external stimulus whereas other types require active sensing elements or the measurement is indirect. Due to the advantage of being direct and active, the sensor can be applicable to very small scales without any problem of integration.

Piezo sensors represent a broad application area. Conventionally piezo sensors were used as vibration recorders in order to detect imbalanced rotating machines or crash detectors in automotive industry. However, they are being used more in ultrasonic level measurements and flow rate measurement applications. In ultrasonic level measurements, the propagation time for the reflected echo of an ultrasonic wave is evaluated. Flow rate measurements are based on either propagation time measurements or on the Doppler Effect which is the measurement of the phase difference.

Piezoceramics can be grouped into two categories namely soft piezo ceramics and hard piezo ceramics. Typical applications of soft piezo ceramics are object identification and surveillance, sound transmitters (buzzers) and sound receivers (microphones) and sound pickups of musical instruments. Hard piezo ceramic materials have high coupling factors and high quality factors as well as good stability under high mechanical loads. Applications of hard piezo ceramic materials include ultrasonic cleaning, machining of materials (ultrasonic welding, bonding, drilling), medical field (ultrasonic dental scale removal, surgical instruments) and sonar technology [28]. Moreover in a piezo lighter, an impulse is used in a piezo igniter in order to generate a high voltage electric spark which ignites a gas flame [29].

On the other hand, ferroelectric polymers like PVDF has advantages of being light weight and flexible over ceramic materials [23]. The piezoelectric films can be used either as accelerometers or dynamic switch elements. They are applicable where the space for the sensing element is limited and also can be a good alternative since they are lightweight and flexible, which makes the films to be compatible for a wide range of surface geometry, as well as being lower in price. In addition, since the piezo film

generates its own signal, it requires no external power which is a major advantage where the power budget is crucial.

In electronics, PVDF film is laminated to the interior surface of the circuit board in order to detect any tempt to gain access where the information of the electronic unit is essential.

The piezoelectric film can also be applied in the security field and even more in the military applications. The security of an area can be established by detecting the unusual sound noises coming from the surrounding of a fence. Therefore, any disturbances like an attempt to cut the fence or climb a fence can easily be detected. In military applications, during the World War I the first sonar was developed using the piezoelectric effect. Furthermore, the piezoelectric cable can be buried underground and it can create a security perimeter detecting the footsteps and the vehicle activity.

Piezoelectric polymers can be fabricated in order to generate sensors that mimic the human hair in nature. The fibrillar structure of the piezoelectric film makes it useful since it distributes the disturbance to the system. Making use of this property, the system can be used as micro/nano force sensors, tactile sensor in minimal invasive surgery, micro-fluidic flow sensor, and small footprint hearing aid and so on.

The key advantage of PVDF as the sensing material over capacitive sensors has two key design parameters namely the increasing charge on the surfaces of the PVDF film and decreasing of the effective capacitance. Both can be useful since the voltage produced can be considered as the ratio between the charge and the capacitance for a capacitive sensor. The geometry of individual micro pillars results in stress amplification increasing the amount of charge for a given pressure level [30].

Moreover, the structural electrode is proposed in order to increase the resolution and the compatibility with the contact surface. In traditional tactile sensing methods, the force is directly transmitted into voltage output. However, in this design since the stress is transmitted via microstructures, the stress concentration is increased. The charge output is increased since the contact surface of the piezoelectric sensor is decreased [31].

Piezoelectricity can also be utilized as actuators using the converse piezoelectric effect. The most widely used practical application of piezo actuators is the piezo positioners where the precise movement is essential. In micro robotics, microsurgery

equipment and micro electro mechanical systems (MEMS), a high torque motor output is needed and this need can be met by ultrasonic motors since they also have simple structures compared to other actuators. Although it is reported that piezoelectric thin film is used for the acceleration in ultrasonic motors, in order to realize high power output, bulk PZT which is a ceramic material having the piezoelectric effect is used [32].

Some other application areas include piezo loudspeakers that create sound waves and continuous ink-jet printers where the high frequency oscillations of a piezoelement spray disperses the ink. Another important application is the Braille lines for blind people. Applying an electric field across the piezoceramic components, tactile keys are pushed upwards enabling the blind people to sense the text written on a PC monitor.

As the piezo effect is always unidirectional, the effective actuation of the piezo actuators can be achieved by proper integration of several piezo elements [29].

4. MODELING AND DESIGN CRITERIA

4.1 Modeling of the Tactile Sensor

The piezoelectric effect is the combined effect of the structural and electric fields, and is totally reversible. In other words, if one applies a stress to the piezoelectric material, charge can be collected from electrode surface whereas applying a voltage causes strain in the material. Since piezoelectric materials are anisotropic, the actuator and sensing capabilities of the piezoelectric materials depend on the axis of applied electrical field or axis of mechanical stress as well as the poling direction. The piezoelectric films are poled in their thickness directions and the tactile sensors are designed to operate in thickness mode of the piezoelectric films. In such mode of operation, applied pressure and voltage output as well as the strain, occur in the direction normal to the surface of the piezoelectric film. There is a direct relation between the displacement and input voltage or vice versa for this operation as follow:

$$\Delta t = d_{33}V \quad (4.1)$$

$$V_0 = g_{33}\sigma t \quad (4.2)$$

where Δt is the total displacement in the thickness direction, d_{33} is the piezoelectric strain constant in the poling and measurement direction, V is the applied voltage for actuator usage whereas V_0 is the open-circuit output voltage, g_{33} is the piezo stress constant in the poling and measurement direction, σ is the stress applied to the fibers in the poling direction, and t is the thickness of the piezoelectric material in the poling direction.

In the design process of a tactile sensor, the piezoelectric PVDF film is needed in order to generate a voltage output in return of a pressure applied on the film. Moreover, the actuation and the sensing capabilities of the piezoelectric film are integrated resulting in active control of the adhesion to the surface. The adhesion to the contacting surface is increased by using a flexible polymer on the top of the piezoelectric film which has high biocompatibility. The flat piezoelectric film and the

patterned piezoelectric film with polymer micro fibers are given in Figure 4.1. In the proposed tactile sensor design, there is a common ground on the top of the piezoelectric film whereas the bottom layer is patterned such that each fiber backing layer is desired to behave as independent electrodes apart from coupling of adjacent fibers.

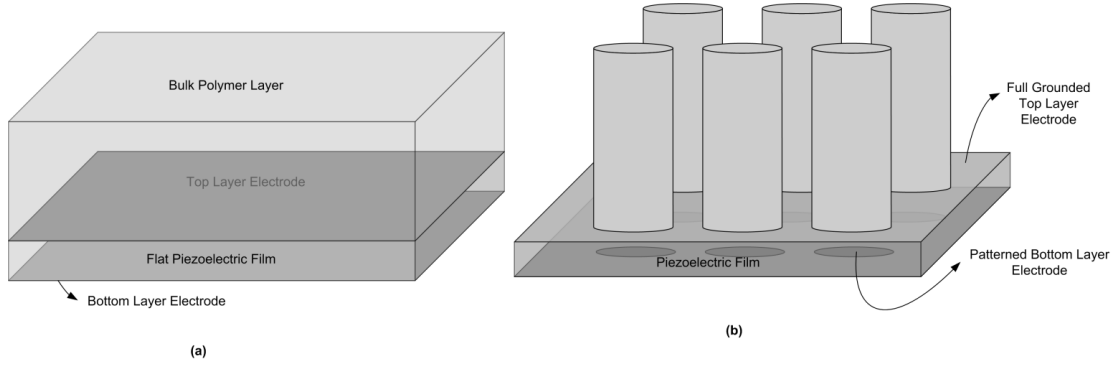


Figure 4.1: (a) PVDF with Bulk PDMS, (b) Patterned PVDF with PDMS Fibers

The proposed design has been compared in terms of the sensitivity which can be expressed by the ratio of the output voltage to the stress acting on the material. The patterned electrode configuration with pillars attached to the contacting surface has been compared to flat piezoelectric film with bulk polymer on top. The sensitivity analysis has been carried out in order to reveal the superiority of the micro-pillar design with patterned electrode configuration.

The sensitivity is given by the Equation 4.3.

$$K = \frac{V_0}{\sigma} \quad (4.3)$$

The output voltage can be expressed in terms of applied pressure which is given in Equation 4.2. Therefore, the sensitivity of the flat PVDF film is calculated as

$$K_1 = g_{33} \cdot t \quad (4.4)$$

Moreover, relative sensitivity has been defined in order to have a comparison of sensitivity of the tactile sensor with respect to flat piezoelectric film case which is simply given in Equation 4.5.

$$K_r = \frac{K_1}{K} \quad (4.5)$$

The relative sensitivity of the flat piezoelectric film is unity whereas the relative sensitivity of the tactile sensor has been calculated by FEM simulations. FEM simulations have been carried out for different spacing ratios where the bottom surface of the piezoelectric film is fixed in all directions and the upper surface of the piezoelectric film is grounded. The stress has been applied in such a way that it is concentrated at the upper surface of the polymer and the voltage output is divided to the flat surface voltage output.

The stress concentration in the fibers can be calculated as given in Equation 4.6 [30].

$$\sigma = \frac{(d + s)(d + s)}{\pi d^2/4} \cdot P \quad (4.6)$$

In the equation d is the diameter of a fiber, s is the edge to edge spacing between the fibers which is given in Figure 4.4. The pressure P is kept constant and the stress per unit fiber is found by rearranging the Equation 4.6.

$$\sigma = \frac{(1 + s/d)^2}{\pi/4} \cdot P \quad (4.7)$$

Therefore the sensitivity has been explored by keeping the applied stress constant and dividing the voltage developed for each case to the voltage output of the flat piezoelectric film. The relative sensitivity has been plotted versus a dimensionless parameter spacing ratio (s/d) which is the ratio of edge to edge spacing between the fibers divided by the diameter of a single fiber. The FEM solutions are given in Figure 4.2. Such dimensionless parameters have been used in the understanding of the effects of design parameters. Spacing ratio which is the ratio of spacing between fibers to fiber diameter and aspect ratio which is the ratio of length of the fibers to their diameter have been utilized so that the design can easily be integrated to micro nano tactile sensor to huge pressure distribution handling problems.

The geometry of individual micro pillars results in stress amplification increasing the amount of charge for a given pressure level. Moreover, the structural electrode is proposed in order to increase the resolution and the compatibility with the contact surface [30]. However, the piezoelectric polymer (polyvinylidene fluoride (PVDF)) utilized in these works reduce the adhesion capability of gecko like fibers since the surface energy of the piezoelectric material is much less than the widely used

polymers (poly(dimethylsiloxane) (PDMS), Poly(methyl methacrylate)(PMMA)) for synthetic fiber production.

Moreover, the elastic modules of piezoelectric material have a higher value than soft polymers giving a decrease in adhesion and rough surface adaptation capability of fibers which results in the deficiency of determining the topography of the contacting surface.

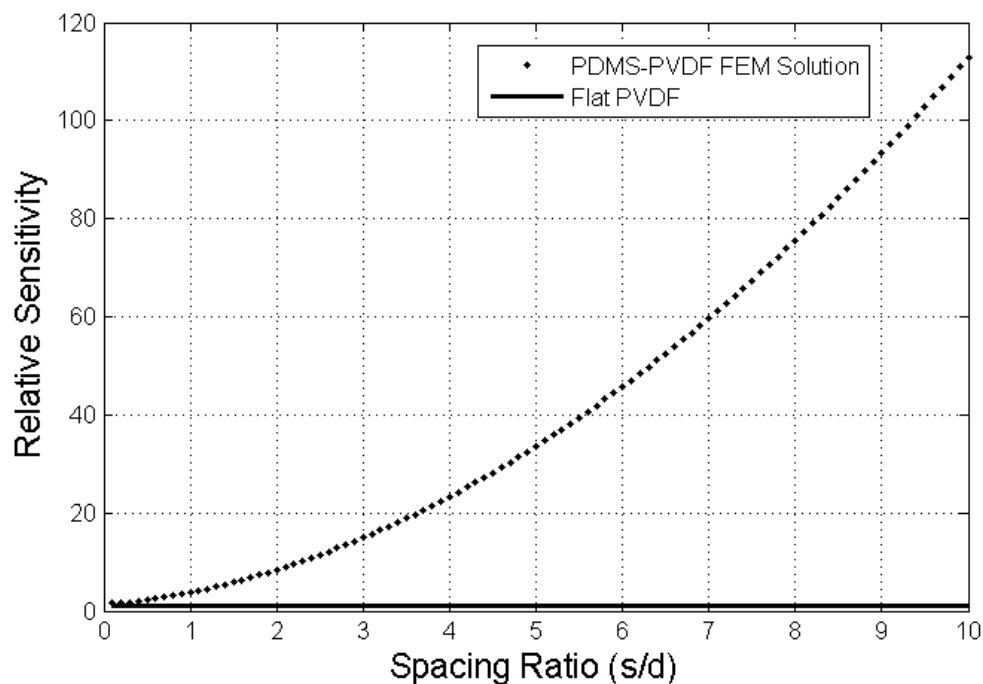


Figure 4.2: Relative Sensitivity Comparison

The sensor mode of the fiber array is utilized for the sensing of the pressure over the upper surface of the array. A voltage is gathered which is related with the normal stress on the piezoelectric film so the design is needed to be optimized in order to generate maximum voltage output. As the voltage is related to the stress on the film, increasing the stress concentration will also increase the voltage output. Another issue about the tactile sensing is to increase the resolution and improve the ability to sense the pressure changes in fine environments. Therefore, the proposed model has been examined both for static and dynamic working environments. This examination has been carried out by simulation tests and the material properties that have been used in the simulations are given in Table 4.1.

Table 4.1: Simulation parameters of materials of PVDF piezoelectric film and PDMS as polymer fiber used in the finite element analysis

Parameter	Symbol	Value	Units
Elastic Modulus (PVDF)	E_{PVDF}	2.0	GPa
Elastic Modulus (PDMS)	E_{PDMS}	1.8	MPa
Shear Modulus (PVDF)	G_{PVDF}	0.775	GPa
Shear Modulus (PDMS)	G_{PDMS}	0.677	MPa
Poisson's Ratio (PVDF)	ν_{PVDF}	0.29	
Poisson's Ratio (PDMS)	ν_{PDMS}	0.33	

The single pillar static analysis carried out to give the limits for the dimensions of a single pillar whereas the fiber array analyses gives the dimensions of spacing between the fibers and the thickness of the piezoelectric polymer film. In designing a single fiber, the polymer fibers are located on the upper surface of the piezoelectric film and the geometry created is given in Figure 4.3.

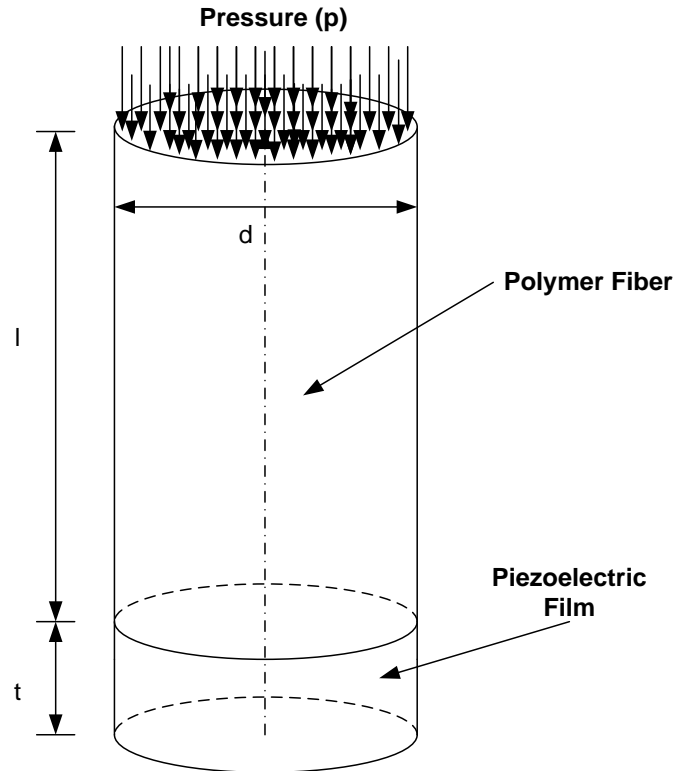


Figure 4.3: Basic Geometry of a Single Pillar

The fiber array is generated by combining the design mentioned for the single pillar. The polymer fibers are located on the upper surface of the piezoelectric film where the fibers are connected to each other. The top electrode layer on the piezoelectric film combined for every pillar and grounded. The bottom electrode layer is patterned and

gives independent potential differences for each pillar. The geometry of a single fiber and the fiber array is given in Figure 4.4.

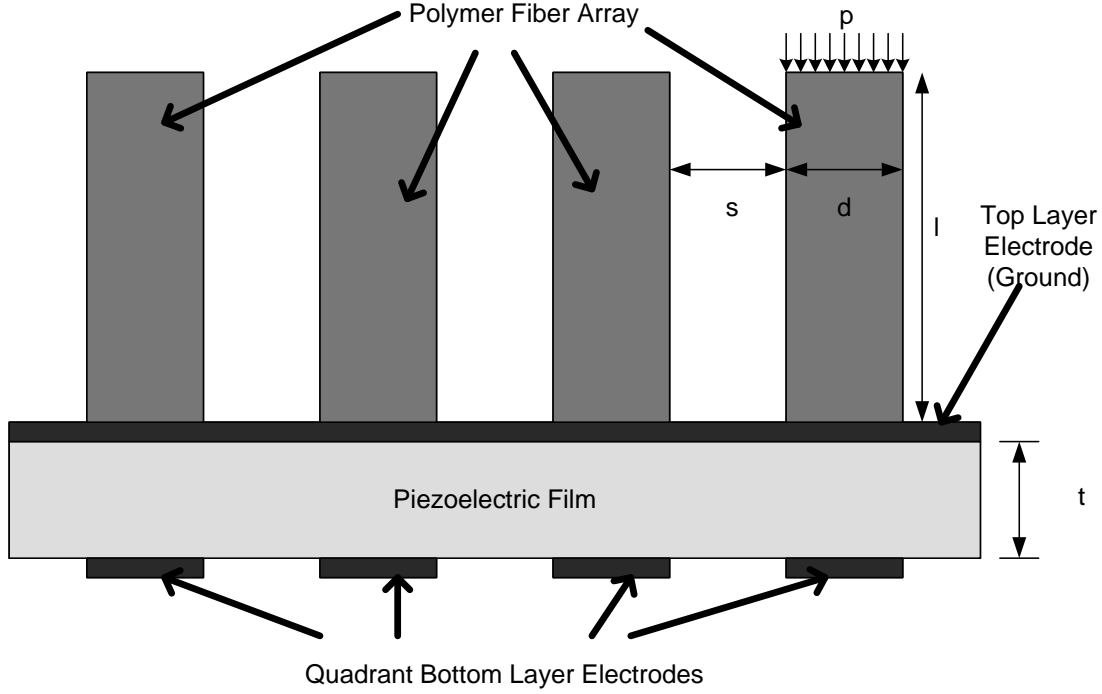


Figure 4.4: Illustration of the Proposed Sensor

4.1.1 Buckling of fibers

The design constraints are considered and the first criterion is the buckling of the polymer fibers. The buckling criterion of a single pillar is given by [33]

$$F = \pi^2 \frac{EI}{(KL)^2} \quad (4.8)$$

Table 4.2: Buckling Formula Abbreviations

Abbreviation	Definition
F	Critical Vertical Load on Pillar (N)
E	Modulus of Elasticity (Pa)
I	Area Moment of Inertia (m ⁴)
K	Effective Length Factor Depending on End Supports
L	Length of Column (m)

Effective Length Factor Depending on End Supports:

- For both ends pinned (hinged, free to rotate), $K = 1.0$
- For both ends fixed, $K = 0.50$
- For one end fixed and the other end pinned, $K = 0.699$
- For one end fixed and the other end free to move laterally, $K = 2.0$

The moment of inertia for cylindrical pillars are given by Equation 4.9

$$I = \frac{\pi d^4}{64} \quad (4.9)$$

The buckling limit inequality is achieved by inserting Equation 4.9 into the buckling equation. Furthermore, the equation is rearranged such that it is presented in terms of non-dimensional parameters.

$$F = \sigma A < \pi^2 \frac{EI}{(Kl)^2} \quad (4.10)$$

$$\sigma \left(\frac{\pi d^2}{4} \right) < \pi^2 \frac{E \left(\frac{\pi d^4}{64} \right)}{4l^2} \quad (4.11)$$

$$(l/d) < \sqrt{\frac{\pi^2 E}{64 \sigma}} \quad (4.12)$$

The human sense of touch exhibits the highest sensitivity at the fingertips. Fingertip of a human can detect stress levels of 10-40 kPa [13]. In order to have a satisfactory design as well as having the maximum integration with the surface, 10 kPa is taken as the design parameter. The relation of stress and the aspect ratio is given in Figure 4.5.

Considering the fiber array, the stress concentration on the fibers is approximated as

$$p(s + d) \approx \sigma d \quad (4.13)$$

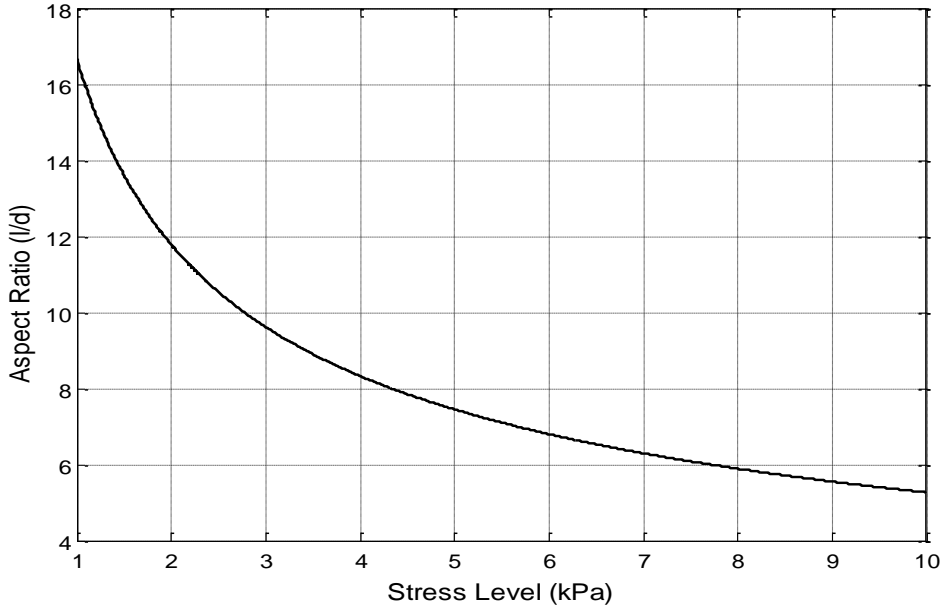


Figure 4.5: Stress Applied versus Aspect Ratio

Therefore, rearranging the Equations 4.12 and 4.13,

$$\frac{p \cdot (s + d)}{d} = \frac{\sigma \cdot d}{d} \quad (4.14)$$

$$p \left(\frac{s}{d} + 1 \right) = \sigma = \frac{\pi^2 E}{64} \frac{1}{(l/d)^2} \quad (4.15)$$

Another dimensionless parameter can be assigned as the spacing ratio s/d . The failure limit of the tactile sensor can be expressed in terms of these two dimensionless parameters. The graph for this limit is given in Figure 4.6. The graph states that the maximum allowable pressure limit increases with the decreasing aspect and spacing ratios. However, decreasing the aspect ratio decreases the surface adaptation whereas decreasing the spacing increases the interaction of adjacent pillars.

In terms of dimensional parameters the length of a single pillar can be limited by the Equation 4.16

$$l^2 < c_1 \frac{d^3}{s + d} \quad (4.16)$$

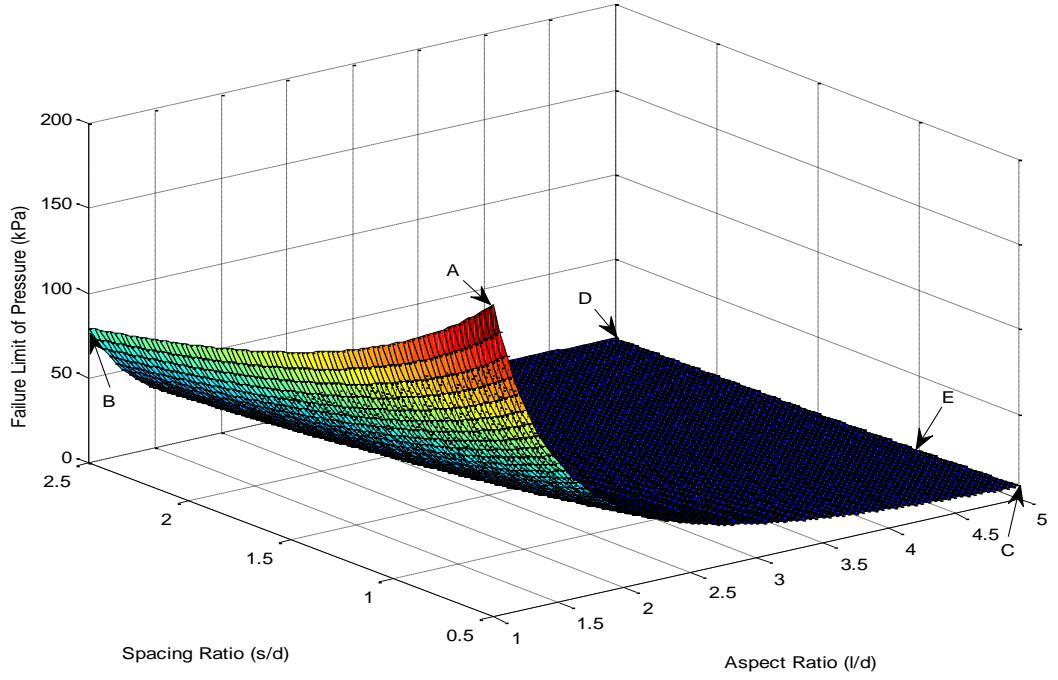


Figure 4.6: Stress Saturation Limit on PDMS Upper Surface

where $c_1 = \pi^2 E / 64 p$ which is a design parameter depending on the applied pressure. Since all of the terms are positive numbers the absolute value remains the same which reduces the length equality to Equation 4.17.

$$l < \sqrt{c_1 \frac{d^3}{s + d}} \quad (4.17)$$

4.1.2 Matting condition

For increased interfacial compliance, slender fibrillar structures with high aspect ratios are preferred. However, this high aspect ratio is limited by their tendency to collapse laterally under the surface loads. Therefore, this limits the ability of fibers adhesion.

Especially for circular cylinders, the height of the fibril must satisfy the inequality given in Equation 4.18 in order not to collapse laterally [34].

$$s > \sqrt[6]{\frac{2^{27} l^{12} \gamma_f^4}{3^3 \pi^4 E_f^* E_f^3 d^{10}}} \quad (4.18)$$

where E_f^* is the plain strain Young's modulus, s is the spacing between the fibers, l is the length of the fibers, γ_f is the surface energy which is half of the work of adhesion and d is the diameter of the fiber. The matting equation can further be rearranged as such:

$$s > \sqrt[6]{\frac{2^{27}\gamma_f^4}{3^3\pi^4 E_f^* E_f^3} \frac{l^2}{d^{5/3}}} \quad (4.19)$$

The non-dimensional terms can be expressed as a single constant.

$$c_2 = \sqrt[6]{\frac{2^{27}\gamma_f^4}{3^3\pi^4 E_f^* E_f^3}} \quad (4.20)$$

Therefore, matting condition can be considered as another inequality as a constraint for the dimensional parameters. This inequality is given in Equation 4.21

$$l < \sqrt{\frac{s d^{5/3}}{c_2}} \quad (4.21)$$

4.1.3 Flaw-insensitive condition

The fiber material properties as well as the structure of the fibers allows them to bend and adopt to many surface roughness and also return back to their original shape after the contact and the pressure is over. Therefore, the polymer fiber would have a repetitive long time usage in many applications.

Assuming that the fibers are cylindrical beams with flat contacting surfaces, the adhesion for a circular punch with flat surface interaction is given as [35]:

$$P_f = \sqrt{\frac{3}{4} \pi d^3 K w_f} \quad (4.22)$$

$$K = \frac{4}{3} \left(\frac{1 - \nu_s^2}{E_s} + \frac{1 - \nu_f^2}{E_f} \right)^{-1} \quad (4.23)$$

where P_f is the adhesion, w_f is the effective work of adhesion, d is the fiber diameter, K is the effective Young's modulus, E_s and E_f are the Young's moduli, ν_s and ν_f are the Poisson's ratio of the surface and the fiber material respectively.

Using the pull-off force of a circular flat punch, the average adhesion strength (σ_0) can be determined as

$$\sigma_0 = \frac{P_f}{\pi \frac{d^2}{4}} \quad (4.24)$$

Therefore, the flaw insensitive condition gives a maximum limit to the diameter of the fiber in order to have good adhesion to the contacting surface. The flaw-insensitive condition is given by the Equation 4.25

$$d < \frac{12Kw_f}{\pi\sigma_0^2} \quad (4.25)$$

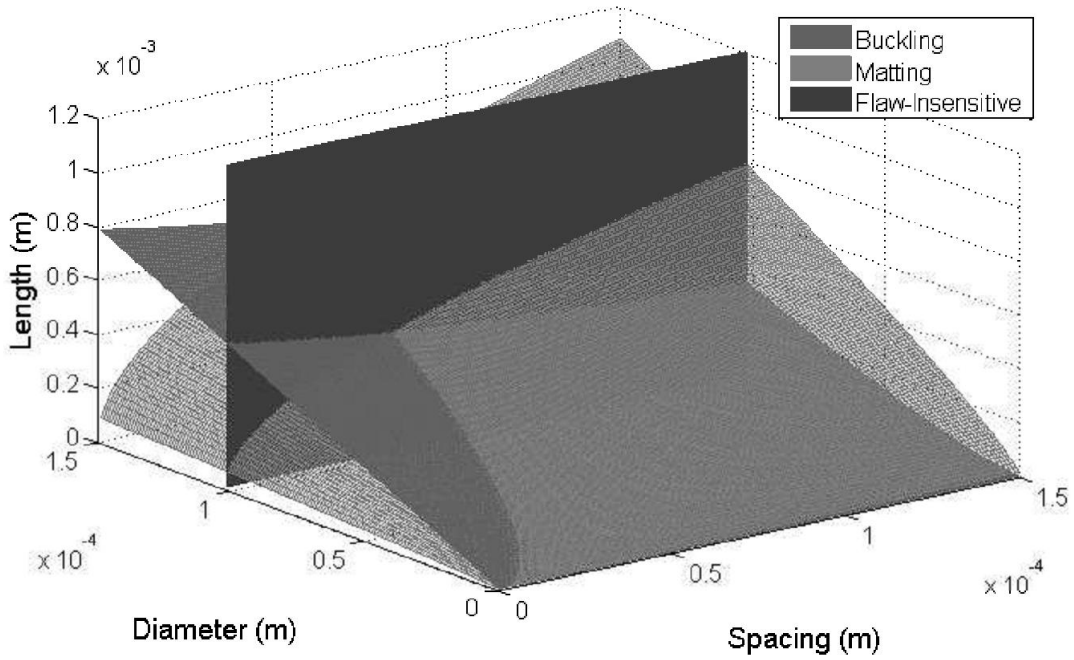


Figure 4.7: Dimensional Constraints for Design Criteria

As a result, a volume that is below the both matting and buckling planes and to the right of the flaw-insensitive plane satisfies the design criteria. In order to have a better view, Figure 4.7 has been plotted for an upper diameter limit of 100 μm eliminating the flaw-insensitive curve. The resultant constraining surfaces have also been plotted

in Figure 4.8 for pressure design criteria of 10, 20 30 and 40 kPa pressure levels. The surface plots reveal that increasing the maximum pressure level as the design parameter lowers the buckling limit curve resulting in shorter polymer fibers. Therefore, the satisfactory design has been developed by the lower limit of the maximum pressure level which is 10 kPa.

The volume below both the buckling limit of the micro pillars and the matting condition of the polymer fiber curves satisfies the design limitations. Increasing the spacing results in eliminating the matting however since it increases the stress concentration sets a limit from the buckling criterion. In order to obtain the parameters another constraint must be accounted. For that purpose a manufacturing limitation of minimum $40\text{ }\mu\text{m}$ comes into play which results in a two dimensional curve.

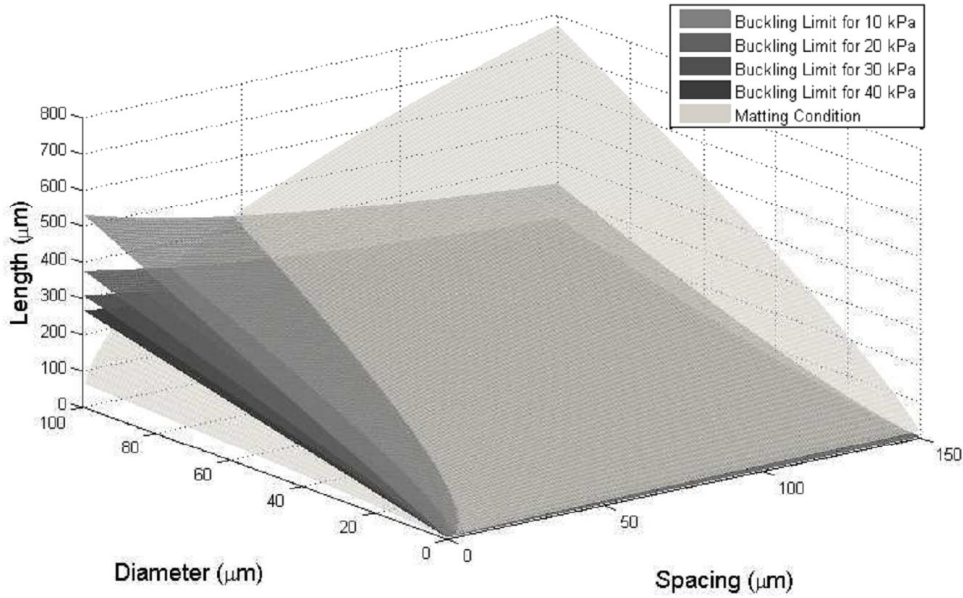
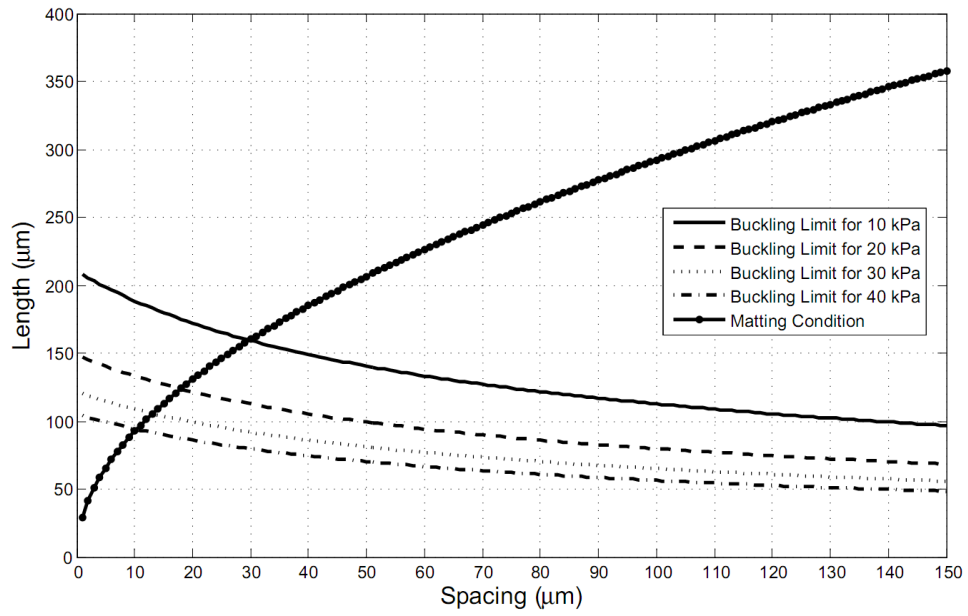
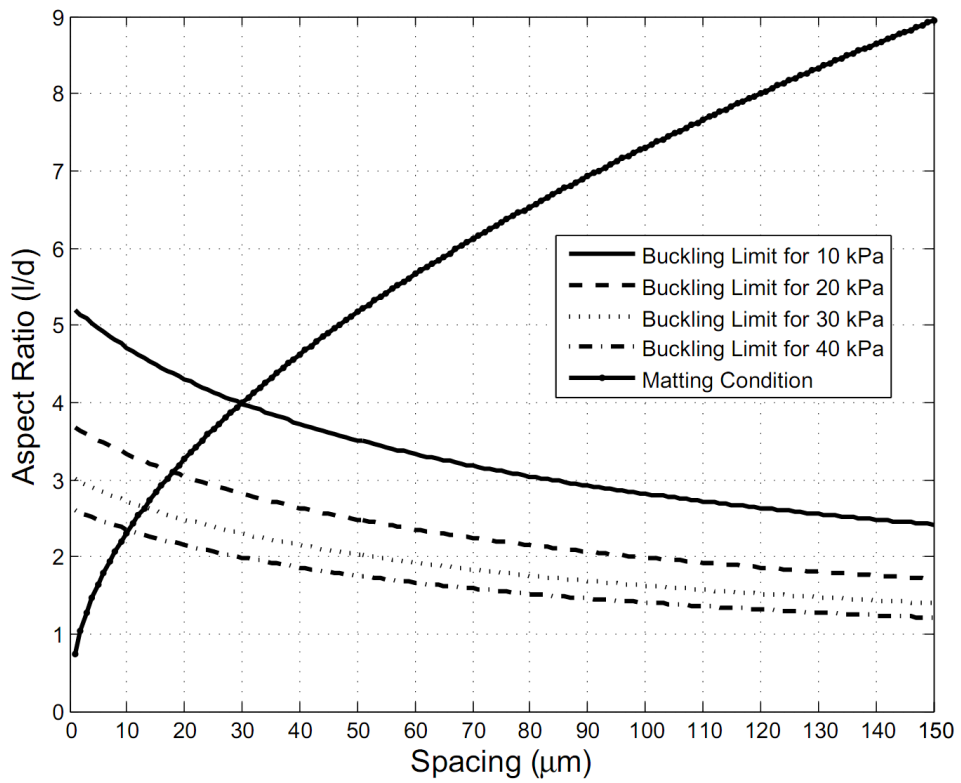


Figure 4.8: Buckling Limit and Matting Condition Inequality for Dimensions

Figure 4.9 (a) is a cross sectional cut of Figure 4.8 with a constant diameter of $40\text{ }\mu\text{m}$. Buckling limit variations can be more clearly seen for the variations in the spacing between the fibers whereas the increase in spacing enables longer fibers. The length of the fiber is also divided by the diameter of the fiber in order to generate a further plot which is given in Figure 4.9 (b) with dimensionless parameter of aspect ratio (l/d).



(a)



(b)

Figure 4.9: a) Two Dimensional Design Criteria for a Diameter of $40\ \mu\text{m}$ b) Design Criteria for Aspect Ratio (l/d)

5. STATIC ANALYSIS OF THE PIEZOELECTRIC TACTILE SENSOR

5.1 Static Single Pillar Analysis

The model has been generated by considering the design criteria for both considering the stability of a single polymer pillar and the interaction of pillars in the fiber array. In the sensor design, it is desired to integrate the sensor and the actuator capability of piezoelectric film. The static analysis of a single fiber include both the behavior of the sensor to applied pressure which is the sensing mode and the stiffness change due to applied voltage which is the actuating mode.

5.1.1 Sensor mode analysis

Piezoelectric films are materials that develop electric charge proportional to the change in the mechanical stress applied. The linear relationship between the applied pressure and the voltage output for piezoelectric film is given in Equation 4.2. In order to evaluate the sensing performance of a single fiber, the applied force, diameter of the fiber and length of the fiber are examined. The differentiation of such geometrical dimensions affects the voltage output of piezoelectric film changing the sensitivity and efficiency of the sensor.

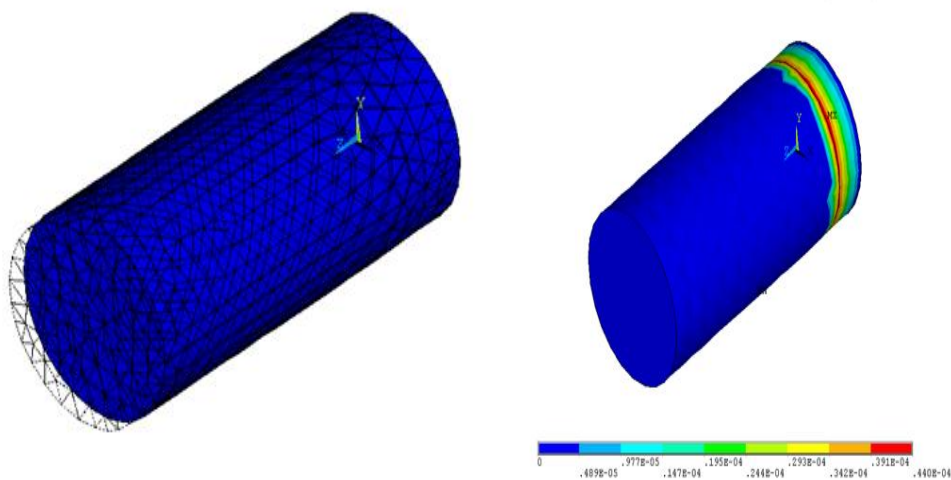


Figure 5.1: a) Deformation of a Single Pillar b) Potential Difference across the Piezoelectric Film

The single pillar analyses have been carried out by a model in which the deformation and the voltage graph is given in Figure 5.1. The sensor mode performance analyses have been carried out by changing the independent variables individually and obtaining the voltage output values for each of those conditions.

5.1.1.1 Force-voltage

The force results in voltage output linearly related to the magnitude of the force. The force is evenly distributed among the upper surface of the polymer pillar. The solutions give close proximity to the analytical solution. The finite element voltage output data and the analytical solution for different force values are plotted in Figure 5.2. The analysis has been carried out for a diameter value of 40 μm , polymer fiber length of 120 μm and piezoelectric film thickness of 25 μm . The bottom surface of the piezoelectric film is fixed whereas the upper surface is grounded. Furthermore, the piezoelectric film and the polymer fiber have been glued in their contacting surfaces.

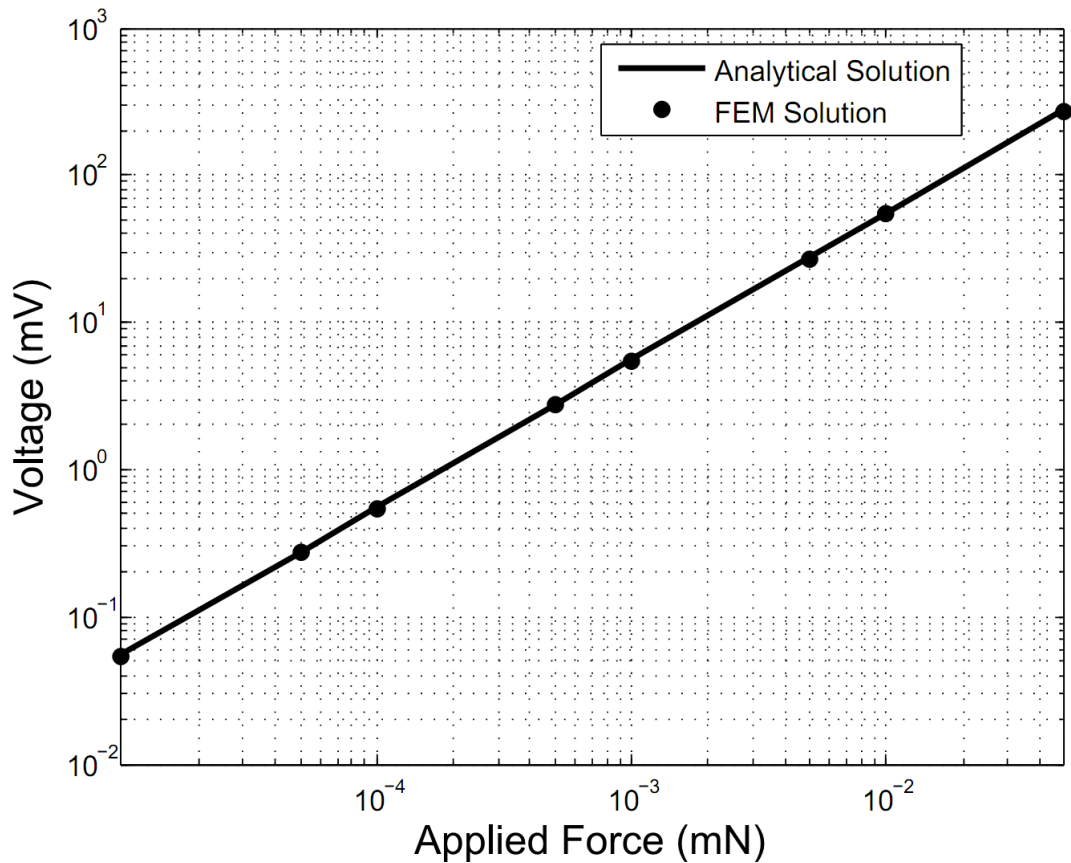


Figure 5.2: Applied Force-Voltage Graph for Single Pillar

The linear range of piezoelectric film is quiet high. The force applied is selected is logarithmic scale so that it can sweep a higher range. The maximum failure limit for

the polymer fibers was selected as 10-40 kPa. The force values applied in the simulations were simply selected in accordance to the design limitations and chosen as $10 \cdot 10^{-9}$ N to $50 \cdot 10^{-6}$ N. The maximum value corresponds to 40 kPa. The mesh size for the single fiber is chosen to be $1 \mu\text{m}$.

The error analysis of the FEM simulations to the analytical solution has further studied. The percent error for the simulations has been calculated as

$$\% \text{ error} = \frac{|\text{FEM Sol.} - \text{Analytical Sol.}|}{\text{Analytical Sol.}} \quad (5.1)$$

The percent error calculations for the applied force versus the voltage output resulted in 1.9 % error between the two solutions for every data point.

5.1.1.2 Thickness-voltage

Furthermore, the applied pressure is kept constant and the PVDF film thickness is varied for constant pillar diameter of $40 \mu\text{m}$. Since the diameter is kept constant, the pressure remains the same but the voltage increases since the film thickness that generates the potential difference increases. The fiber length is kept constant at $120 \mu\text{m}$. The thickness versus the voltage output graph is given in Figure 5.3.

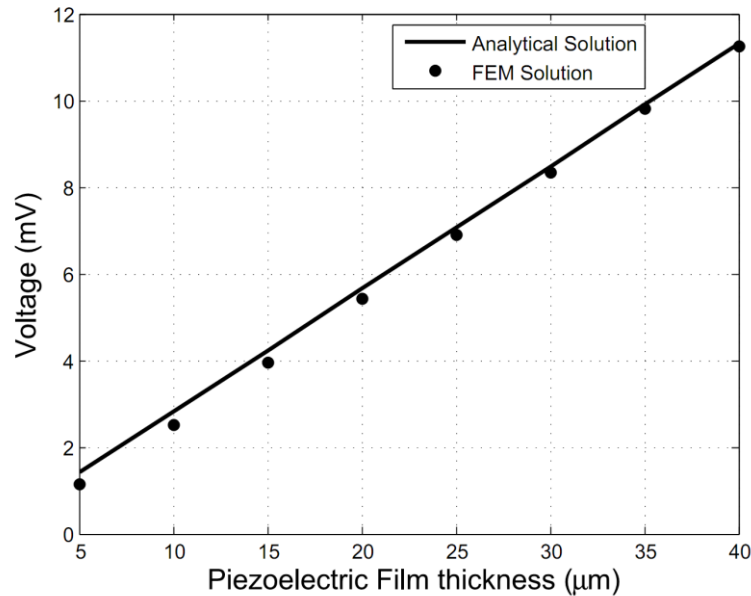


Figure 5.3: Thickness of Piezoelectric Film versus Voltage Graph for 1 kPa Upper Surface Pressure

As can be seen from Figure 5.3 the FEM solution differs from the ideal analytical solution as the piezoelectric film thickness reduces. The error analysis has been carried out for different meshing sizes of 1 μm , 5 μm and 10 μm . The percent error for piezoelectric film thickness of 25 μm reduces below 3-4 percent. The meshing element size for the dimensional analysis of single pillar has been chosen to be 5 μm .

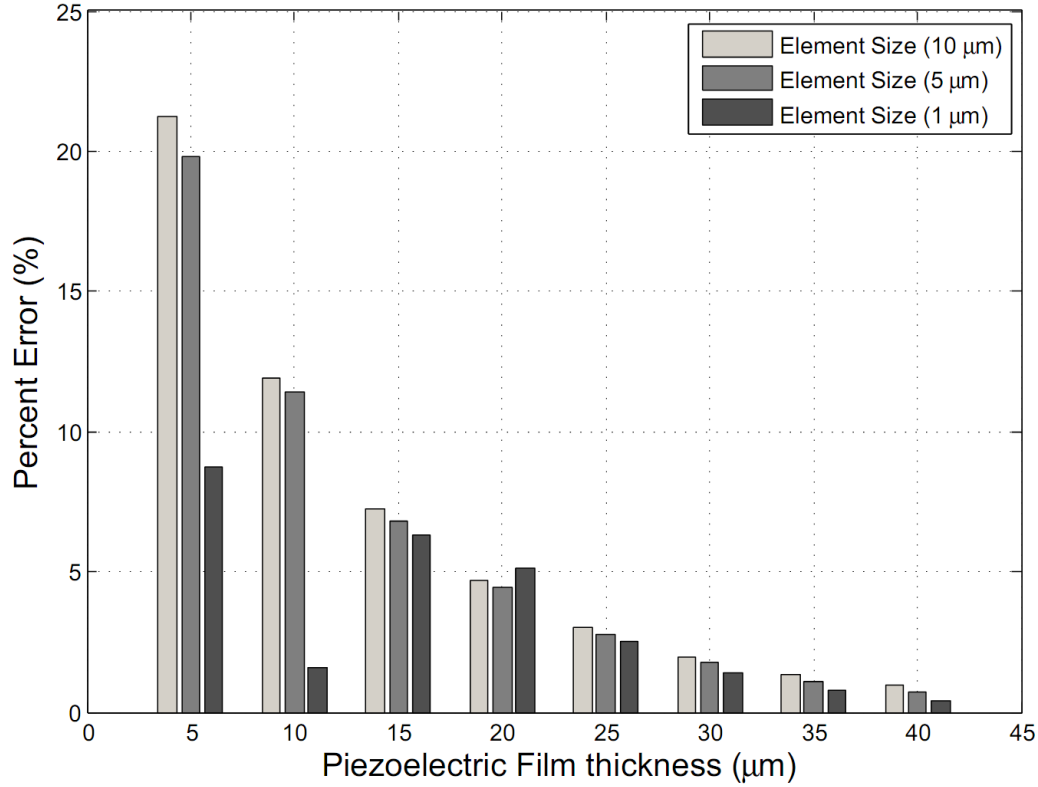


Figure 5.4: Percent Error for Different Meshing Sizes

5.1.1.3 Diameter-voltage

The diameter of the fiber is also an important parameter in the design process of the fibers. The diameter values are also varied and the resultant voltage values are drawn in Figure 5.5. The diameter is inversely proportional to the stress concentration since it increases the pillar cross sectional area reducing the pressure. The same force is transmitted by a larger area by increasing the pillar area. The increase in this area is also limited by the constraint equations of buckling and matting of fibers. Moreover, the pillar diameter should satisfy the flaw-insensitive condition. The simulations have been carried out for piezoelectric film thickness of 25 μm and fiber length of 120 μm .

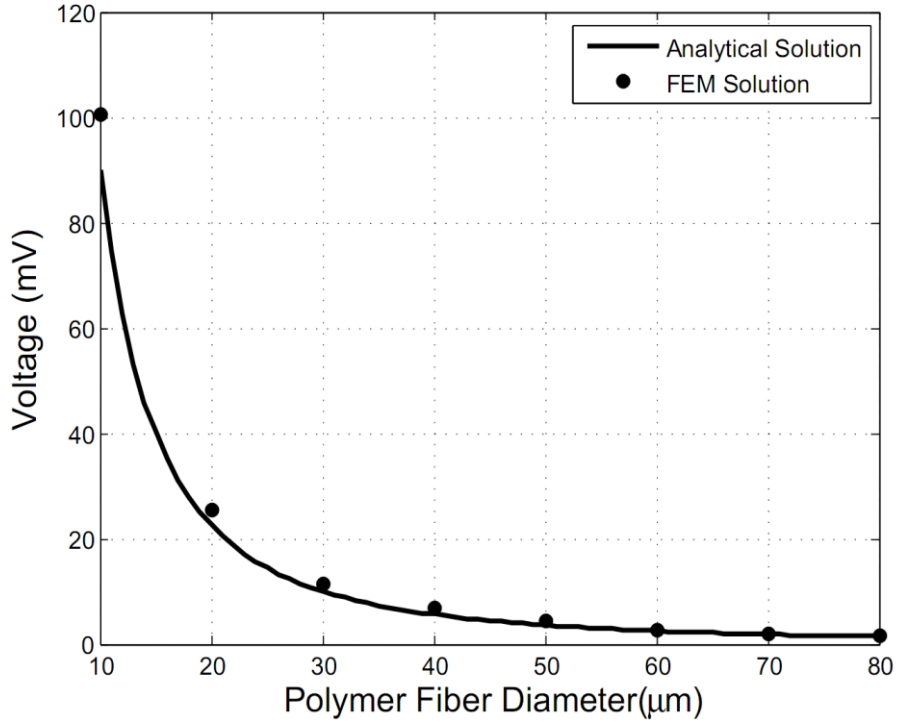


Figure 5.5: Fiber Diameter versus Voltage Graph for Single Pillar of 25 μm Piezoelectric Film Thickness

5.1.2 Actuator mode analysis

After the sensor mode has been deeply explored, the actuation capability of the sensor is also compared for different piezoelectric materials. For this purpose, PVDF polymer is compared with two ceramic piezoelectric compounds. The sensor mode comparison is given in Figure 5.6. Furthermore, the actuator capability of the same piezoelectric materials is given in Figure 5.7.

The stiffness change of the beam is also calculated by the simple beam equation given by,

$$\Delta x = \frac{F_x l}{4E\Delta y^2} \quad (5.2)$$

The stiffness is the ratio of applied force to the displacement which reduces the Equation 5.2 to

$$k_x = \frac{4E\Delta y^2}{l} \quad (5.3)$$

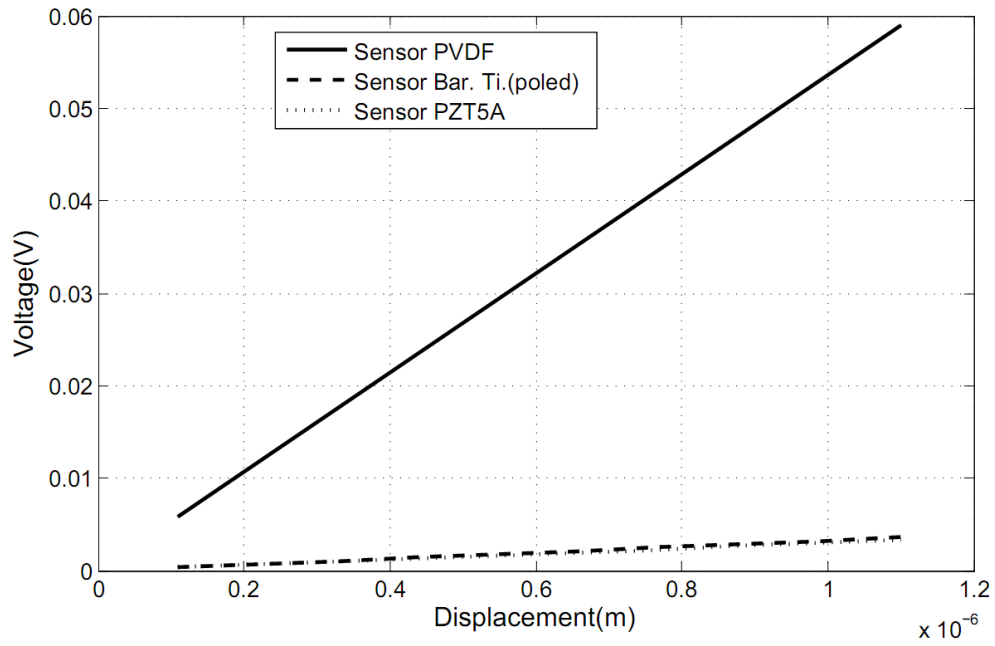


Figure 5.6: Sensor Mode Comparison of Piezoelectric Materials

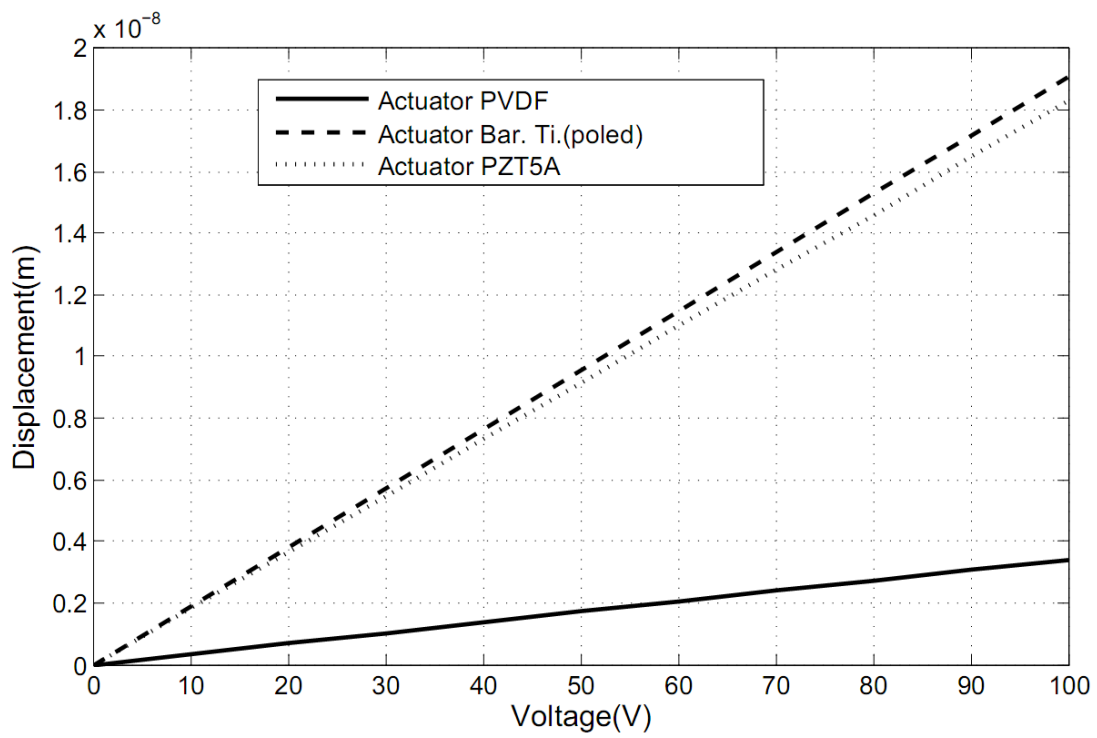


Figure 5.7: Actuator Mode Comparison of Piezoelectric Materials

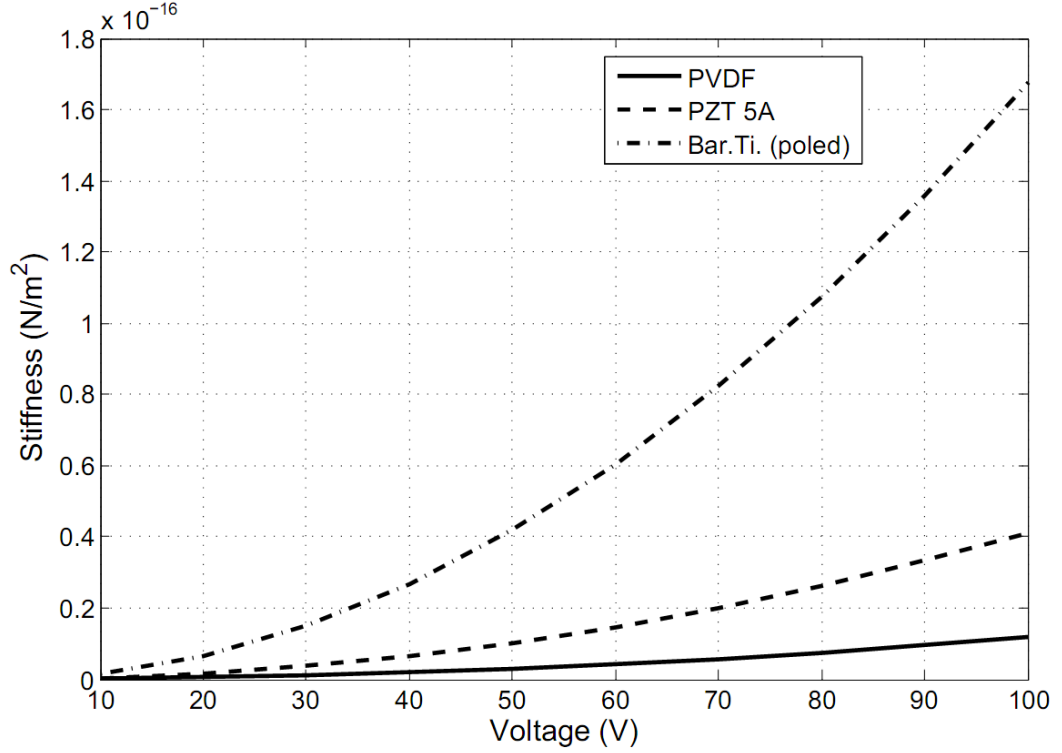


Figure 5.8: Stiffness Change of Piezoelectric Materials

5.2 Static Fiber Array Analysis

Array of pillars are designed to give spatial pressure distribution measurement capability to the proposed model. A constant pressure value is applied on the upper surfaces of the fiber array. After the single pillar analysis has been made, an array of fibers and the interaction of adjacent fibers are analyzed. For this purpose, the following model has been used in the simulations.

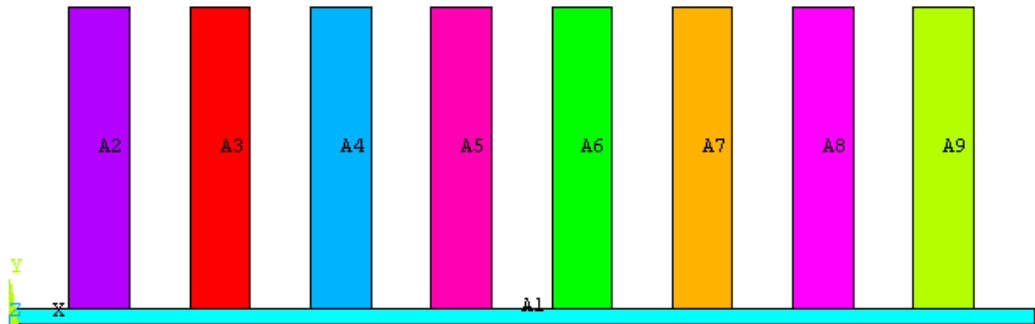


Figure 5.9: Geometry of the Fiber Array

The deformation of the fiber array is given in Figure 5.10.

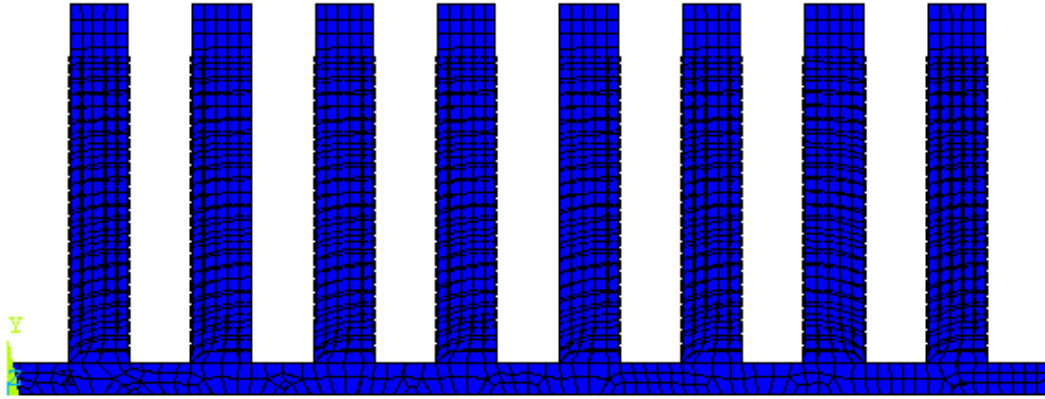
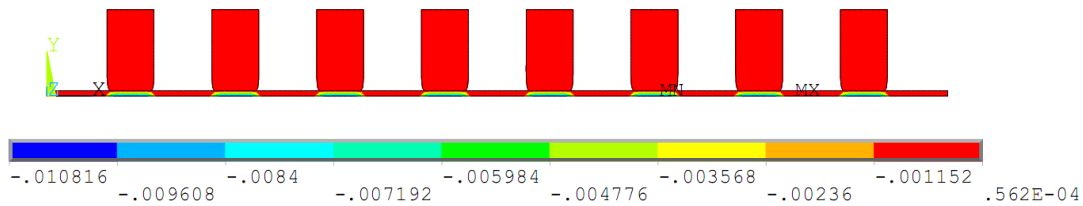


Figure 5.10: Deformation of the Fiber Array

Related with the deformation and the stress on the PVDF film, an electric potential is generated and the output voltage is collected to a signal processing unit. The distributed electrodes on the backing layer of each fiber give a finite and distinct output voltage. However, the spacing ratio (s/d) should be optimized to find the limit of the spatial resolution. Moreover, the backing layer thickness should be investigated to analyze the thickness of the backing layer as well as the cross-talk for the adjacent fibers.

5.2.1 Thickness of piezo film & coupling

The thickness of the piezoelectric film (backing layer) is needed to be tuned such that it will minimize the coupling effect of the adjacent fibers. However, minimizing the thickness will reduce the voltage output of the overall tactile sensor. Therefore, a trade off is needed. Figure 5.11 shows 5 different cases where the piezoelectric film thickness has been varied. The same amount of 10 kPa pressure has been applied on the upper surface of the pillars and the voltage output values have been plotted.



(a)

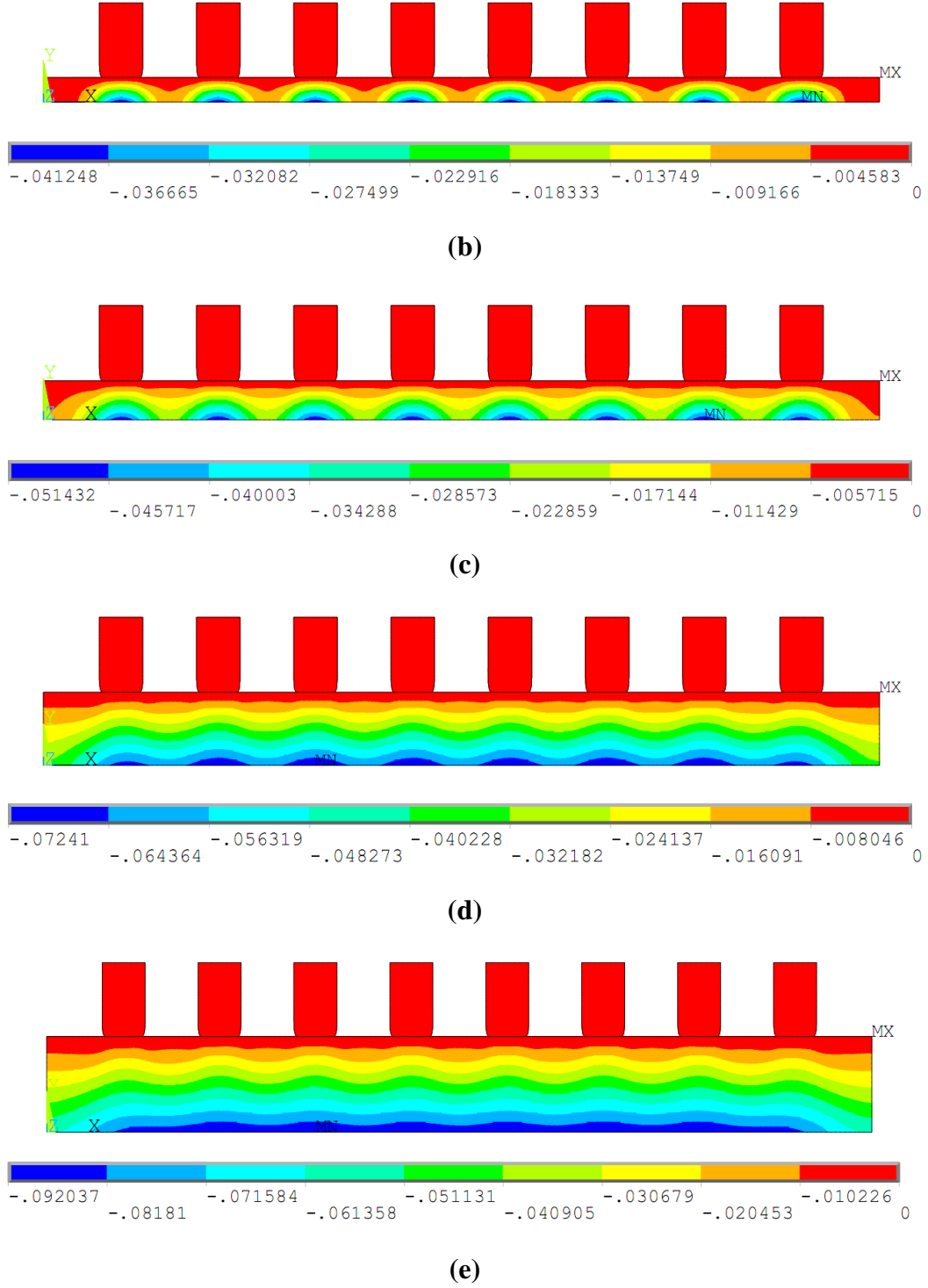


Figure 5.11: Voltage Distribution for (a) 5, (b) 25, (c) 40, (d) 75, (e) 100 μm Film Thickness

It is observed that increasing the PVDF film thickness results in a higher potential difference but on the other hand an applied pressure on a pillar generates potential difference on other pillars which leads to cross-talk between fibers. As the piezoelectric layer thickness decrease, the voltage outputs can distinctly be monitored

as in Figure 5.12. Higher backing layer thickness results with a higher output voltage value but it approaches to a simple flat film case, and patterning effect disappears.

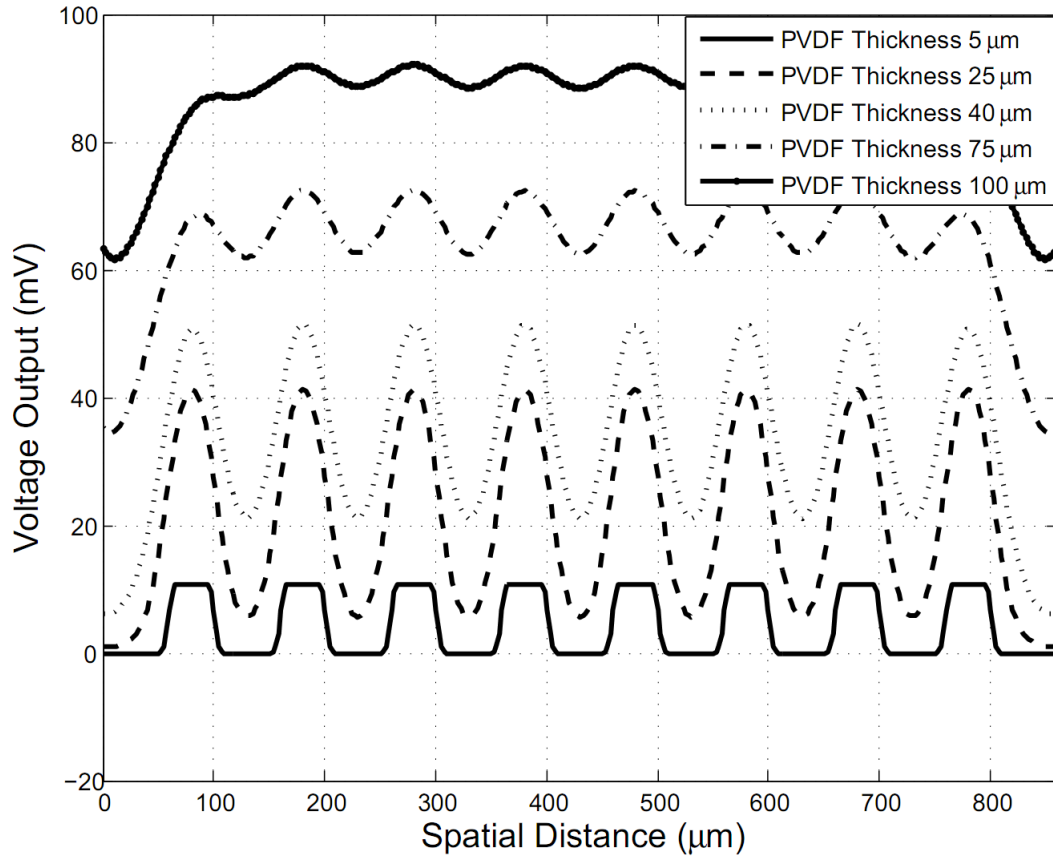


Figure 5.12: Effect of Piezoelectric Film Thickness on Voltage Output

The coupling between the fibers has been explored in terms of percent coupling of fibers. For this purpose two different nodal voltage values have been compared as given in Figure 5.13.

The percent coupling is given by the formula:

$$\% \text{ coupling} = \frac{\text{Voltage}(DP2)/2}{\text{Voltage}(DP1)} * 100 \quad (5.4)$$

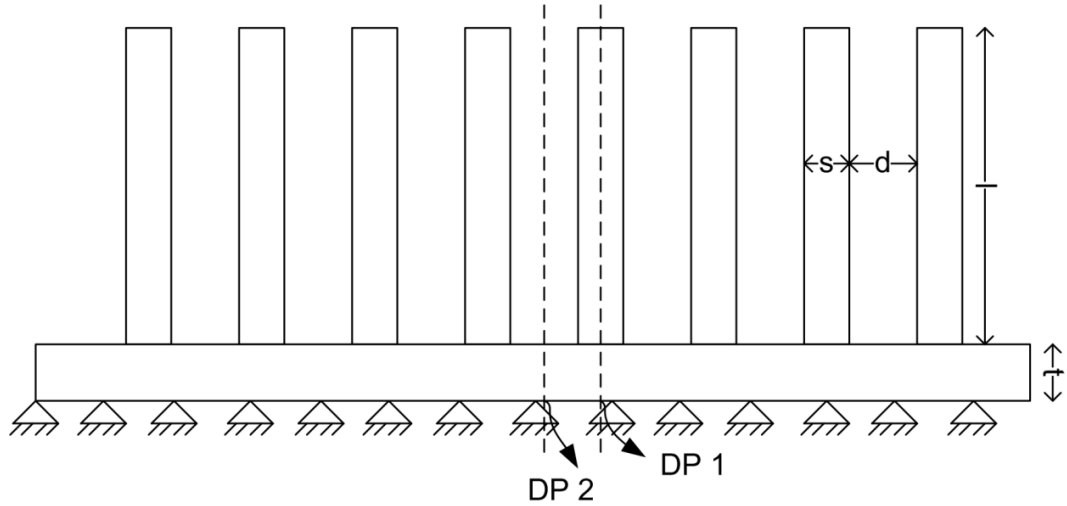


Figure 5.13: Illustration of Fiber Array for Coupling of Fibers

The voltage developed on the film free of fibers contains effects of both adjacent fibers which doubles the potential difference. Therefore the voltage of data point 2 has been divided into two and this voltage value has been compared to the voltage at data point 1. Figure 5.14 shows the percent coupling values which increases with the increasing film thickness. This validates the potential difference generation given in Figure 5.12. It converges to flat piezoelectric film case as the film thickness increases which lower the dominance of the polymer fibers.

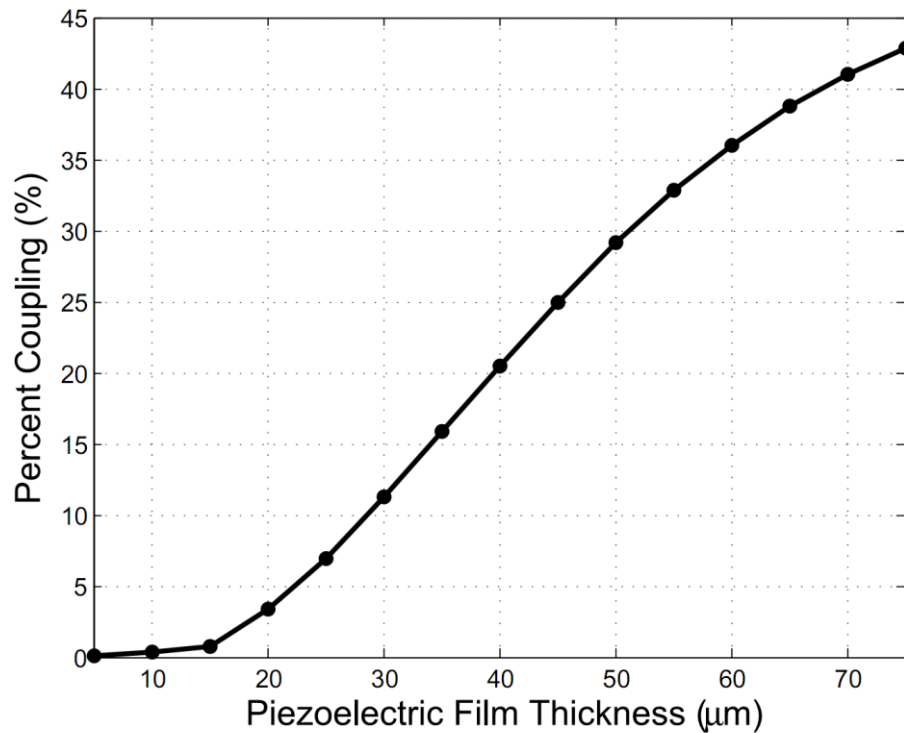
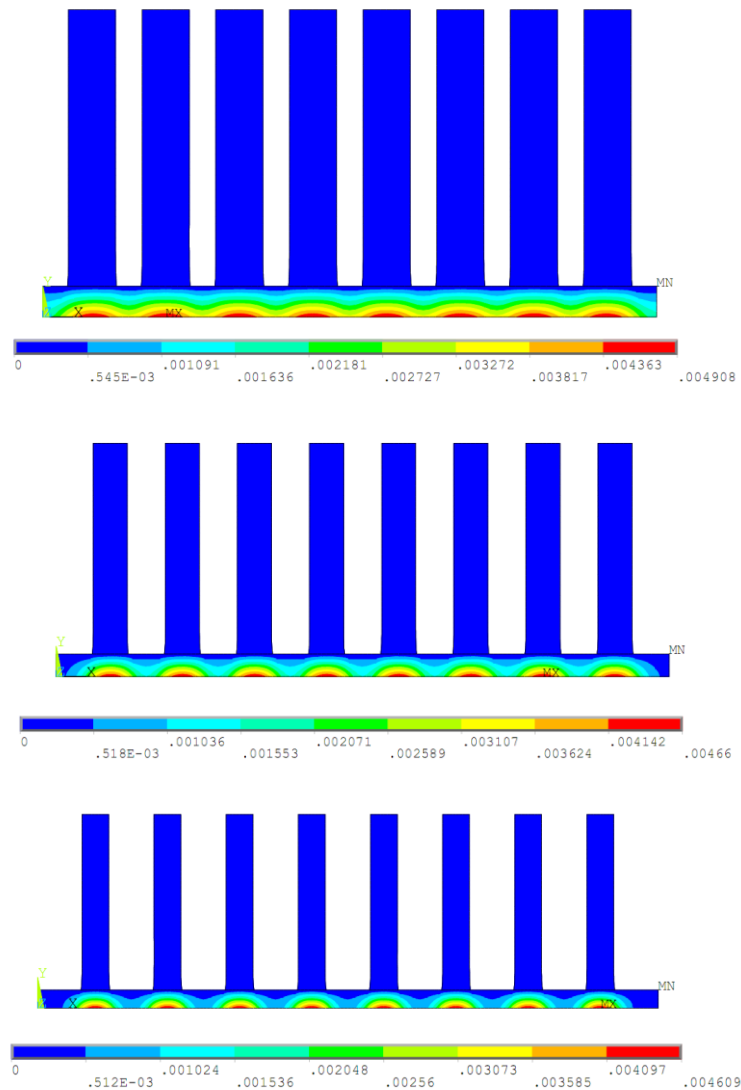


Figure 5.14: Percent Coupling of Fibers for Different Piezoelectric Film Thicknesses

5.2.2 Spacing of fibers & coupling

The spacing ratio of the fibers determines the spatial resolution of the tactile sensor. As the spacing value of two fibers decrease, the spatial resolution will increase. The maximum voltage output and the cross-talk over the fibers are strongly affected by the gap distance. Thus, it is necessary to find the minimum spacing of the fibers without coupling of the electrical signal for adjacent fibers.

The critical spacing value of fiber array is investigated in Figure 5.15 which gives the electric potential across the fiber array. These plots provide a clear representation of the cross-talk between two electrodes. As the spacing ratio of the fibers decrease, the coupling effect decreases quadratic as shown in Figure 5.16. The spacing value greater than 60 μm approximately results decoupling of each electrode, and this would be the spatial resolution limit for the proposed design.



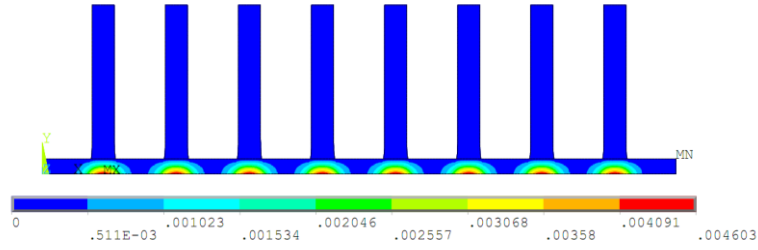


Figure 5.15: Voltage Distribution for 20, 40, 60, 80 μm Spacing

The diameter is kept constant at 40 μm and the spacing has been varied. The voltage returns to a horizontal line meaning that increasing the spacing does not affect the voltage output which further means that the fibers have been decoupled. The spacing between the fibers has been plotted by an increment of 5 μm up to 100 μm and the maximum voltage values are given in Figure 5.16.

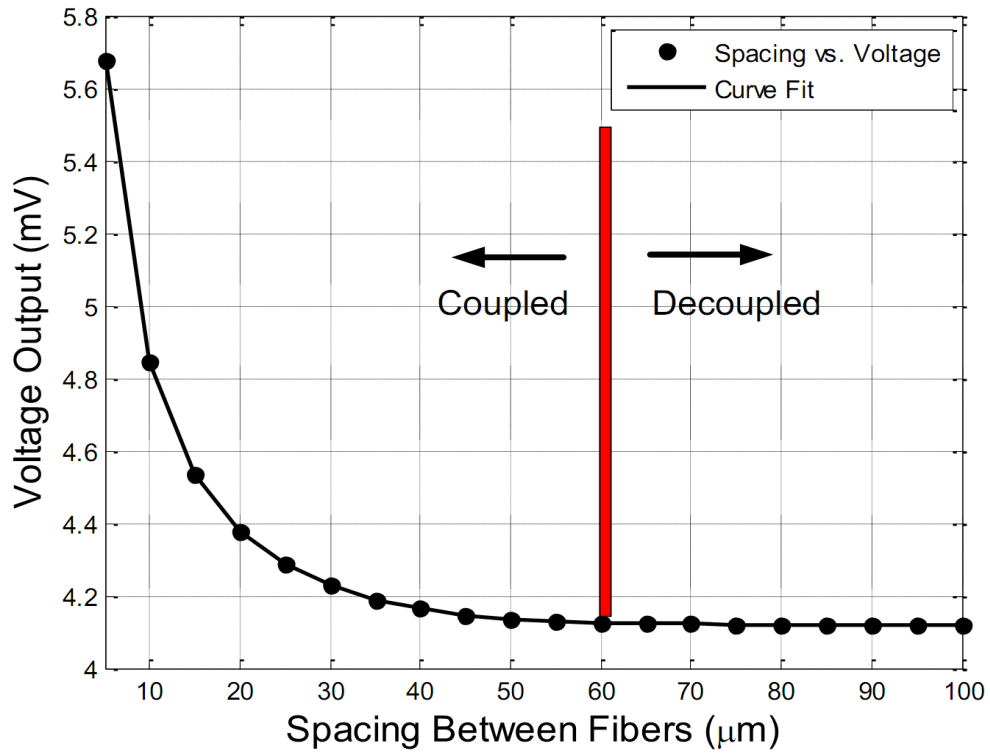


Figure 5.16: Coupling Effect Limit for Spacing Between the Fibers

As can be seen from Figure 5.16, the voltage values converges to 4.12 mV as the spacing is increased. The coupling limit is chosen to be 0.1 % of this limit. The absolute difference of the voltages have been compared and as shown in Figure 5.17, the 60 μm edge to edge spacing between the fibers results in a decoupled fiber array design.

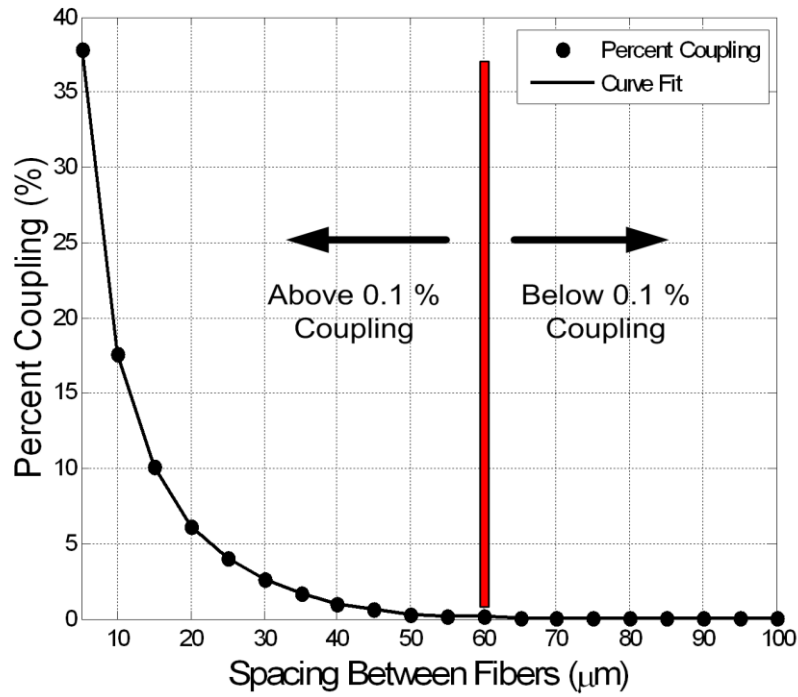


Figure 5.17: Percent Coupling for Spacing Change Between the Fibers

Furthermore, the diameter has also been included as another parameter and the voltage output for two independent variables have been plotted in Figure 5.18 with the constraining curve that limits the voltage change below 0.1 % limit.

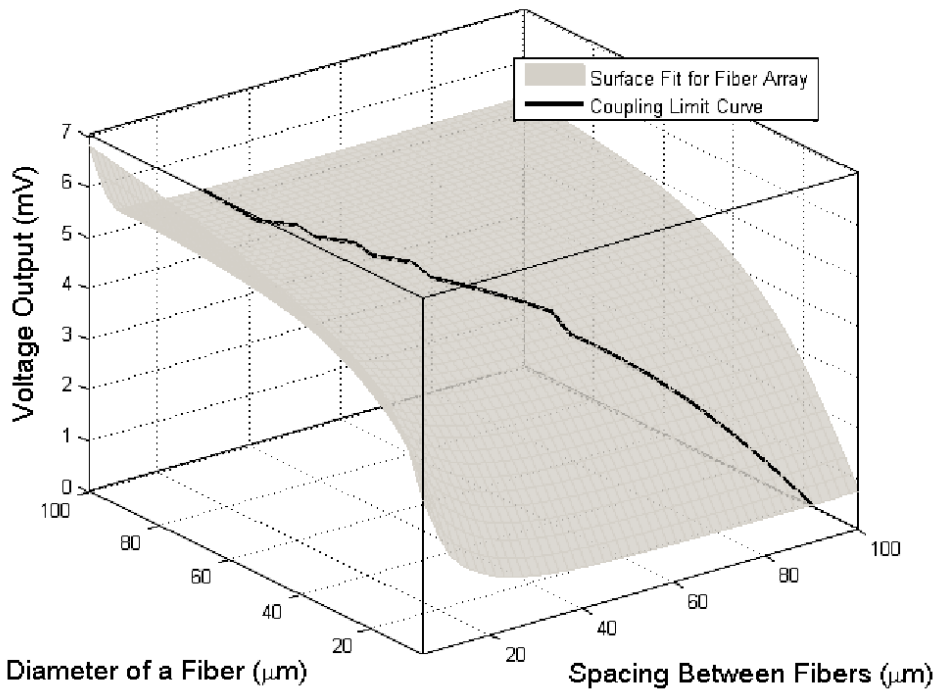


Figure 5.18: Voltage Coupling Limit for Fiber Diameter and Fiber Spacing

Figure 5.18 states that the voltage output for every diameter has a coupling limit of 0.1 for different spacing ratios. The spacing should be far enough to lower the voltage to the steady state voltage where the spacing is considered to go to infinity.

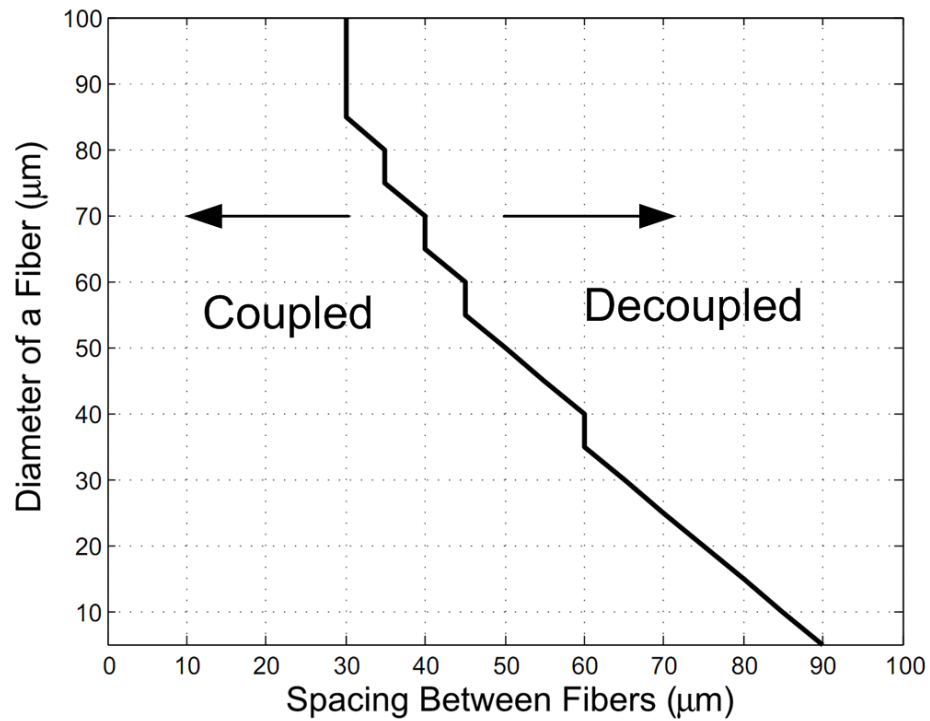


Figure 5.19 : Two Dimensional Coupling Limit Curve

6. VISCOELASTICITY OF PDMS

6.1 Viscoelastic Material Models

Viscoelasticity is the property of materials that exhibit both viscous and elastic characteristics when undergoing deformation [36]. All materials exhibit some viscoelastic response. In common metals such as steel or aluminum, as well as in quartz, at room temperature and at small strain, the behavior does not deviate much from linear elasticity. Synthetic polymers, wood, and human tissue as well as metals at high temperature display significant viscoelastic effects. In some applications, even a small viscoelastic response can be significant. To be complete, an analysis or design involving such materials must incorporate their viscoelastic behavior. Knowledge of the viscoelastic response of a material is based on measurement.

Some phenomena in viscoelastic materials are:

- if the stress is held constant, the strain increases with time (creep)
- if the strain is held constant, the stress decreases with time (relaxation)
- the effective stiffness depends on the rate of application of the load

Viscoelasticity is studied using dynamic mechanical analysis. When we apply a small oscillatory strain and measure the resulting stress.

- Purely elastic materials have stress and strain in phase, so that the response of one caused by the other is immediate.
- In purely viscous materials, strain lags stress by a 90 degree phase lag.
- Viscoelastic materials exhibit behavior somewhere in the middle of these two types of material, exhibiting some lag in strain [36].

6.1.1 Mathematical models of viscoelastic behavior

In these models springs and dashpots are used to simulate the elastic and viscous components of the stress/strain response.

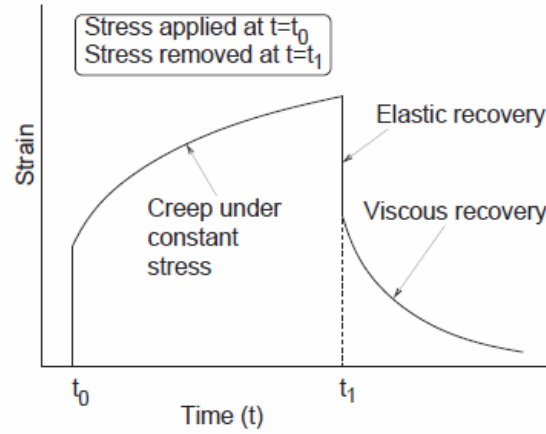


Figure 6.1: Typical Creep and Recovery [37]

The spring (elastic component of the response) obeys the relations for tensile and shear stress

$$\sigma = E \cdot \varepsilon \quad (6.1)$$

$$\tau = G \cdot \gamma \quad (6.2)$$

The dashpot (viscous component of the response) obeys the relations for tensile and shear stress

$$\sigma = \eta \cdot \dot{\varepsilon} \quad (6.3)$$

$$\tau = \mu \cdot \dot{\gamma} \quad (6.4)$$

Simple models using combinations of springs and dashpots do not correspond directly to discrete molecular structures, but they do aid in understanding how the materials will respond to stress/strain variations. In general, the more complex the model the better the experimental fit, but the greater the number of experimental constants required [38].

6.1.1.1 Maxwell model

The Maxwell model can be represented by a purely viscous damper and a purely elastic spring connected in series, as shown in the diagram.

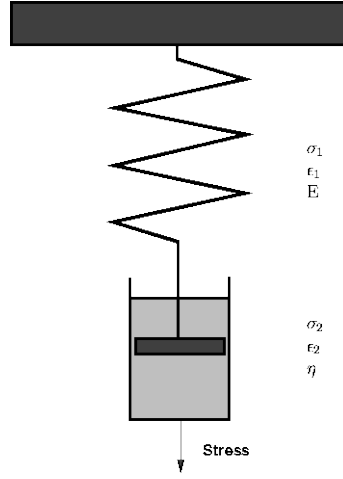


Figure 6.2: Maxwell Viscoelastic Model [39]

Strain and stress equilibrium gives,

$$\sigma = \sigma_1 = \sigma_2 \quad (6.5)$$

$$\varepsilon = \varepsilon_1 + \varepsilon_2 \quad (6.6)$$

Combining the equilibrium with the stiffness and damper equations, the governing equation for the Maxwell model can be obtained as:

$$\dot{\varepsilon} = \frac{\dot{\sigma}}{E} + \frac{\sigma}{\eta} \quad (6.7)$$

Creep

Applying a constant stress of σ , the governing equation takes the form

$$\dot{\varepsilon} = \frac{\sigma}{\eta} \quad (6.8)$$

Differentiating both sides gives

$$\int \dot{\varepsilon} = \int \frac{\sigma}{\eta} \quad (6.9)$$

$$\varepsilon(t) = \frac{\sigma}{\eta} t + C \quad (6.10)$$

Since at time zero, the strain only comes from the stiffness of the spring the constant can be found at $t=0$.

$$\varepsilon(t) = \frac{\sigma}{\eta}t + \frac{\sigma}{E} \quad (6.11)$$

Relaxation

For a constant strain

$$0 = \frac{\dot{\sigma}}{E} + \frac{\sigma}{\eta} \quad (6.12)$$

Solving the equation at $t=0$,

$$\sigma(t) = \sigma_0 e^{\left(-\frac{E}{\eta}t\right)} \quad (6.13)$$

Recovery

When the stress is removed there is instantaneous recovery of the elastic strain.

$$\varepsilon_R = \frac{\sigma}{E} \quad (6.14)$$

Under this model, if the material is put under a constant strain, the stresses gradually relax, When a material is put under a constant stress, the strain has two components. First, an elastic component occurs instantaneously, corresponding to the spring, and relaxes immediately upon release of the stress. The second is a viscous component that grows with time as long as the stress is applied. The Maxwell model predicts that stress decays exponentially with time, which is accurate for most polymers. One limitation of this model is that it does not predict creep accurately. The Maxwell model for creep or constant-stress conditions postulates that strain will increase linearly with time. However, polymers for the most part show the strain rate to be decreasing with time.

Application to soft solids: thermoplastic polymers in the vicinity of their melting temperature, fresh concrete (neglecting its ageing), numerous metals at a temperature close to their melting point.

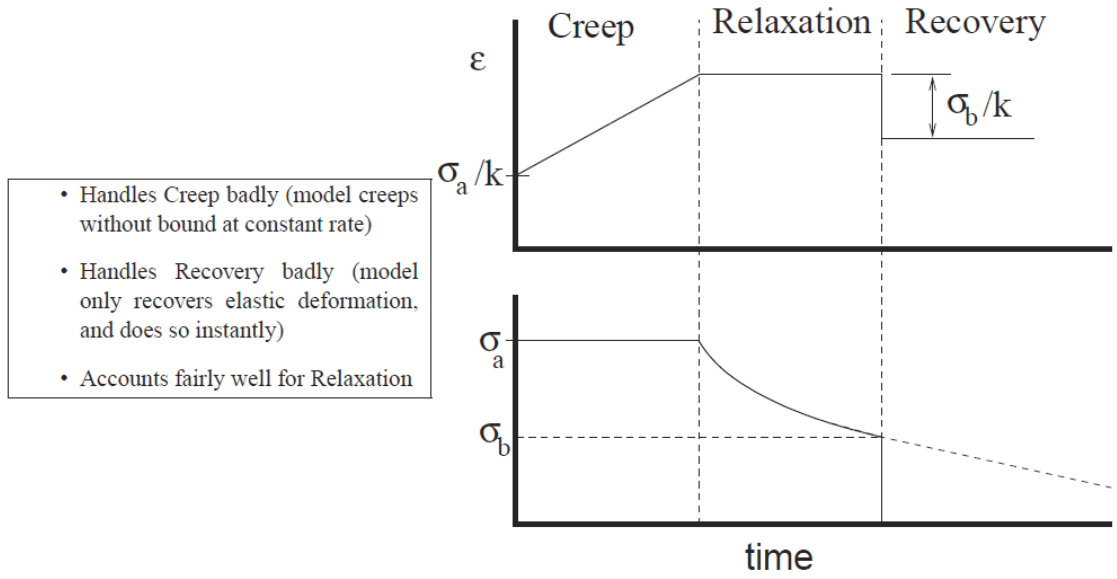


Figure 6.3 : Creep and Recovery for Maxwell Model [39]

6.1.1.2 Kelvin–Voigt model

The Kelvin–Voigt model, also known as the Voigt model, consists of a Newtonian damper and Hookean elastic spring connected in parallel, as shown in the picture. It is used to explain the creep behavior of polymers.

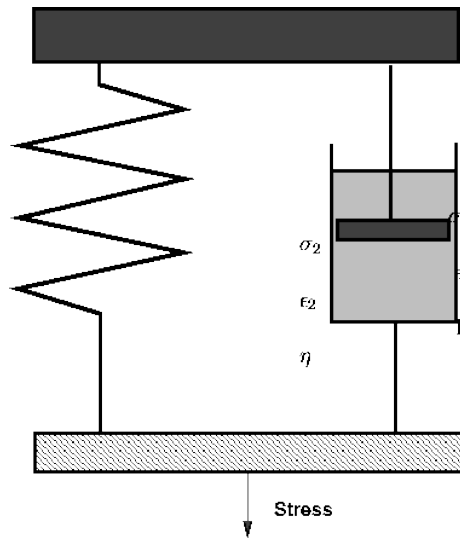


Figure 6.4: Kelvin–Voigt Viscoelastic Model [38]

Strain and stress equilibrium gives,

$$\sigma = \sigma_1 + \sigma_2 \quad (6.15)$$

$$\varepsilon = \varepsilon_1 = \varepsilon_2 \quad (6.16)$$

Combining the equilibrium with the stiffness and damper equations, the governing equation for the Kelvin-Voigt model can be obtained as:

$$\sigma = E \cdot \varepsilon + \eta \cdot \dot{\varepsilon} \quad (6.17)$$

Creep

Solving this differential equation for total strain,

$$\varepsilon(t) = \frac{\sigma}{E} \left(1 - e^{\left(-\frac{E}{\eta} t \right)} \right) \quad (6.18)$$

Relaxation

For a constant strain

$$\sigma = E \cdot \varepsilon \quad (6.19)$$

Recovery

When the stress is removed there is instantaneous recovery of the elastic strain.

$$0 = E \cdot \varepsilon + \eta \cdot \dot{\varepsilon} \quad (6.20)$$

Solving the Equation 7.20,

$$\varepsilon(t) = \varepsilon \cdot e^{\left(-\frac{E}{\eta} t \right)} \quad (6.21)$$

This model represents a solid undergoing reversible, viscoelastic strain. Upon application of a constant stress, the material deforms at a decreasing rate, asymptotically approaching the steady-state strain. When the stress is released, the material gradually relaxes to its undeformed state. At constant stress (creep), the Model is quite realistic as it predicts strain to tend to σ/E as time continues to infinity. Similar to the Maxwell model, the Kelvin–Voigt model also has limitations. The model is extremely good with modeling creep in materials, but with regards to relaxation the model is much less accurate.

Applications: organic polymers, rubber, wood when the load is not too high.

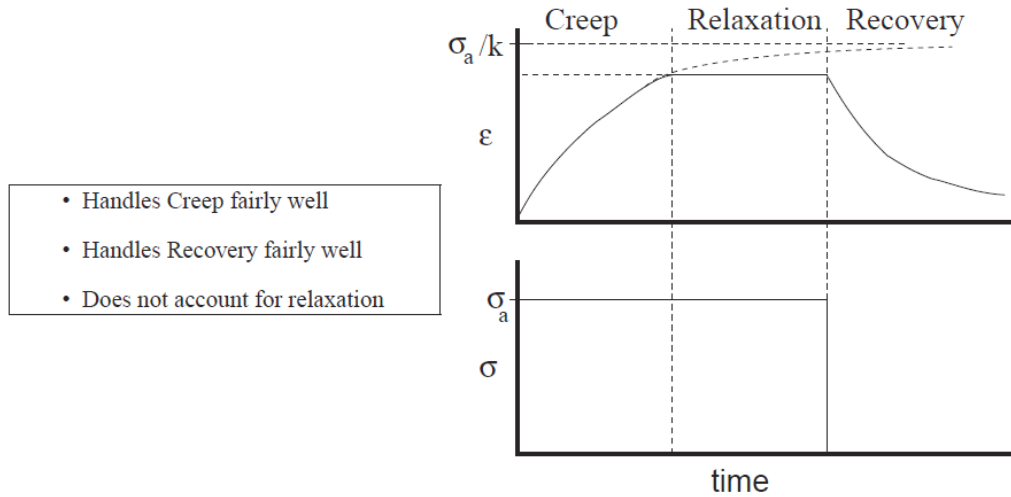


Figure 6.5 : Creep and Recovery for Kelvin–Voigt model [39]

6.1.1.3 Standard linear solid model

The Standard Linear Solid Model effectively combines the Maxwell Model and a Hookean spring in parallel. A viscous material is modeled as a spring and a dashpot in series with each other, both of which are in parallel with a lone spring.

$$\dot{\epsilon} = \frac{\frac{E_2}{\eta} \left(\frac{\eta}{E_2} \dot{\sigma} + \sigma - E_1 \epsilon \right)}{E_1 + E_2} \quad (6.22)$$

Under a constant stress, the modeled material will instantaneously deform to some strain, which is the elastic portion of the strain, and after that it will continue to deform and asymptotically approach a steady-state strain. This last portion is the viscous part of the strain. Although the Standard Linear Solid Model is more accurate than the Maxwell and Kelvin-Voigt models in predicting material responses, mathematically it returns inaccurate results for strain under specific loading conditions and is rather difficult to calculate.

- Exhibits the following behavior:
 - Instantaneous elastic strain when stress applied
 - Under constant stress, strain creeps towards a limit
 - Under constant strain, stress relaxes towards a limit

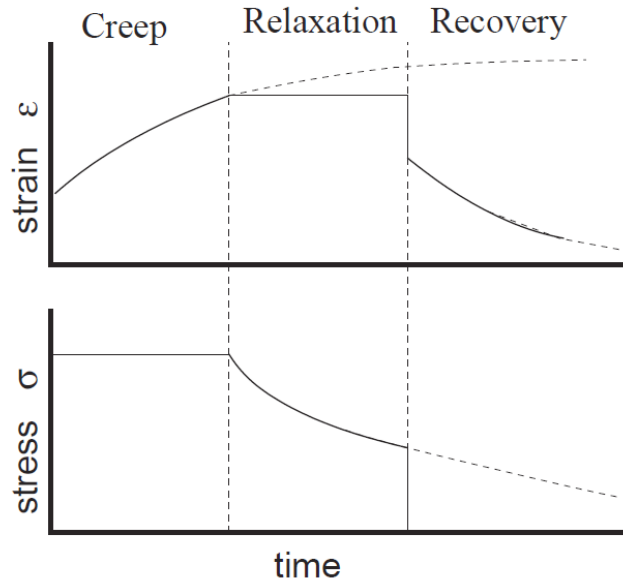


Figure 6.6 : Creep and Recovery for standard linear solid model [39]

- When stress is removed, instantaneous elastic recover, followed by gradual recovery towards zero strain.
- Two time-constants:
 - * One for creep/recovery under constant stress
 - * One for relaxation under constant strain

6.1.1.4 Generalized Maxwell model

The Generalized Maxwell also known as the Maxwell-Weichert model is the most general form of the models described above. It takes into account that relaxation does not occur at a single time, but at a distribution of times. Due to molecular segments of different lengths with shorter ones contributing less than longer ones, there is a varying time distribution. The Weichert model shows this by having as many spring-dashpot Maxwell elements as are necessary to accurately represent the distribution. The Figure 6.7 represents a possible Wiechert model.

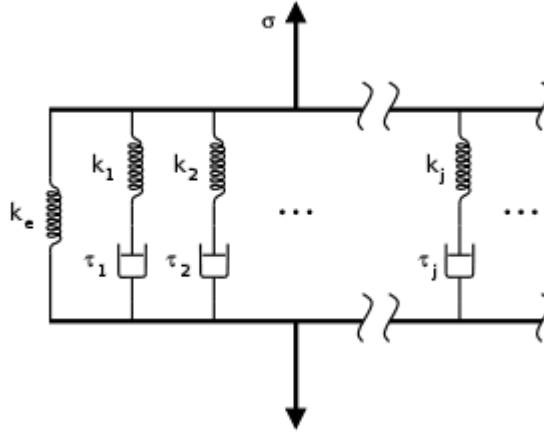


Figure 6.7 : Generalized Maxwell Model [36]

Applications: metals and alloys at temperatures lower than one quarter of their absolute melting temperature.

6.2 Experimental Work

PDMS was used to model as an elastic material in the analyses. In reality, the PDMS polymer not only acts as an elastic material but also has a viscous property, which means that the behavior of the material against a disturbance, changes with time. Therefore, for a more accurate analysis the fiber should be modeled as a viscoelastic material which is described by a generalized Maxwell model [40]. Moreover, the relaxation function of the model was extracted in which the modulus of elasticity is given by Prony Series [41]. Therefore, the creep and relaxation behavior of the material can be obtained. Indentation test has been carried out for this purpose. The indentation test set up is given in Figure 6.8.

In the evaluation of the modulus of elasticity for PDMS, different mixing ratios of Sylgard 184 (Dow Corning) have been prepared and indentation test has been applied on the prepared specimen. The following formula from contact mechanics has been used in the calculation process [42]:

$$E^* = \frac{E}{1 - \nu^2} = \frac{P}{hD} \quad (6.23)$$

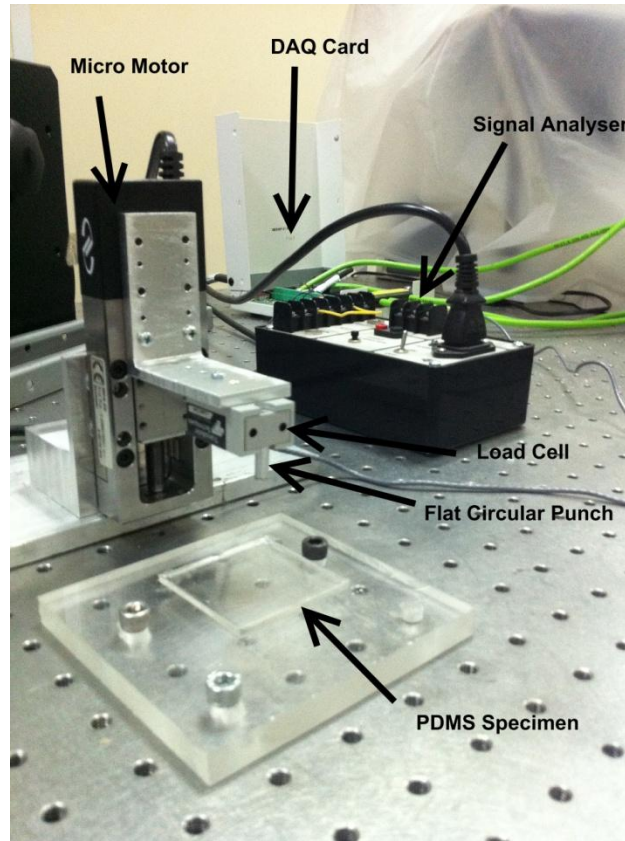


Figure 6.8: Indentation Test Set-up

where E^* is the plain strain Young's modulus, E is the modulus of elasticity, ν is Poisson's ratio, P is the load on the specimen, h is the deformation in the thickness of the PDMS and D is the diameter of the tip.

The specimen was indented by a load stem of flat circular punch which is integrated to a load cell. The micro stage motor was used to move the stem into the specimen. In the analysis, 0.25mm displacement was given by the stage and the force was measured as a voltage output from the load cell. The output voltage was fed to a data acquisition board via a signal analyzer. The basic illustration of the indentation experiment is given in Figure 6.9.

The experiments have been carried out by a micro stage motor and a load cell attached to it. The micro stage motor is utilized in the vertical adjustment and the load cell is used in the gathering of the force data. The load cell is indented into the specimen by a load stem attached on it which has a diameter of 4.4 mm.

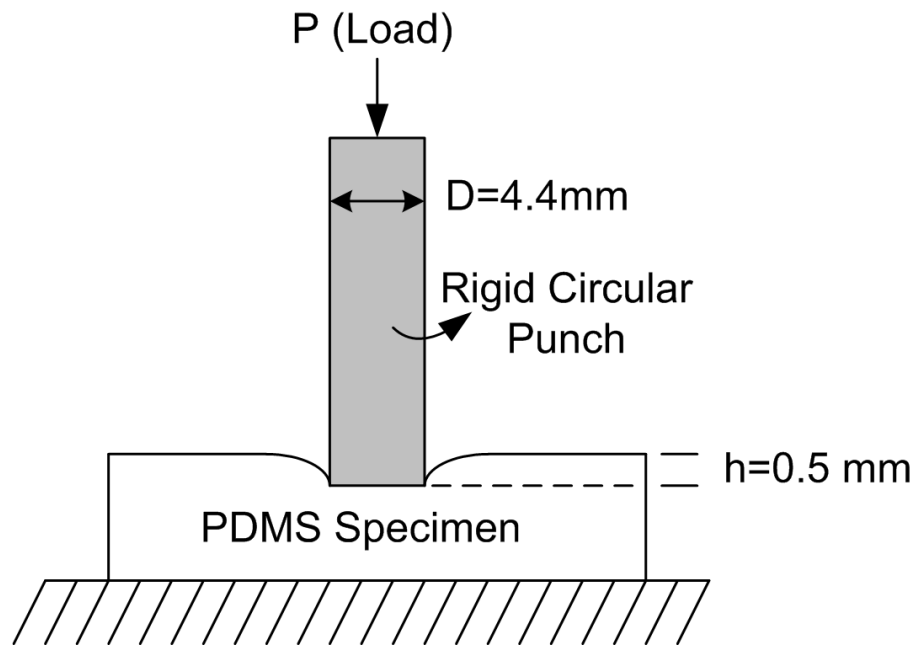


Figure 6.9: Illustration of Indentation into PDMS Polymer

The load cell creates an electrical signal proportional to the load on it and the analog voltage output is fed to a PC via a data acquisition card. The voltage output data from the load cell is converted into load by a calibration constant of the load cell. In the analysis a 250 gr load cell is used with a calibration constant of 0.7255 V/N. The force data for different mixing ratios is plotted in Figure 6.10.

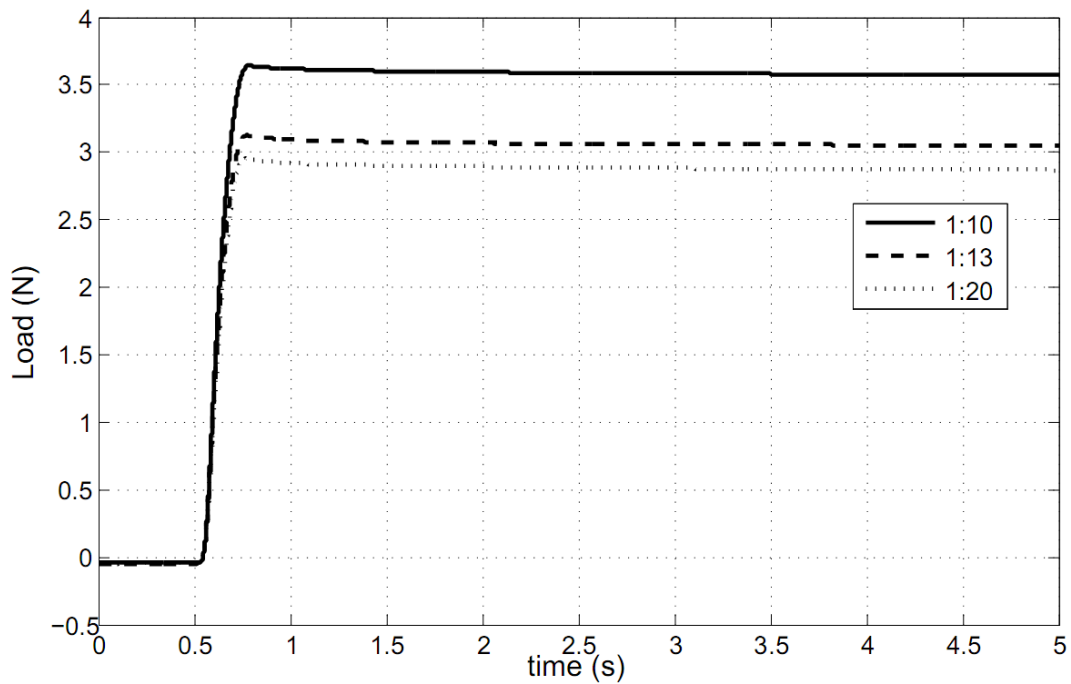


Figure 6.10: Force Data of Indentation Experiments

Moreover, the Poisson's ratio is taken as 0.5 [43]. The force and the displacement data is collected at the loading curve and the slope of P/h is taken in the evaluation of the Young's modulus. For this purpose two points on the loading curve are selected and the modulus of elasticity is calculated by the Equation 7.23. Three different mixing ratios are prepared with A-B ratios of 1:10, 1:13, 1:20 with total masses of 3.56, 3.87 and 4.81 grams. Those three specimens have been examined and Young's modulus of 1.88 MPa, 1.65 MPa and 1.45 MPa are found, respectively.

The relaxation curve gives the time dependent behavior of the modulus of elasticity. The relaxation-time experimental data is first filtered and then fitted to a Prony series which is given as:

$$E(t) = E_0 \left(1 - \sum_{i=1}^N a_i \left(1 - e^{-\frac{t}{\tau_i}} \right) \right) \quad (6.24)$$

a_i and τ_i are coefficients are experimentally obtained material parameters. Two set of coefficients from time series representation of elasticity are chosen in order to introduce the viscoelasticity. Change of elasticity in time with selected experimentally obtained coefficients is represented in Table 6.1.

Table 6.1: Prony Series Coefficients

Mixing Ratio (A:B)	a_1	a_2	τ_1	τ_2
1:10	0.008206	0.01386	0.1945	2.403
1:13	0.01251	0.01355	0.1588	1.686
1:20	0.01219	0.01913	0.2247	2.581

The relaxation curves for different mixing ratios are filtered and together with the curve fitting, are plotted in Figure 6.11.

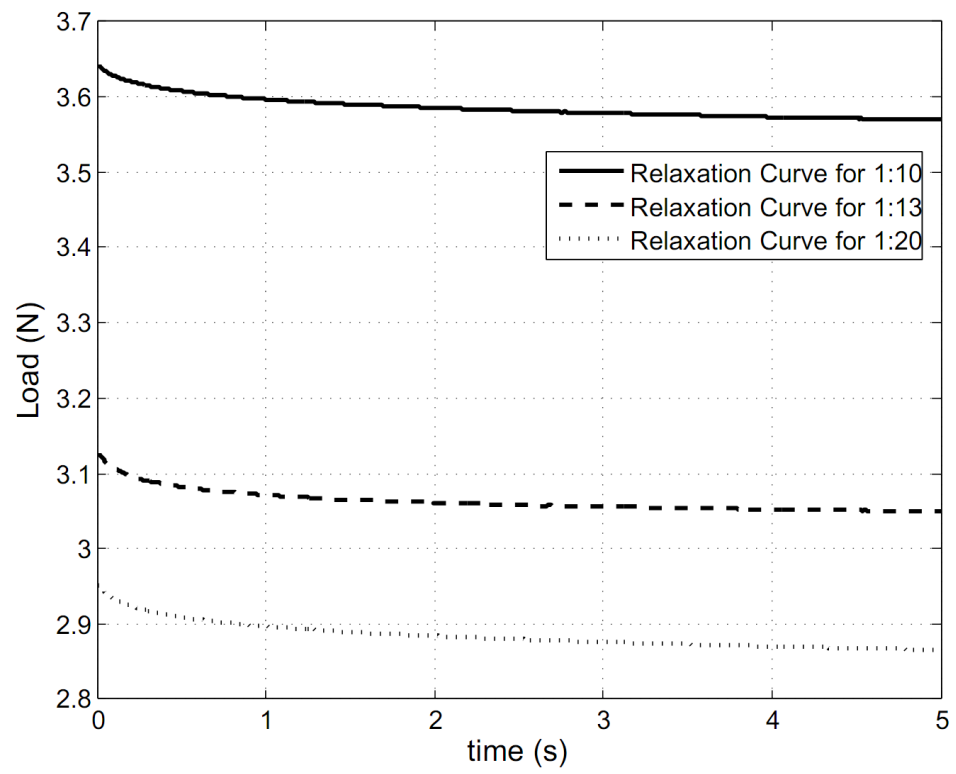


Figure 6.11: Relaxation Curves for 1:10, 1:13, 1:20 Mixing Ratios

7. DYNAMIC ANALYSIS OF THE PIEZOELECTRIC TACTILE SENSOR

7.1 Single Pillar Frequency Analysis

7.1.1 Contribution of viscoelasticity to FEM analysis

The experimental data is further compared with different material models for PDMS. The viscoelastic coefficients which are tabulated in Table 6.1 are given as an input for FEM simulations and the change in the dynamic behavior is examined.

The comparison of material models have been carried out such that the vertical displacement of the PDMS upper surface and the stress on the bottom layer of the PDMS fiber are investigated as given in Figure 7.1. Furthermore, the FFT graphs of the collected data are drawn in order to observe the contribution of every frequency to the output of the system.

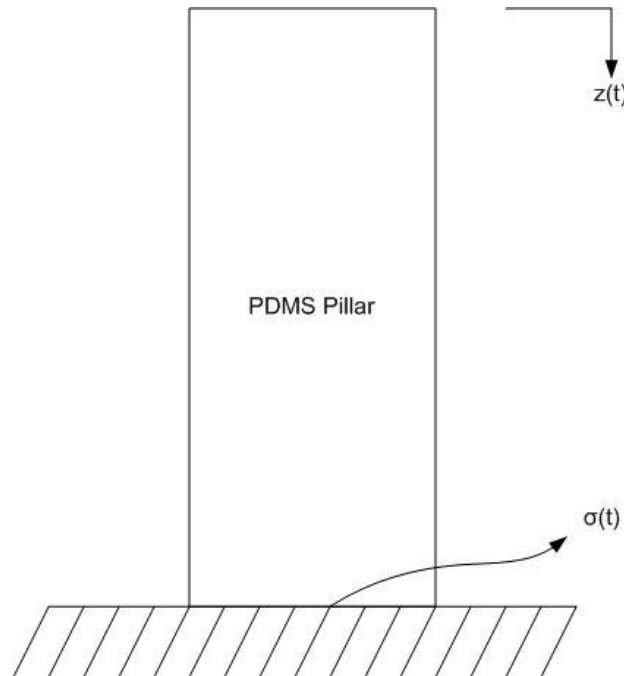


Figure 7.1 : Demonstration of the parameters for Viscoelastic PDMS Pillar

The dynamic analyses have been carried out and in frequency domain a shift in dominant frequencies of the response is observed. The comparison of viscoelastic

modeling is simulated and in order to have a rich set of data, an impulsive force is given as an input and the displacement and the stress values are given as a function of time.

Furthermore, the output of Figure 7.2 is examined in frequency domain in order to reveal the shift of the dominant frequencies. For the principle natural frequency, the value is not much different but as the natural frequency increases there exists a delay in the frequency curve. This is demonstrated in the FFT graph which is given in Figure 7.3.

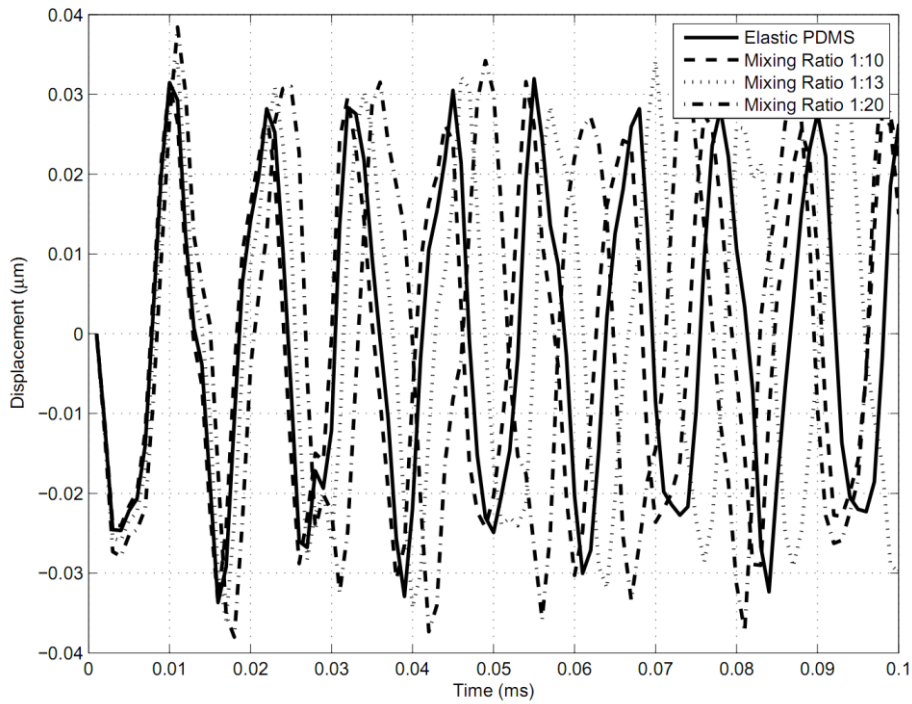


Figure 7.2: Vertical Displacement of Polymer Fiber Upper Surface

Moreover, the stress generated on the bottom surface of the PDMS pillar is also examined. The voltage output from the PVDF film is directly proportional to the stress generated on the bottom surface of the PDMS pillar. For this purpose, the contribution of viscoelasticity is examined. The comparison graph is given in Figure 7.4.

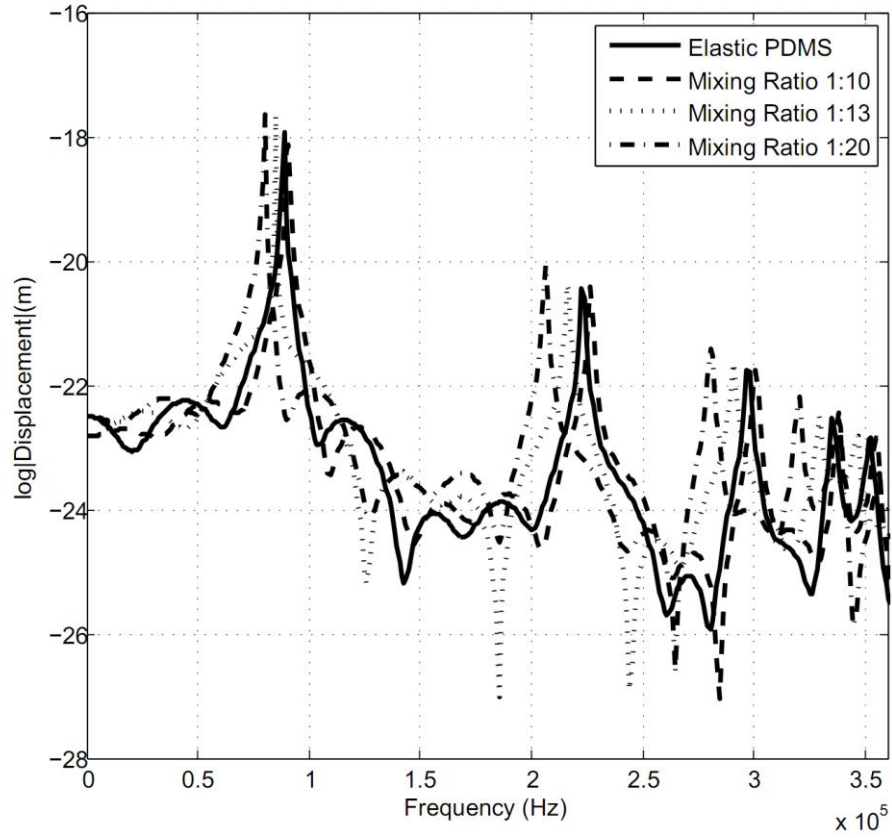


Figure 7.3: Displacement Response in Frequency Domain

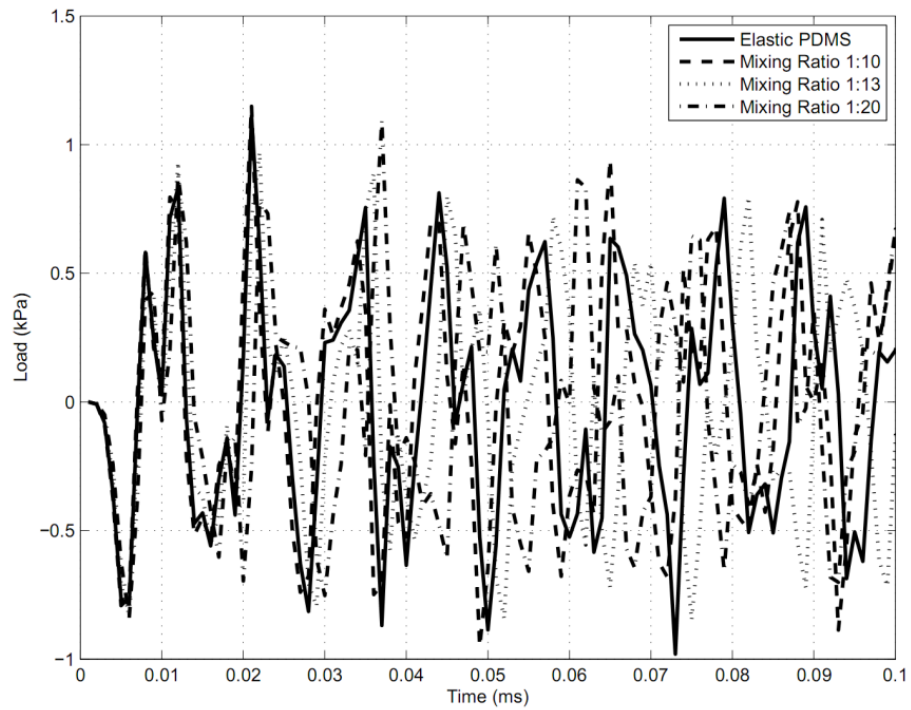


Figure 7.4: Stress Exerted to Piezoelectric Film by Polymer Fiber

The dynamic behavior of the stress on PVDF film is observed with the frequency contribution which is given in Figure 7.5.

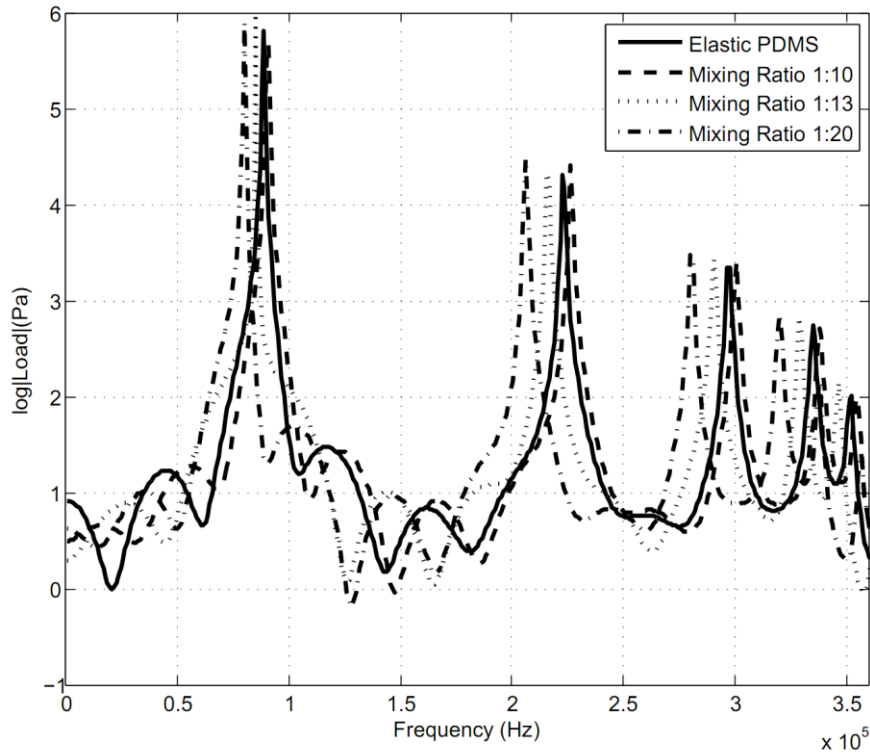


Figure 7.5: Stress Developed Response to Impulse in Frequency Domain

7.1.2 Single pillar modal analysis

The dynamic analyses have also been performed in order to observe the behavior of the tactile sensor in dynamic working environments like vibrating surfaces or to dynamic loadings where the load distribution among the upper surface of the tactile sensor changes with time. For this purpose, the single fiber is first analyzed and the modal analysis has been performed in order to get the natural frequencies of a single fiber. After the frequencies have been obtained, frequency sweep has been applied in order to observe the changes of voltage output at or near the natural frequencies and see the linearity of the output for a high frequency range of inputs. Finally, transient analysis has been performed as applying an impulsive load to the upper surface of the polymer and the displacement and the voltage output is observed in both time and frequency domains.

The single fiber dynamic analysis starts with the modal analysis where the natural frequencies can be found. The modal analysis has been performed by Block Lanczos iterative algorithm. It is the most widely used iterative method of solving the

eigenvalue problem. The eigenvalues are used in determining the natural frequencies of the system whereas the eigenvectors are used in determining the mode shapes. The Block Lanczos method is chosen since it can handle complex models of different materials and complex shapes accurately and calculate natural frequencies of first 40 very fast and accurate.

In modal analysis of ANSYS the frequencies are calculated and the results are tabulated in Table 7.1. The natural frequencies operate for longitudinal, torsion and lateral vibration modes. The frequencies have been separated in their operation mode by the eigenvector or mode shape that they correspond to.

Those natural frequency values are separated into the modes that they operate. The Table 7.1 describes which natural frequency values refer to which mode of operation. The dominant frequencies which have the lowest natural frequencies are given from 1 to 4.

Table 7.1 : Natural Frequency Distribution for Single Pillar

Frequency Number	Longitudinal (Hz)	Lateral (Hz)	Torsion (Hz)
1	90927	16103	55182
2	$2,68 \cdot 10^5$	77760	$1,65 \cdot 10^5$
3	$4,31 \cdot 10^5$	$1,74 \cdot 10^5$	$2,76 \cdot 10^5$
4	$4,99 \cdot 10^5$	$2,76 \cdot 10^5$	$3,87 \cdot 10^5$

The frequency values are also plotted in Figure 7.6 in order to get a better view and comparison for each mode of operation.

7.1.3 Single pillar harmonic response analysis

The response of a single fiber is examined for harmonic input given on the upper surface of the polymer. Figure 7.7 shows the directions and the displacement applied. The value of z_0 has been calculated as the displacement that corresponds to application of static pressure with magnitude of 10 kPa. Therefore, the analysis starts with applying a distributed load of 10 kPa and observing the vertical displacement on the upper surface of the polymer. This displacement is considered to be the maximum displacement of the harmonic input and the frequency has been swept up to 300 Hz with a step size of 10 Hz.

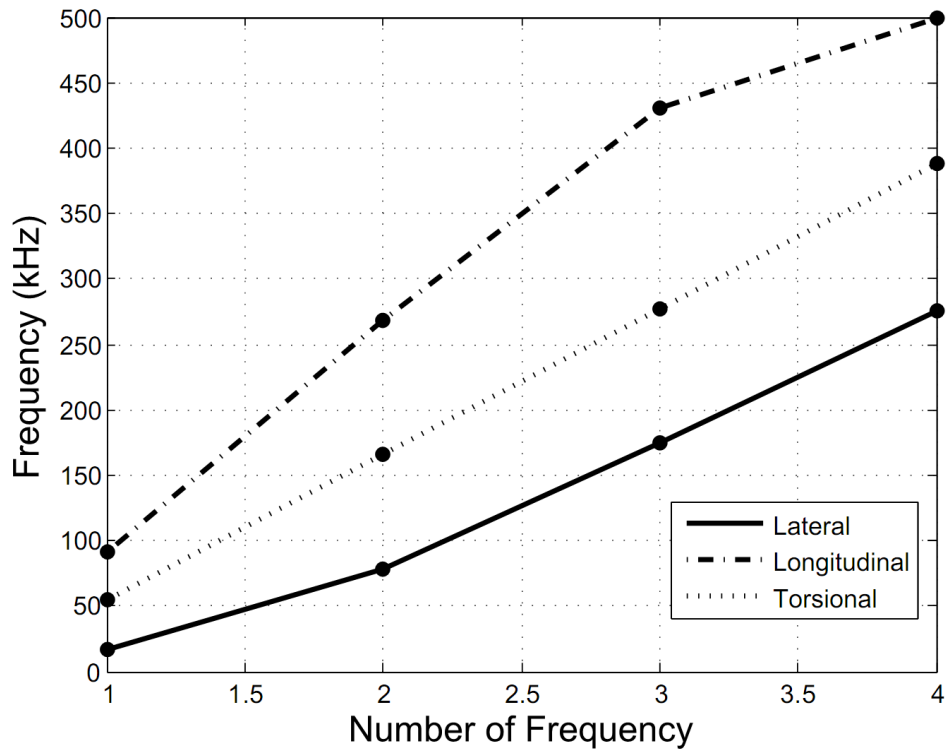


Figure 7.6: Natural Frequencies for Single Fiber

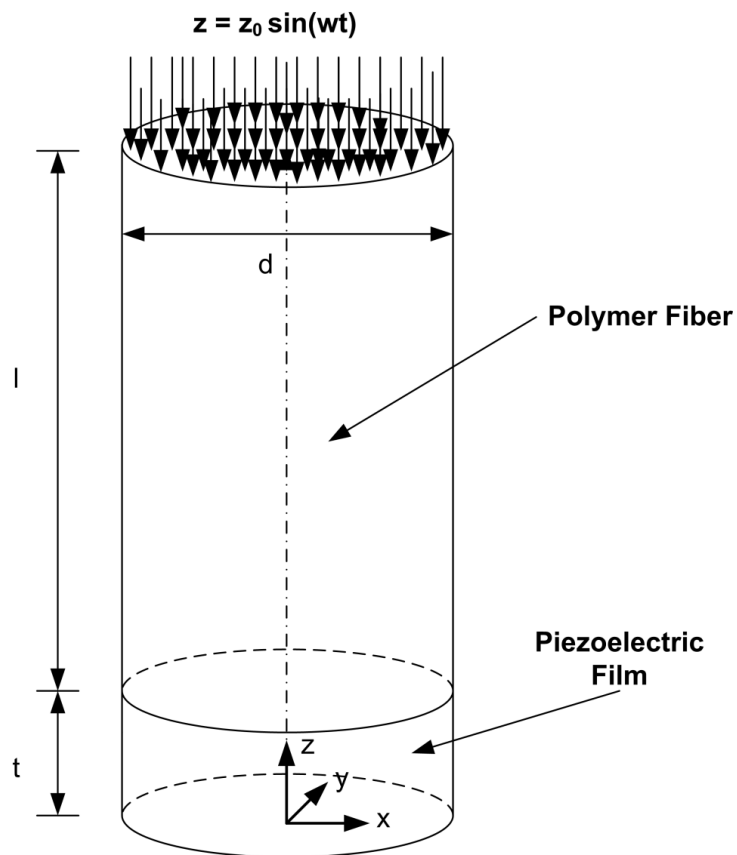


Figure 7.7: Harmonic Input for Single Fiber Analysis

The analysis of fixed magnitude and varying frequency has been developed in order to observe the linearity of the voltage output from the piezoelectric film. Figure 7.8 states that the voltage output remains almost the same as the frequency is varied meaning that the gain of the system remains the same for this frequency range.

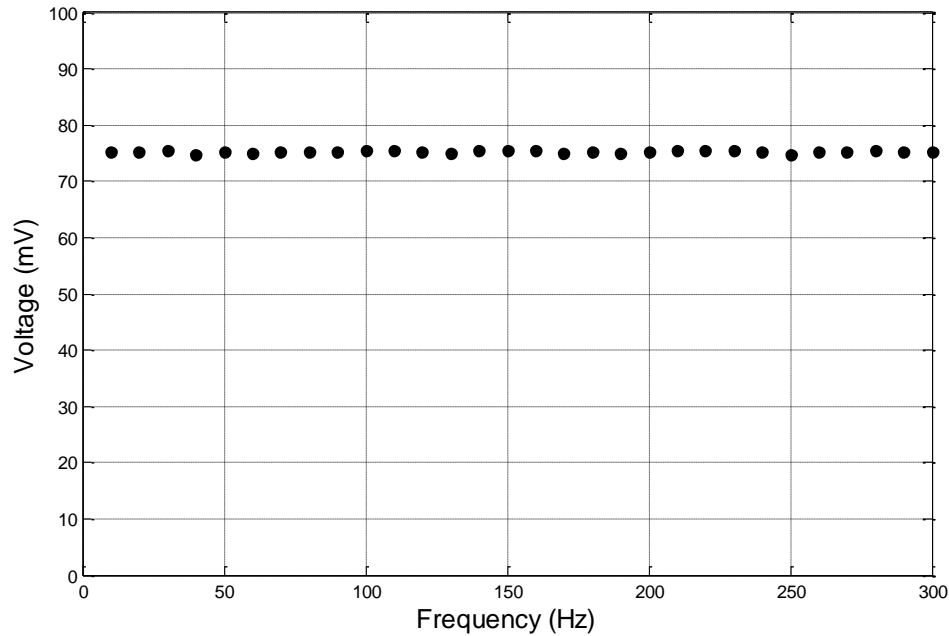


Figure 7.8: Frequency Sweep up to 300 Hz vs. Voltage Output

Furthermore, in single fiber harmonic response analysis, a sinusoidal force with a magnitude of 1 μN is applied on the center node of the upper surface of the PDMS. The applied force is swept such that it starts from a frequency of 10 kHz and goes up to 300 kHz so that the effect of every mode of vibration can be observed and the contributions to the output voltage can be determined.

Figure 7.9 illustrates the application of the harmonic analysis. The fiber is allowed to move in any direction as the force is concentrated on the center node and as the force is applied in the positive z-direction, the following displacement values are observed.

The frequency sweep in lateral direction match in frequency values meaning that it has symmetry among these directions. However the tactile sensor is designed to operate in longitudinal direction. The z-direction displacement is given in Figure 7.10 and has its own peak resonance value in longitudinal vibration mode shape.

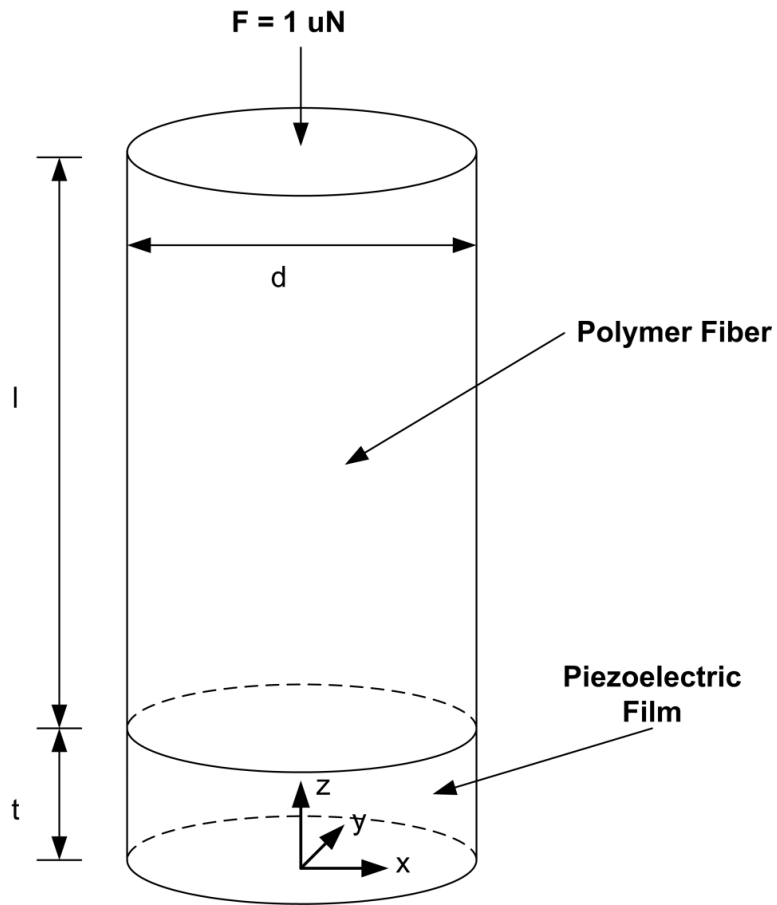


Figure 7.9: Natural Frequency Harmonic Input Sweep

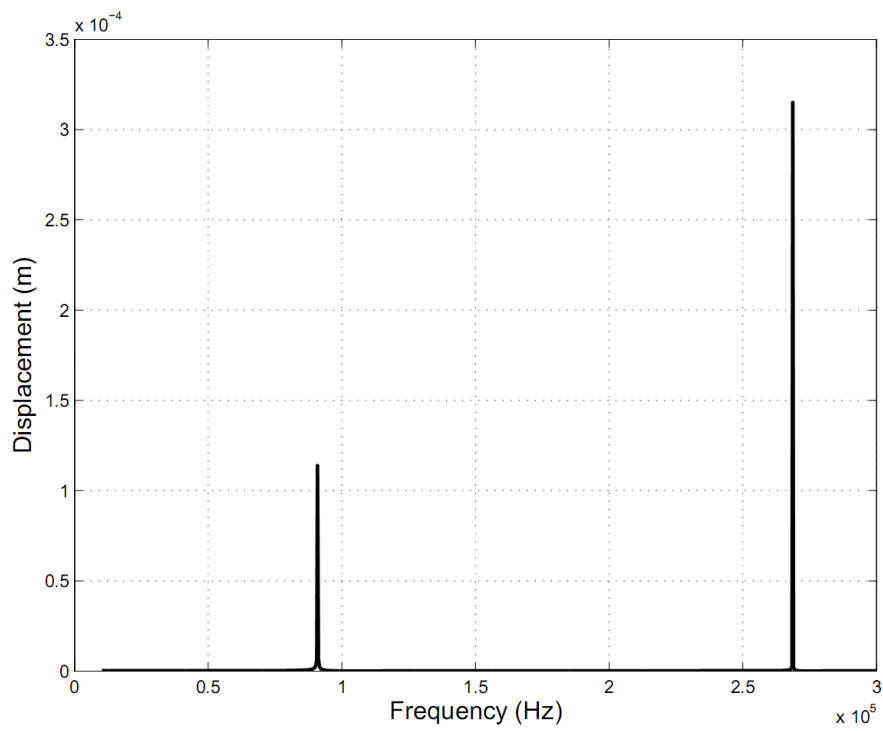


Figure 7.10: Frequency Sweep of Z-Displacement for FZ

The voltage output is directly related to the applied normal stress on the piezoelectric film therefore, the voltage graph is expected to have similarity with the z-displacement curve.

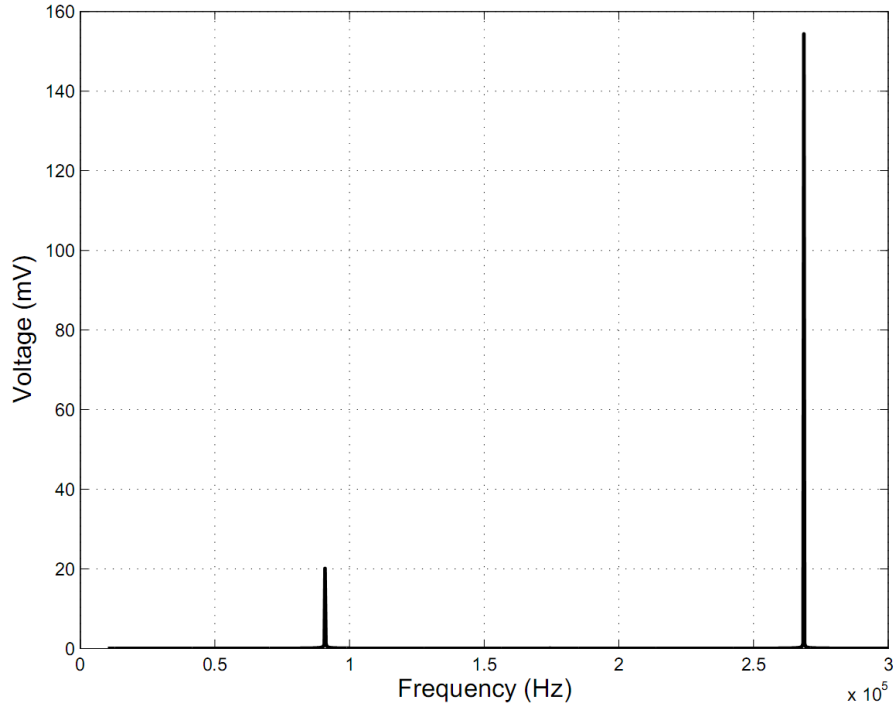


Figure 7.11: Frequency Sweep of Voltage Output for FZ

7.1.4 Single pillar transient response analysis

The frequency sweep shows that the response of the pillar to harmonic excitation makes peaks at the frequencies that match the natural frequency of the pillar. The further step will be to have an idea about the behavior of the system over time. The transient analysis is made for this purpose.

In the analysis an impulsive force input is given to the upper surface of the PDMS polymer and the responses which are the deflection on the upper surface of the PDMS and the voltage output on the bottom surface of the piezoelectric PVDF film are examined.

Since an ideal impulsive force cannot be created in reality, an approximation is made in order to create the desired force input. In this transient response analysis, a force is applied for a single sampling time period and then removed for the rest of the simulation. This way a high energy input is fed to the system in a very small amount of time and then totally removed so that the system responses freely. The simulations

have been carried out as in Figure 4.3. The simulation results reveal that the transient response is mainly affected by the first mode on the related type of loading. In the analysis, a pressure is applied on the upper surface so the longitudinal vibration is mostly considered.

The analyses have been carried out for both elastic and viscoelastic modeling of polymer. The elastic polymer analysis contains a constant elastic modulus of 1.8 MPa whereas for viscoelastic modeling the coefficients of A:B mixing ratio of 1:10 which is also given in Table 6.1 are used.

The displacement of the polymer is given in Figure 7.12. In order to have a better understanding of the system, it is transferred into frequency domain which is given in Figure 7.13.

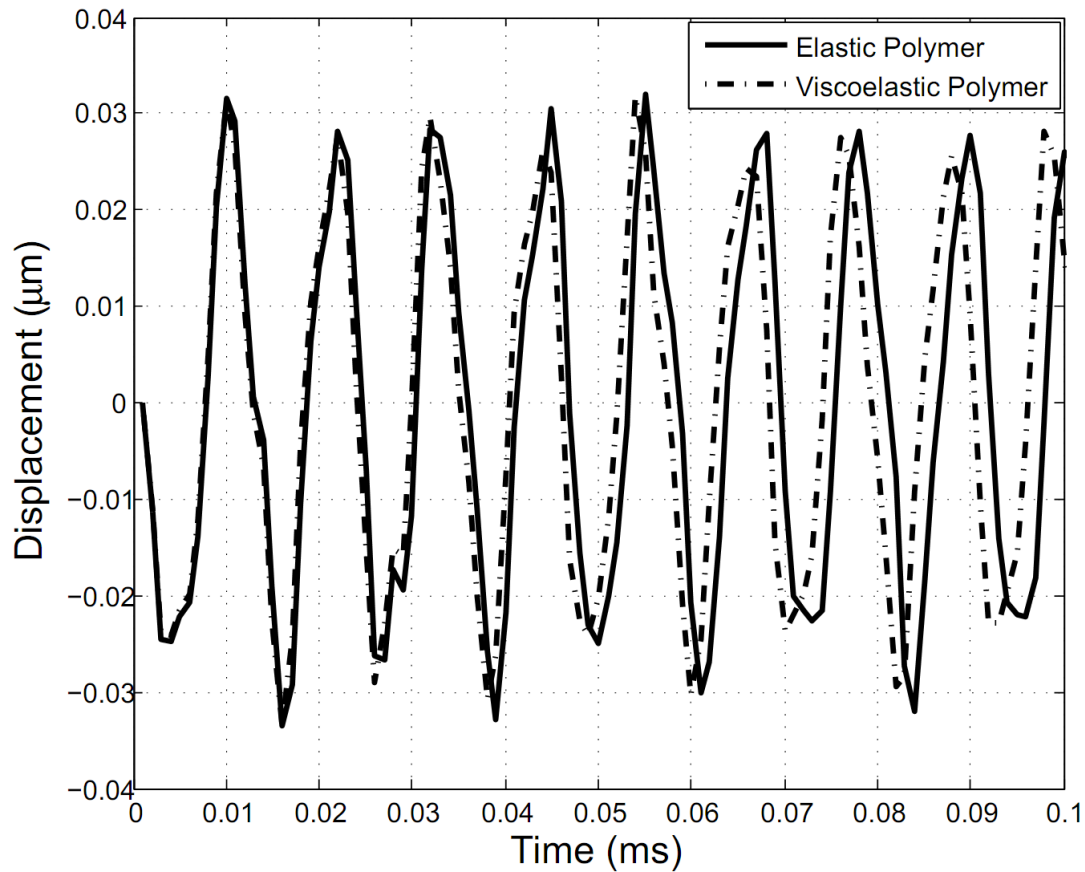


Figure 7.12: Displacement on the Upper Surface of the PDMS

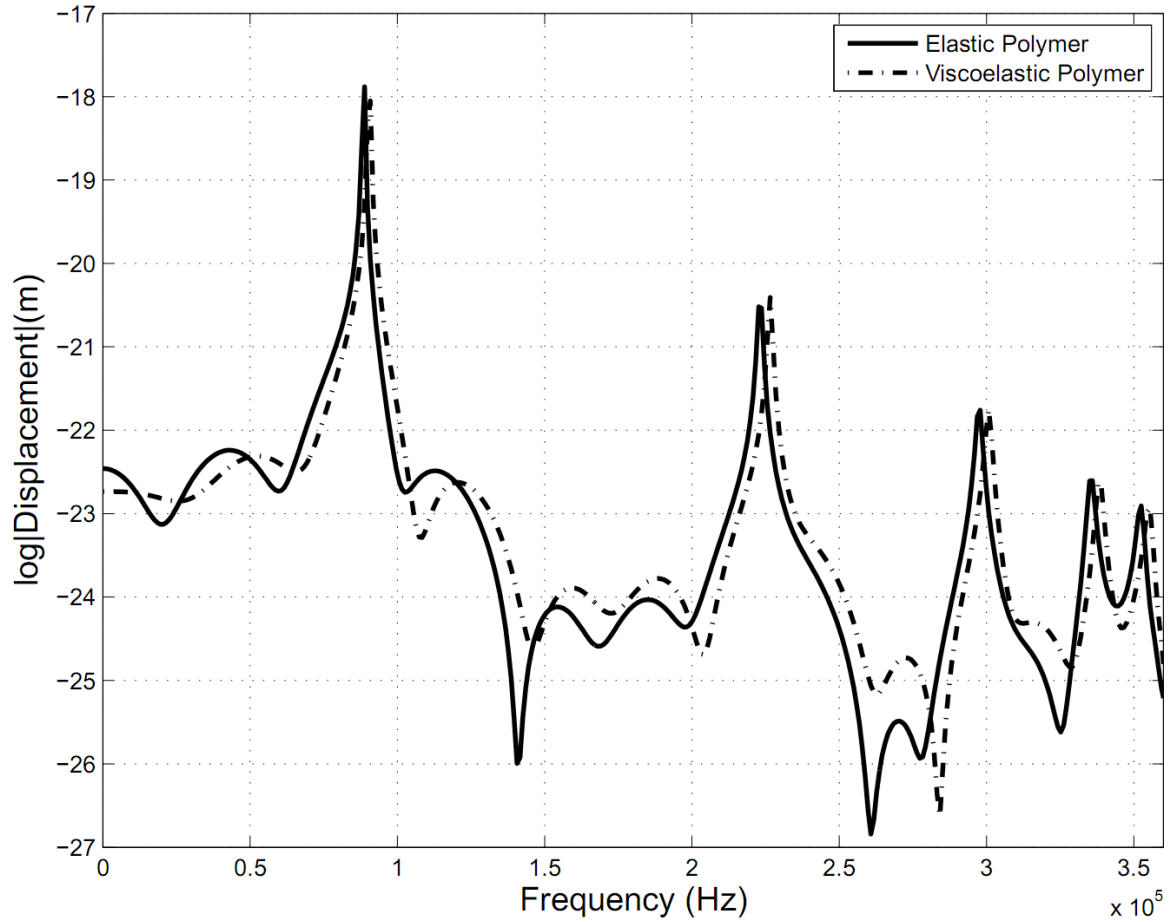


Figure 7.13: FFT of Displacement on the Upper Surface of the PDMS

In transient analysis, the voltage output is also affected by the contribution of the modes of the system. The pressure on the surface is related to the displacement on the surface and since the displacement makes peaks at the natural frequencies, the stress value changes. Furthermore, since the displacements on the surfaces of the pillars are not the same, the stress values vary resulting in a more complicated voltage output.

The voltage on the upper surface of the PVDF film is zero since it is grounded and the voltage output on the lower surface which is to be collected is given in Figure 7.14.

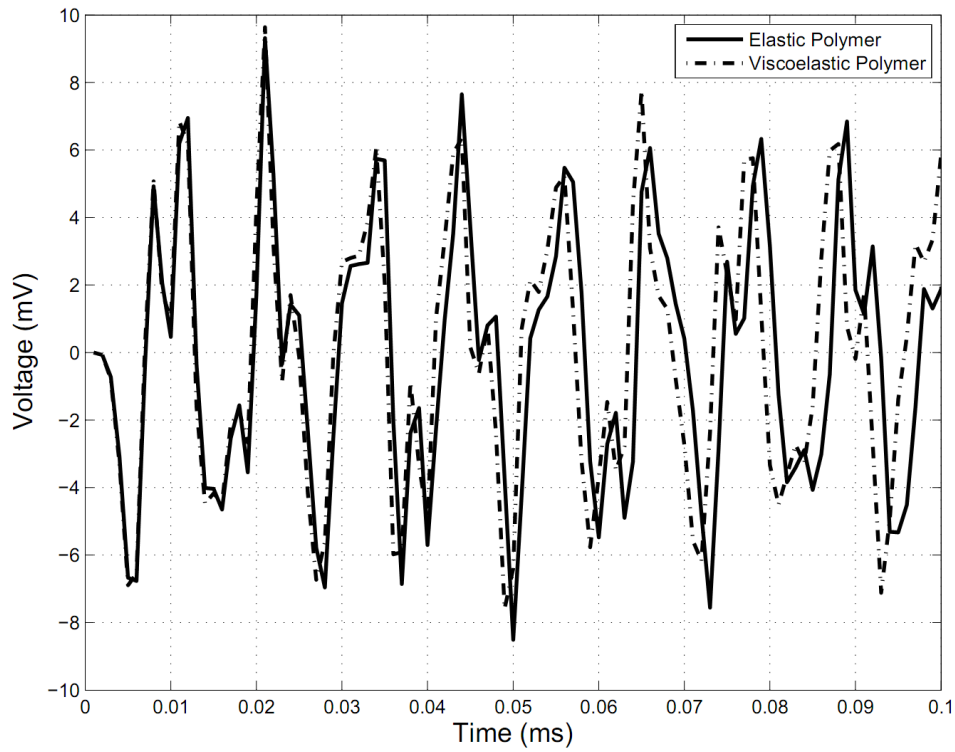


Figure 7.14: Voltage Output from the PVDF Film

The voltage output is affected by many harmonics of different frequencies and the frequency domain graph which is shown in Figure 7.15 gives the following graph.

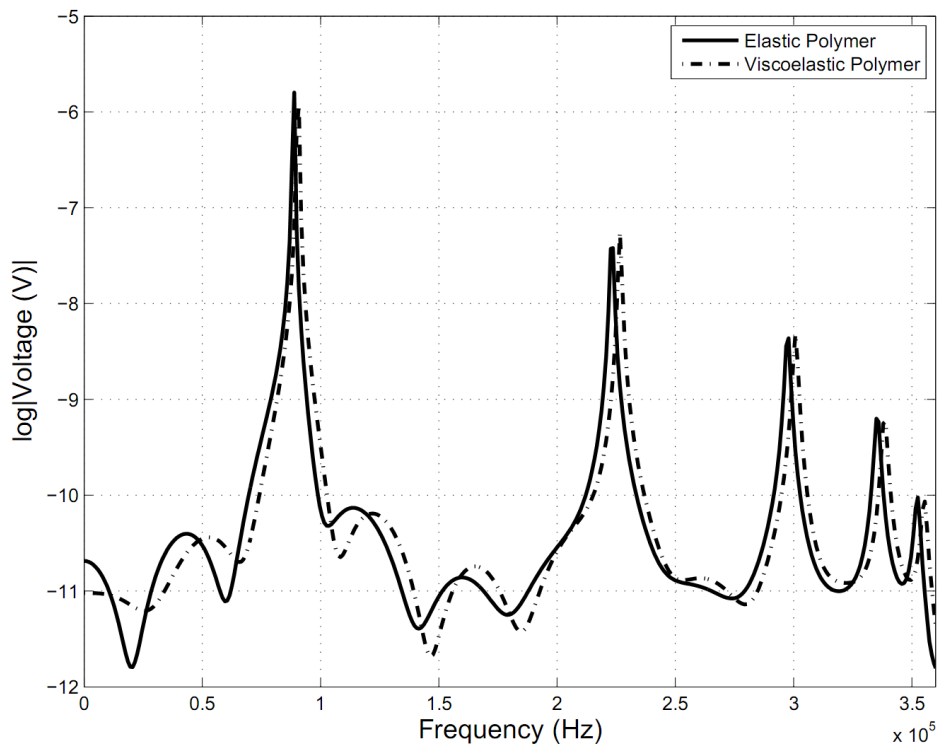


Figure 7.15: FFT of Voltage Output from the PVDF Film

7.2 Fiber Array Frequency Analysis

7.2.1 Fiber array modal analysis

The dynamic analysis is further examined by the modal analysis of the fiber array. The modal analysis consists of determination of the natural frequencies of the array. After the frequencies have been defined, the harmonic analysis and the transient analysis have been performed. The harmonic analysis is done by the frequency sweep in order to obtain the dynamic range for the tactile sensor and the transient analysis which is done by applying an impulsive force is done for determining the behavior of the sensor over time.

The natural frequency values have been calculated by the modal analysis in ANSYS. The model given in Figure 7.16 contains 8 pillars which results in 8 times repetition of each natural frequency. The natural frequencies have been separated to the modes of operation by the mode shape that they correspond to.

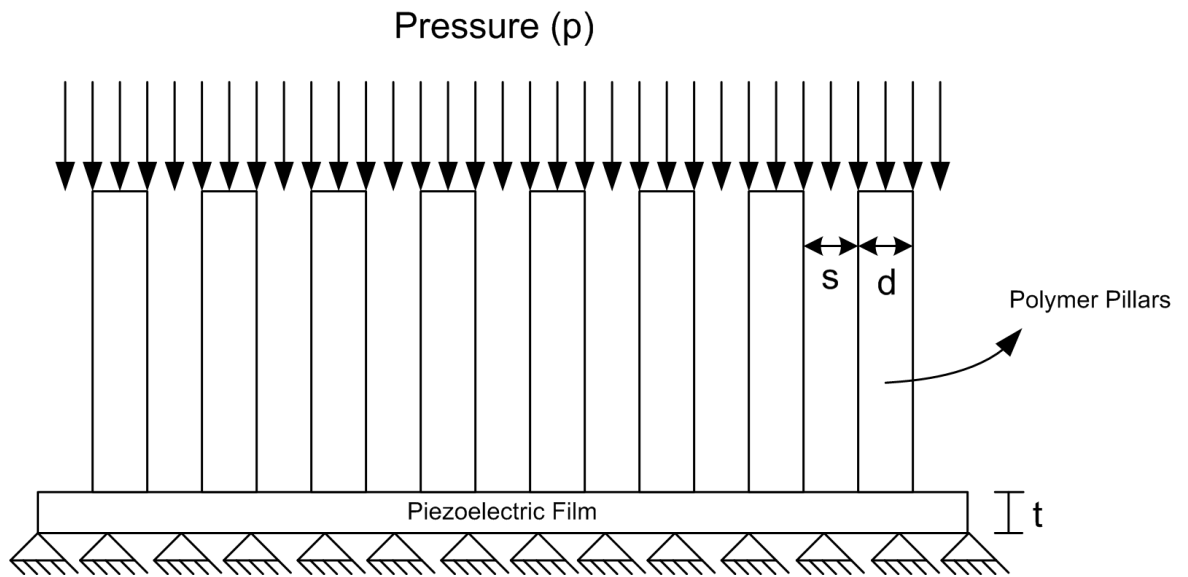


Figure 7.16: Fiber Array Dynamic Analysis Model

Different from the single pillar analysis, the fiber array analysis has been carried out two dimensional. Therefore, the natural frequency values do not contain the values of torsion. The values both contain the transverse and the longitudinal values. The first 4 values are tabulated in Table 7.2.

Table 7.2 : Natural Frequency Distribution of the Fiber Array

Frequency Number	Longitudinal (Hz)	Lateral (Hz)
1	90321	17962
2	$2.68 \cdot 10^5$	82045
3	$4.24 \cdot 10^5$	$1.80 \cdot 10^5$
4	$4.74 \cdot 10^5$	$3.60 \cdot 10^5$

The table can also be represented in terms of a simple graph in order to visualize the relativity of the different modes of natural frequencies.

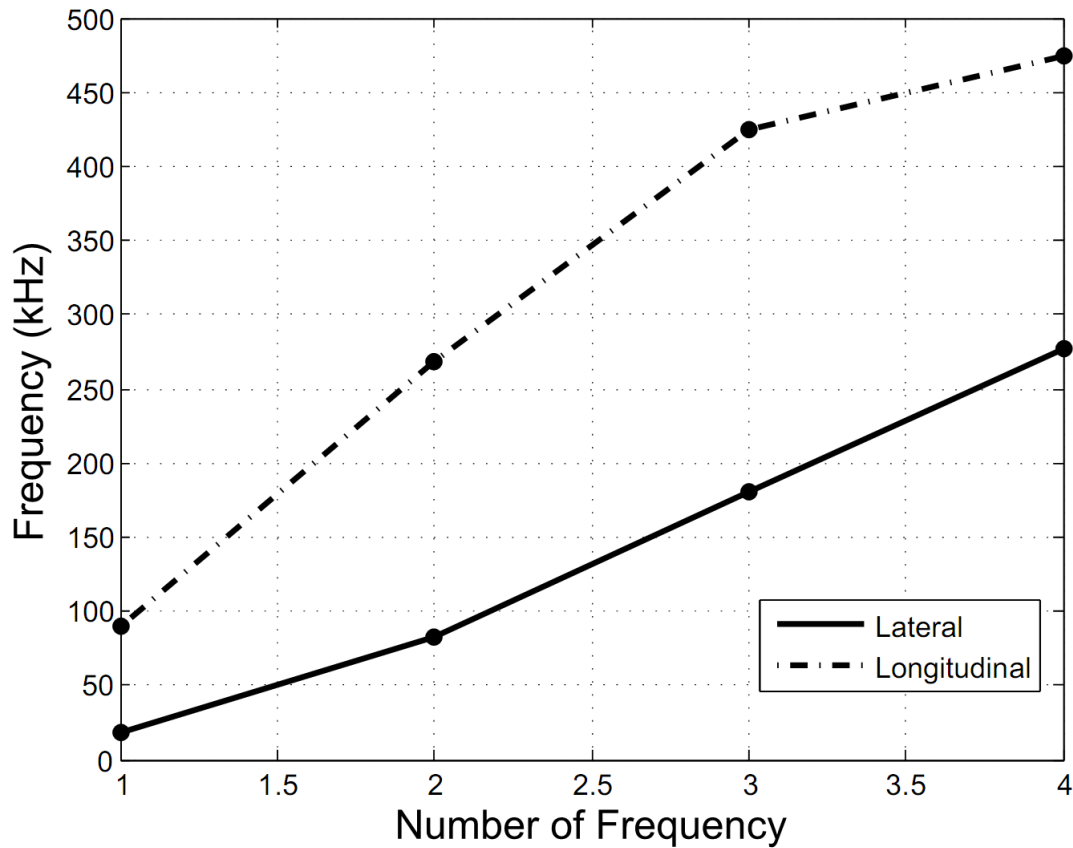


Figure 7.17 : Demonstration for the natural frequency values

7.2.2 Fiber array harmonic response analysis

After the natural frequencies of the structure have been determined, the response of the fiber array to harmonic excitation which is applied on the top surface of the PDMS layer has been examined. On this analysis, a unit pressure is applied and the voltage output on the lower surface of the PVDF film is plotted. The plots also show that what frequencies correspond to the normal mode operation of the fiber array. As these frequencies have been applied a voltage output much more than the normal system response can be gathered.

As given in Figure 7.17, the frequency corresponds to the transverse vibration mode is the third value given in the table of natural frequencies. The voltage output is also expected to have its peak on this frequency value. The voltage output graph is given Figure 7.18:

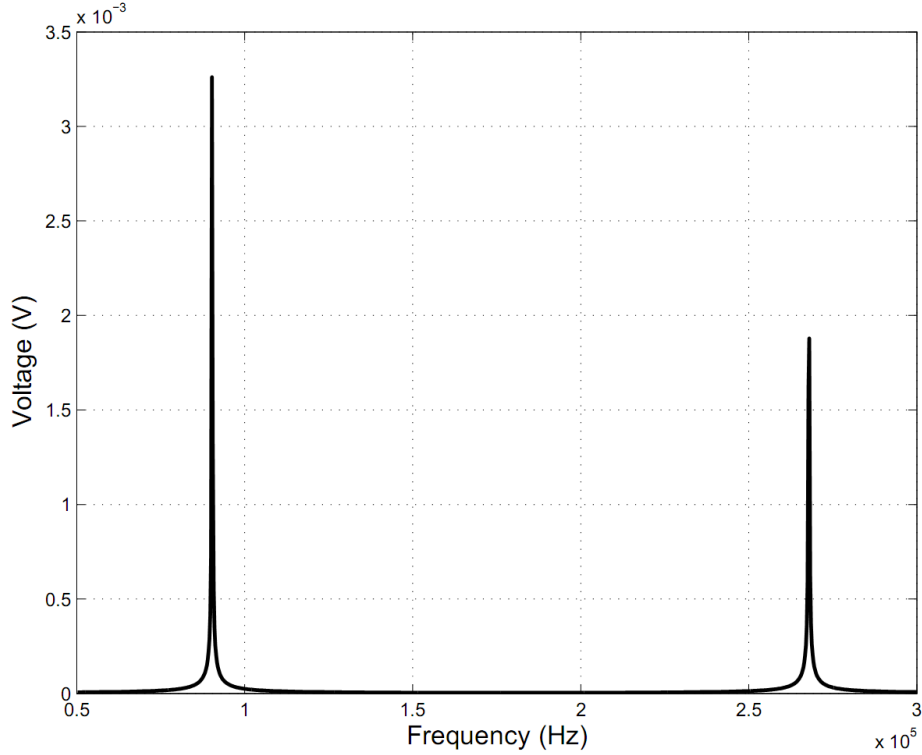


Figure 7.18: Frequency Sweep of Voltage Output for Applied Pressure on the Upper Surface of PDMS

7.2.3 Fiber array impulsive response analysis

The frequency sweep gives which frequencies have the most contribution on the voltage output from the piezoelectric film. The next step would be to examine the transient response characteristics of the fiber array. This can be achieved by applying a vertical impulsive force on the upper surface where the contact of the fiber will occur. In order to see the effect of the natural frequencies, the time step of the simulation is calculated from the Equation 7.1.

$$t_{step} = \frac{1}{20 f} \quad (7.1)$$

The y-displacement and the voltage output values are given for both applying a force on single fiber and applying force on the whole upper surface. For the whole upper surface case the following graphs are acquired.

The transient response is formed mainly by the harmonic excitations of the frequency values related to longitudinal vibration mode which is given in the frequency sweep.

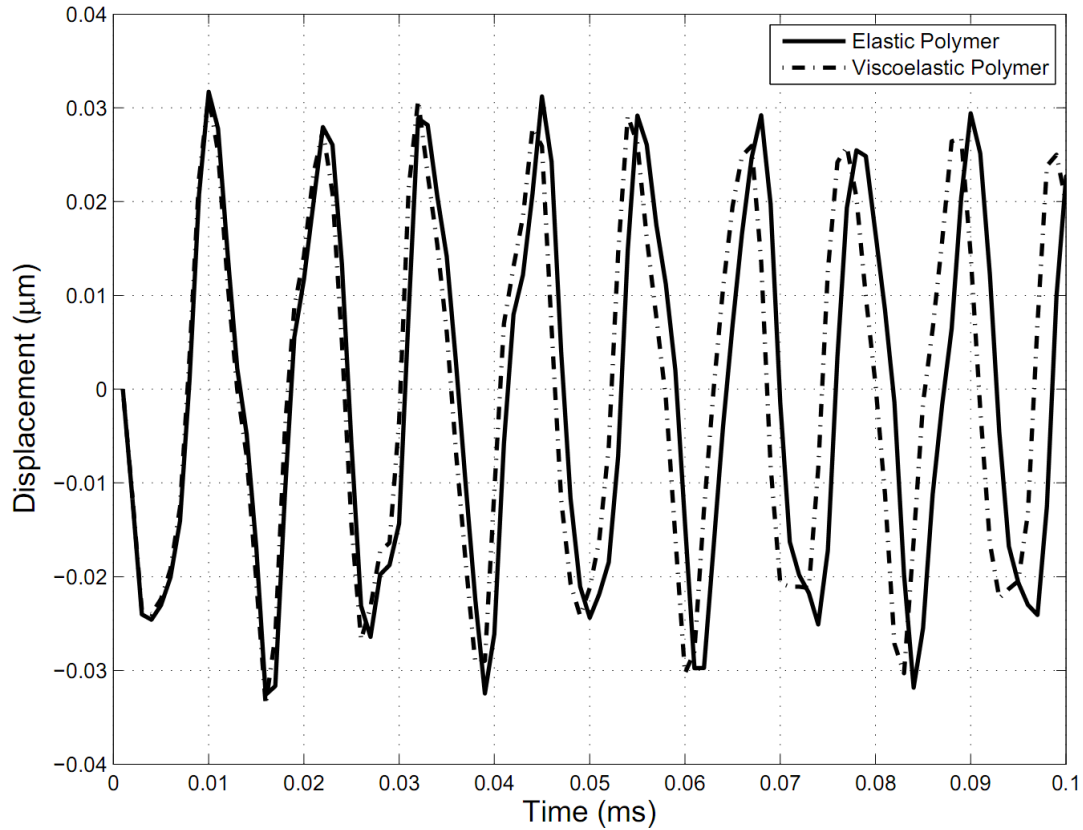


Figure 7.19: Y-Displacement on the Upper Surface for Upper Surface Pressure

The y-displacement transient response is formed mainly by the first mode of the transverse vibration mode. The higher frequency values create deviations from an ideal harmonic sinusoidal response curve. However, a general form of a harmonic response can be observed. In order to observe the dominant frequency values, an FFT analysis has been performed.

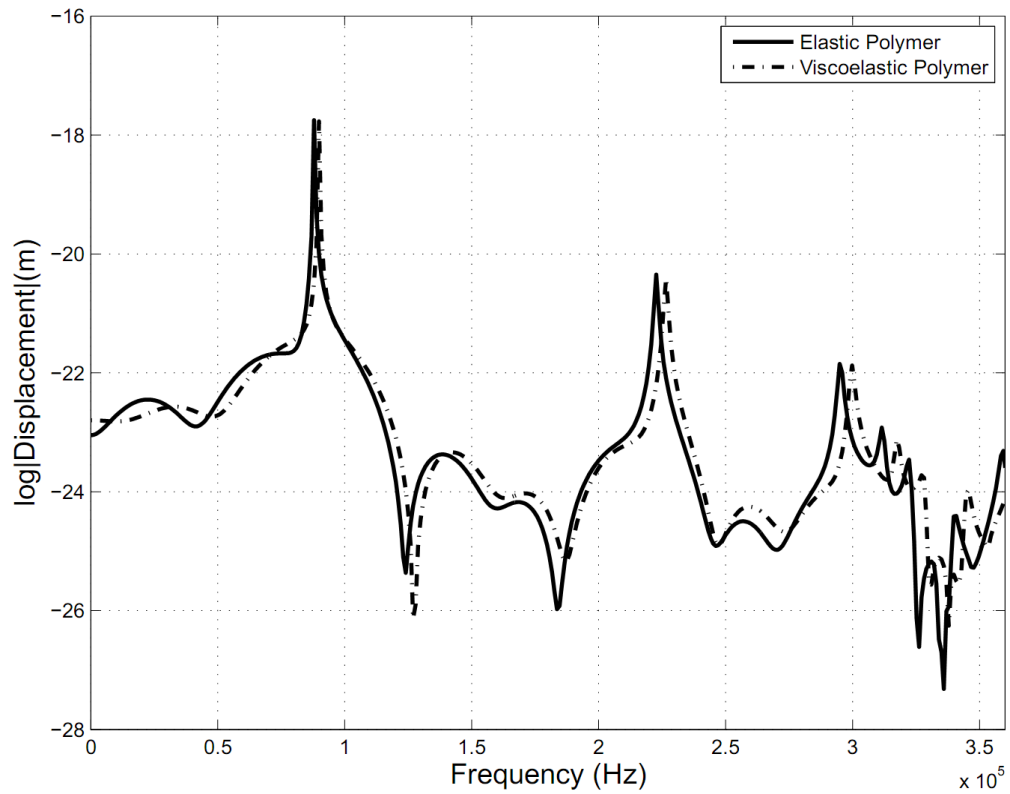


Figure 7.20: FFT of Y-Displacement on the Upper Surface for Upper Surface Pressure

The voltage value graph for an impulsive input is given in Figure 7.21.

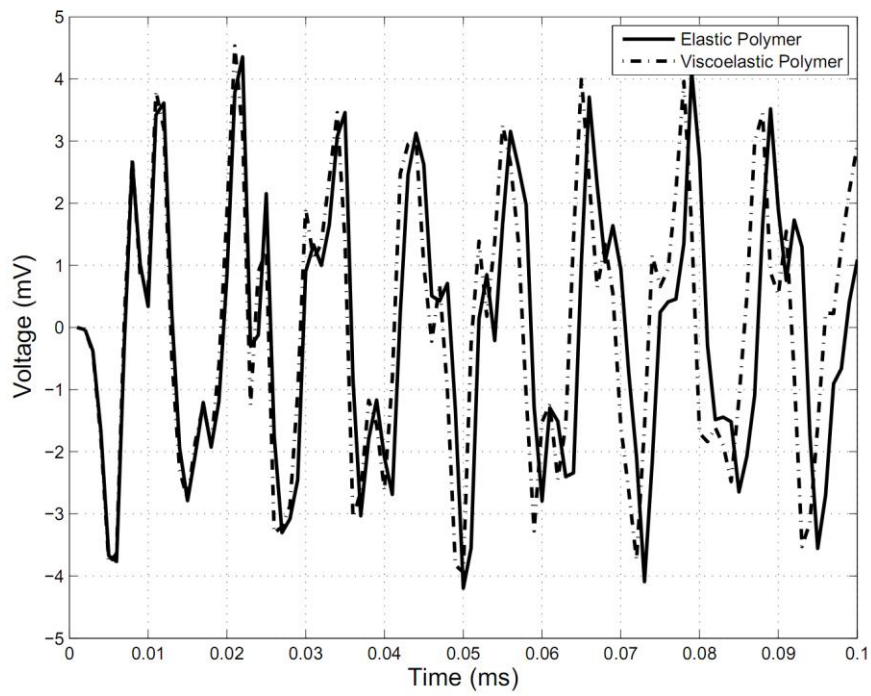


Figure 7.21: Voltage Output on PVDF Film for Upper Surface Pressure

Although the Figure 7.21 gives a general idea about the behavior of the system, the frequency based analysis can give a better view in understanding the dominant frequency values. This can be seen in Figure 7.22.

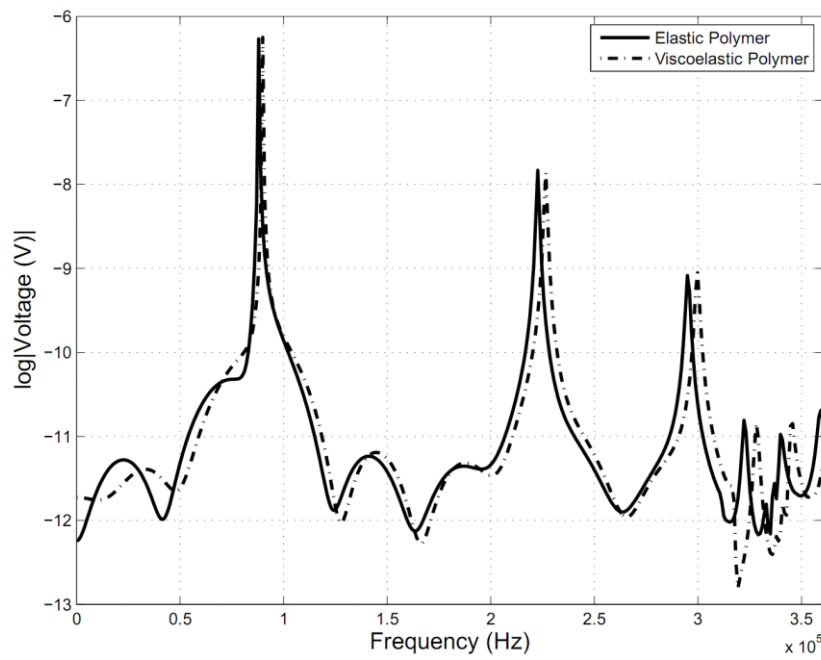


Figure 7.22 : FFT of Voltage Output on the Upper Surface for Upper Surface Pressure

8. TACTILE SENSING SIMULATION TESTS

Tactile sensing simulation tests have been carried out after the dimensions and the dynamical behavior of the array is examined. For this purpose, two cases have been explored in order to evaluate the performance of integration to the surface topography. The first case includes the rough surface adaptation. Second one is a development in the design where a shear force sensing capability is added.

8.1 Hemispheric Tip Indentation

The first case is generated to evaluate the performance of the tactile sensing of the sensor by modeling a rough surface and measuring the response of the system. Furthermore, piezoelectric film with bulk PDMS, which is given in Figure 8.1, on top has been compared with the design of the fiber array. The simulations carried out for this purpose includes the excitation of the fiber array by a hemispheric rigid glass tip. A distributed load has been applied on the upper contacting surface of the PDMS and a comparison has been made for the patterning of the PDMS layer.

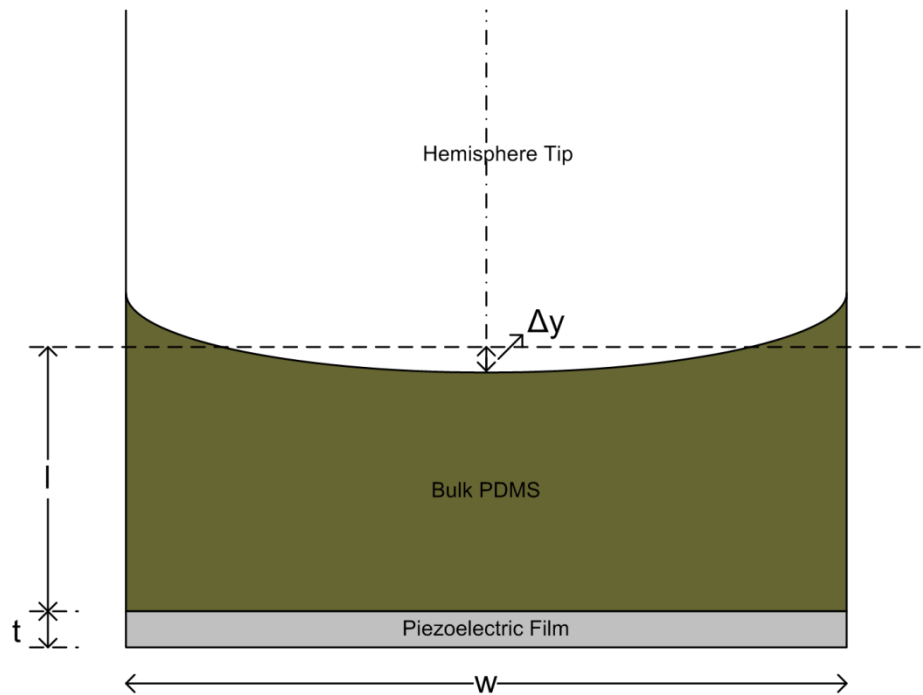


Figure 8.1: Piezoelectric film with unpatterned PDMS bulk

Figure 8.1 demonstrates the interaction of the glass tip with bulk PDMS with a piezoelectric film as backing layer. The voltage output is expected to have smooth changes since the hemispheric tip has the same characteristics. The same distributed load has been applied on the upper surface of the PDMS pillars. The 6 pillars in the middle are in compression whereas the pillars on the end are assumed to be stuck to the glass tip and are under tension. As a result, the potential difference is assumed to be reversed. This demonstration is given in Figure 8.2.

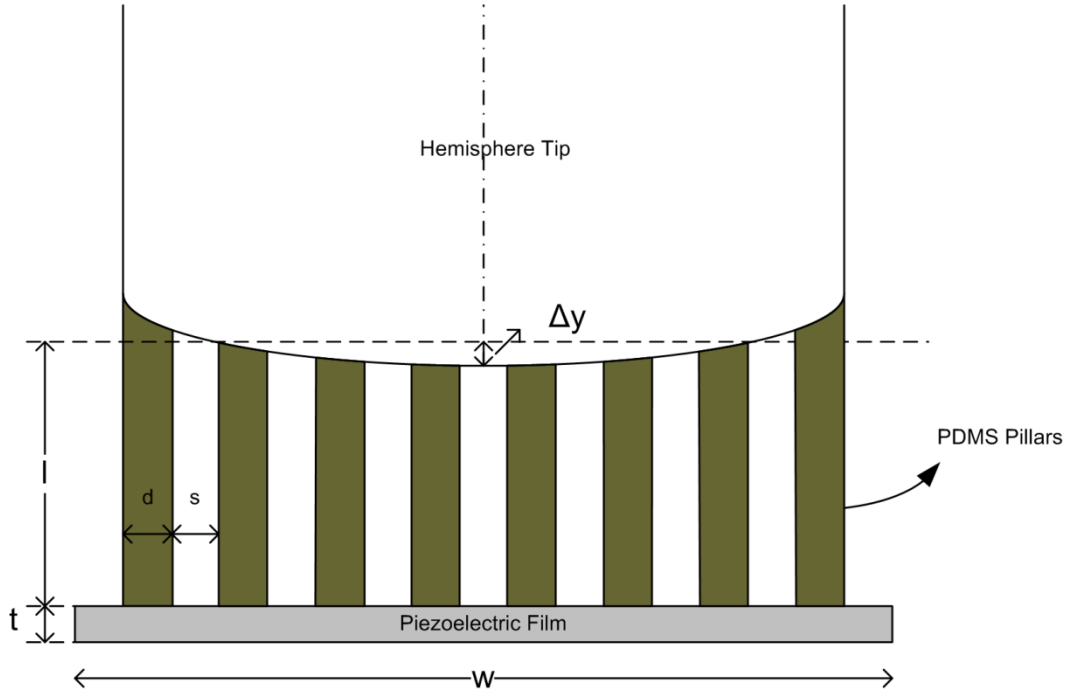


Figure 8.2: Piezoelectric film with patterned structure: PDMS pillars

The hemispheric glass tip has been modeled as a rigid punch inserted into the polymer. Therefore, the FEM simulations have been carried out such that there exists a vertical displacement on the upper surface. The radius of the displacement is given by the following formula.

$$r^2 = (r - \Delta y)^2 + \left(3d + \frac{5s}{2}\right)^2 \quad (8.1)$$

The dimensional parameters are given such that the spacing is 60 μm , the diameter is 40 μm and the Δy is 10 μm . The equation gives a punch radius of 3650 μm .

The vertical displacement can be given as a function of the horizontal displacement. This equation is simply the equation of circle with the radius calculated in Equation 8.1.

$$\Delta y(x) = \sqrt{(3650 \cdot 10^{-6})^2 - (x - 430 \cdot 10^{-6})^2} - 3640 \cdot 10^{-6} \quad (8.2)$$

The voltage output for bulk PDMS and pillar fiber array is given in Figure 8.3. It is shown that patterning the PDMS layer results in higher voltage difference on the bottom surface of the piezoelectric film. This is due to the stress concentration on the pillars. The general behavior of the voltage can represent topography of the contacting surface since it has finer resolution and higher voltage output compared to flat PDMS layer. Therefore, the blurring effect seen on flat design disappears with the patterned one and roughness adaptation capability increases.

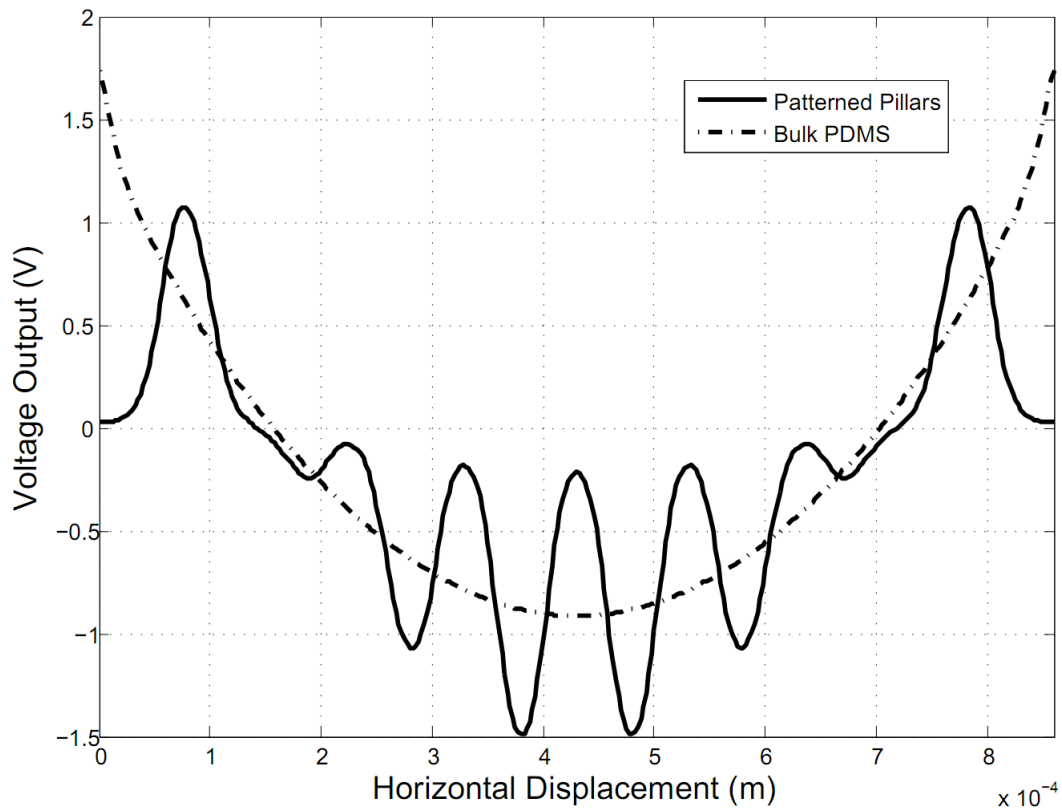


Figure 8.3: Comparison of voltage output in response to pressure distribution between patterned and unpatterned PDMS samples

8.2 Shear Force Sensing Capability & Quadrant Method

The shear sensing capacity is developed by dividing the electrode into 4 parts to the proposed design as shown Figure 8.4. In this method four different voltage values which are the numbered areas are gathered and making the comparison of these voltage values, the shear stress on the upper surface of the pillar can be calculated.

This configuration is similar to the measuring of normal and lateral forces of atomic force microscopy (AFM).

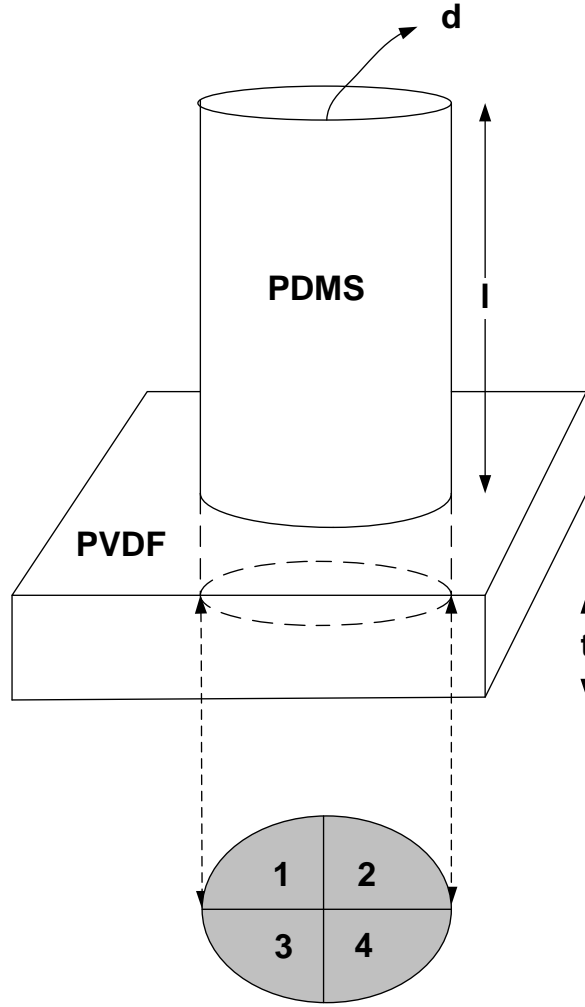


Figure 8.4: Model of the Quadrant Electrode Pillar

Each pillar can detect stresses in all three directions by either adding or subtracting the voltage values of each electrode. The model given in Figure 8.4 illustrates the structure of a single pillar. The shear stress generates different potential differences on PVDF film depending on the tension or compression on the film. the numerical values are then used for the calculation of the shear stress level acting on the sensor. The following equations give the stress values:

$$F_N = C_N(V(1) + V(2) + V(3) + V(4)) \quad (8.3)$$

$$F_x = C_x \left(\frac{(V(2) + V(4)) - (V(1) + V(3))}{2} \right) \quad (8.4)$$

$$F_y = C_y \left(\frac{(V(1) + V(2)) - (V(3) + V(4))}{2} \right) \quad (8.5)$$

Therefore, since the voltage values are linearly proportional with the stress on them, the forces can be calculated by calibrated constant gains (C_N, C_x, C_y) of voltages.

The shear force sensor simulation has been carried out such that there exists a force parallel to the upper surface of the polymer pillar and the resultant voltage distribution among the bottom surface of the piezoelectric film is given in Figure 8.5.

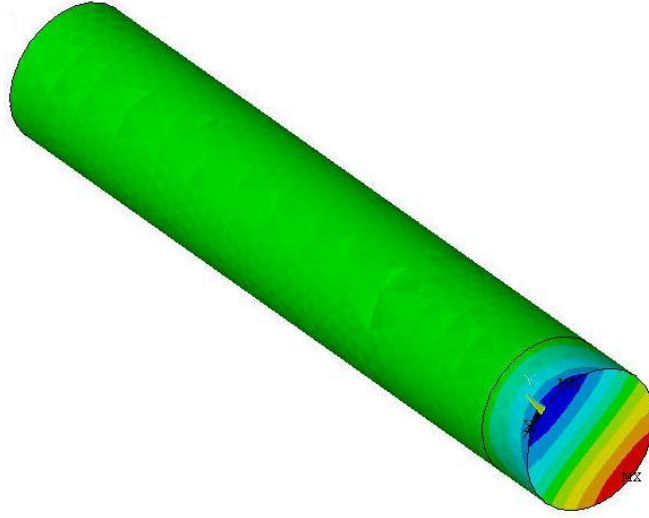


Figure 8.5: Voltage Graph for Shear Stress

The potential difference between the two surfaces of the piezoelectric film is collected and since the upper surface is grounded, the potential on the bottom surface is crucial. The voltage distribution gathered from the bottom surface of the piezoelectric film is given in Figure 8.6.

After all the voltage data is taken, the four electrodes are demonstrated by separating the data points into four quadrants according to their locations. For this purpose the voltage data is taken into a data array of “*x_y_voltage*” where the first column represents the x values, the second represents the y values and the last column gives the voltage values corresponding to these coordinates¹.

¹ The MATLAB code for this process is given in APPENDIX A.1

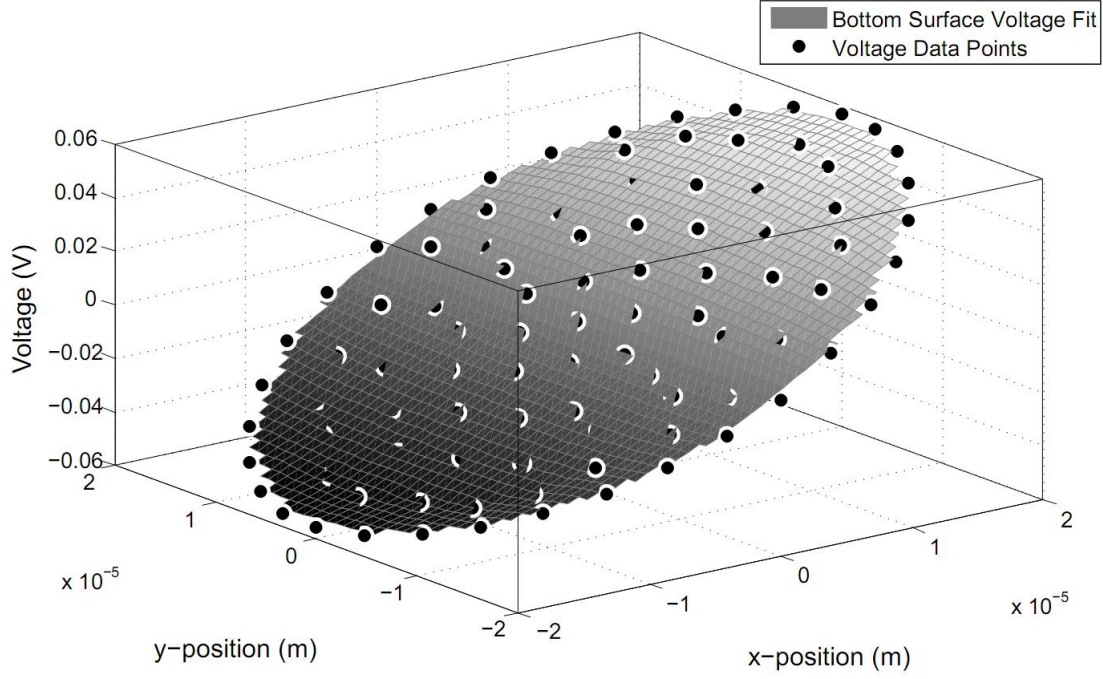


Figure 8.6: Bottom Voltage Output for Shear Stress on PDMS Upper Surface

8.3 Rough Surface Adaptation

The simulations carried out for this purpose includes the excitation of the fiber array by a random rough surface topography. The surface has a Gaussian height distribution function and Gaussian autocovariance function, where the length of the surface is chosen as $10\text{ }\mu\text{m}$, the RMS height is 0.25 and the correlation length is chosen to be 0.75. The distributed load from the random surface has been modeled by approximating the surface roughness with an 8th order polynomial with an RMSE of $4.365\text{ }10^{-10}$. This distributed load has been applied on the upper contact surface of the PDMS and a comparison has been made for the patterning of the PDMS layer. Figure 8.7(a) demonstrates the interaction between the random surface and the bulk PDMS with a piezoelectric film as backing layer. The voltage output is expected to behave the same as the surface topography at the voltage peaks which correspond to the voltage output at the projection of the bottom of the pillars. The same distributed load has been applied on the upper surface of the PDMS pillars. It is assumed to have the same indentation depth as the flat bulk PDMS case which is demonstrated in Figure 8.7(b).

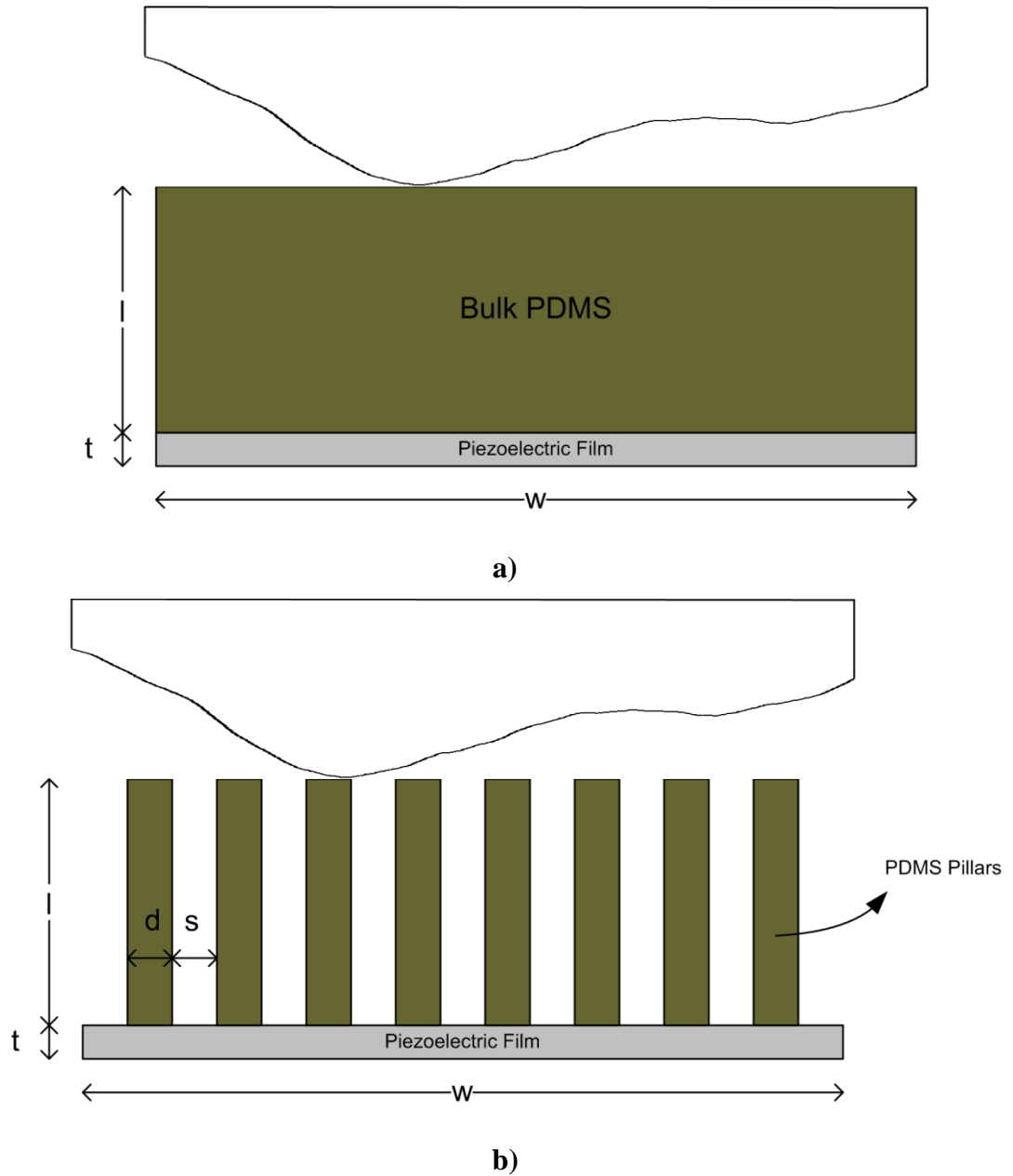


Figure 8.7 : a) Rough surface on bulk PDMS, b) Rough surface on patterned pillars

The voltage output for bulk PDMS and pillar fiber array is also given in Figure 8.8. The fiber array given in Figure 8.7(b) is a small portion of a fiber array so in order to eliminate the edge effects the graphs has been plotted with a limited horizontal displacement. It is shown that patterning the PDMS layer results in higher voltage difference on the bottom surface of the piezoelectric film. This is due to the stress concentration on the pillars. The general behavior of the voltage can represent topography of the contact surface since it has finer resolution and higher voltage

output compared to flat PDMS layer. Therefore, the blurring effect seen on flat design disappears with the patterned one and roughness adaptation capability increases.

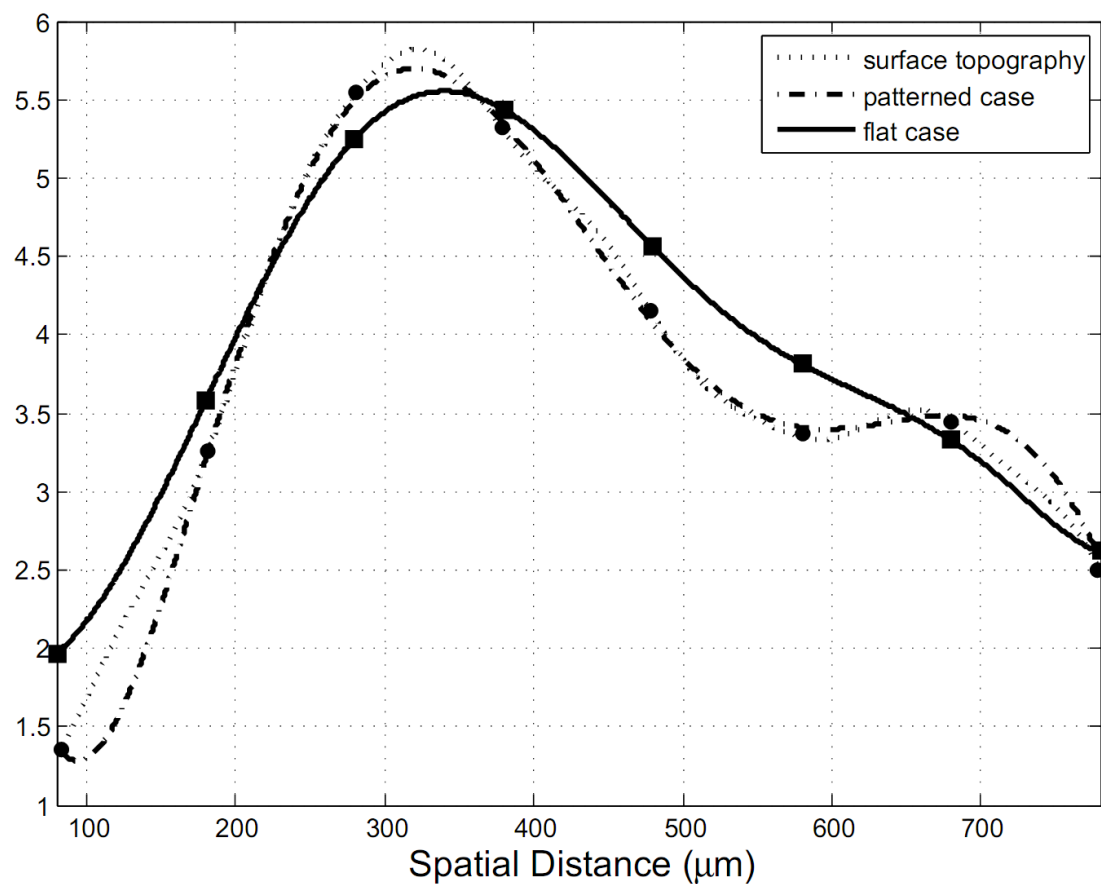


Figure 8.8: Rough surface adaptation for patterned and flat case

9. CONCLUSION AND RECOMMENDATIONS

The contribution of this research is designing the actuator and sensor integrated synthetic polymer fiber array. Unlike the passive mode operation of the fiber array, the actuator and sensor integrated synthetic polymer fiber array have capability of ease adaptation to the surface roughness and increase the adhesion with respect to passive synthetic polymers and thin film polymers.

The design parameters such as the fiber diameter, spacing ratio and aspect ratio are analyzed for the fiber array, and the limits for the cross-over talk of the electric charges are found. The electrical limit, which is the cross-talk between the electrodes, determines the spatial resolution limit of the proposed design. The spacing value of two fibers greater than 60 μm results decoupling of each electrode, and this would be the spatial resolution limit for the proposed design. Using suitable decoding electronics and micro-electro-mechanical (MEMS) techniques, it is feasible to produce the fiber with this resolution. Thus, it is expected to approach the spatial resolution of the human hand (40 μm) with the proposed design.

The proposed design can adapt to the surface as it has vertical fibers that can integrate into the surface roughness of the contacting object. Therefore, the sensor can be used in order to map the pressure distribution. This is basically the static usage of the sensor. Moreover, the sensor can be used as shear sensor as the electrode on the bottom surface is divided into four parts. Making use of this quadrant electrode concept, the sensor can both be used as normal force sensor and the shear force sensor.

The dynamical analyses have been performed in order to design a sensor that can work on vibrating environments. The crack detection can be obtained in dynamically working environments as the sensor is placed on the critical area. The charge generated is proportional to the stress on the film. Therefore, the design is made such that the energy coming from the environment is mostly absorbed not by the piezoelectric film but kept by the pillars which creates more inertial load increasing the voltage output of the sensor. Also the sensor can be used in climbing robots where the touching surface is always changing and there is a need for understanding and

mapping the surface roughness of the new surface in order to achieve the best contacting surface area and therefore increase the adhesion of the robots.

In human tactile sensing, the design will lead to the touch sense of the human hand. In humanoid robots, the tactile sensor placed on the tip of the gripper will lead the precise force and local pressure data that cannot be calculated by the force sensors at the joints. Furthermore, in applications where the precise force control is needed as in the case of minimally invasive surgeries, the sensor will have major advantages.

Since the mechanical design is simple as compared to capacitive or optical sensors as the material itself can generate the sensor signal, it is more compact that can lead to increase in the resolution of the tactile sensor. However, the main limitation is the manufacturing limitations since the dimensions are very small so that MEMS production is needed and the manufacturing processes are much limited than the conventional manufacturing processes.

REFERENCES

- [1] **Provancher, W. R.** (2003). On Tactile Sensing and Display, *Unpublished doctoral dissertation*, Stanford University, California, USA
- [2] **Liu, C.** (2007). Micromachined biomimetic artificial haircell sensors. *Bioinspiration & Biomimetics*, vol. **2**, no. 4, pp. 162-169.
- [3] **Qasaimeh, M. A., Sokhanvar, S., Dargahi J., Kahrizi M.** (2009). PVDF-Based Microfabricated Tactile Sensor for minimally invasive surgery, *Journal of Microelectromechanical Systems*, vol. **18**, no. 1, pp. 195-207
- [4] **Najarian, S., Dargahi, J., Molavi, M., & Singh, H.** (2006). Design and Fabrication of Piezoelectric-based Tactile Sensor for Detecting Compliance. *2006 IEEE International Symposium on Industrial Electronics*, vol. **4**, no. 424, pp. 3348-3352
- [5] **Keissner, A., Brücker, C., Jacobs, P., & Kashefi, A.** (2009). Multi- tactile sensor concept for the autonomous navigation in human blood vessels. *4th European Conference of the International Federation for Medical and Biological Engineering*, pp. 1544–1547. Springer.
- [6] **Tegin, J., & Wikander, J.** (2005). Tactile sensing in intelligent robotic manipulation – a review. *Industrial Robot An International Journal*, vol. **32**, no. 1, pp. 64-70
- [7] **Liu, W., Sumer, B., Stefanini C., Menciassi A., Li, F., Chen, D., Dario, P., Sitti, M., Fu, X.** (2009). A novel artificial hair receptor based on aligned PVDF micro/nano fibers, *2008 IEEE International Conference on Robotics and Biomimetics*, pp. 49-54
- [8] **Westling G. and Johansson R. S.** (1984). Factors influencing the force control during precision grip, *Experimental Brain Research*, vol. **53**, pp. 277–284
- [9] **Engel, J. M., Chen, J., Liu, C., & Bullen, D.** (2006). Polyurethane Rubber All-Polymer Artificial Hair Cell Sensor. *Journal of Microelectromechanical Systems*, vol. **15**, no. 4, pp. 729-736
- [10] **Dahiyal, R. S., Valle, M., Metta, G., Lorenzelli, L., & Collini, C.** (2007). Tactile sensing arrays for humanoid robots. *2007 PhD Research in Microelectronics and Electronics Conference*, pp. 201-204
- [11] **Howe R.D.** (1993). Tactile Sensing and Control of Robotic Manipulation, *Advanced Robotics*, vol. **8**, no. 3, pp 245-261
- [12] **Tegin J. and Wikander J.** (2005). Tactile Sensing in Intelligent Robotic Manipulation – A Review, *Industrial Robot: An International Journal*, vol. **32**, no. 1, pp 64-70

- [13] **Sumer, B., Aksak, B., Sahin, K., Chuengsatiansup, K., Sitti, M.** (2011). Piezoelectric Polymer Fiber Arrays for Tactile Sensing Applications, *Sensor Letters*, vol. **9**, no. 2, pp. 457-463
- [14] **Del Campo, A., Greiner, C., & Arzt, E.** (2007). Contact shape controls adhesion of bioinspired fibrillar surfaces. *Langmuir The Acs Journal Of Surfaces And Colloids*, vol. **23**, no. 20, pp. 10235-10243.
- [15] **Greiner, C., Campo, A. D., & Arzt, E.** (2007). Adhesion of bioinspired micropatterned surfaces: effects of pillar radius, aspect ratio, and preload. *Langmuir The Acs Journal Of Surfaces And Colloids*, vol. **23**, no. 7, pp. 3495-3502.
- [16] **Yao, H., Rocca, G. D., Guduru, P. R., & Gao, H.** (2008). Adhesion and sliding response of a biologically inspired fibrillar surface: experimental observations. *Journal of the Royal Society Interface the Royal Society*, vol. **5**, no. 24, pp. 723-733
- [17] **Geim, A. K., Dubonos, S. V., Grigorieva, I. V., Novoselov, K. S., Zhukov, A. A., & Shapoval, S. Y.** (2003). Microfabricated adhesive mimicking gecko foot-hair. *Nature Materials*, vol. **2**, no. 7, pp. 461-463
- [18] **Sitti, M., & Fearing, R. S.** (2003). Synthetic gecko foot-hair micro/nano-structures for future wall-climbing robots. *2003 IEEE International Conference on Robotics and Automation Cat No03CH37422*, pp. 1164-1170
- [19] **Url-1** <http://en.wikipedia.org/wiki/Tactile_sensor>, date retrieved 20.04.2011
- [20] **Url-2** <<http://www.soton.ac.uk/~rmc1/robotics/artactile.htm>>, date retrieved 20.04.2011
- [21] **Url-3** <<http://en.wikipedia.org/wiki/Photoelasticity>>, date retrieved 22.04.2011
- [22] **Ramos, M., Correia, H., Lanceros-Mendez, S.** (2005). Atomistic modelling of processes involved in poling of PVDF, *Computational Materials Science*, vol. **33**, pp. 230-236
- [23] **Ng, N., Ma, J., Boey, F.** (2007). Polymer piezoelectric tubular transducers, *Electrochemical and Solid-State Letters*, vol. **10**, no. 2, page 5
- [24] **Lu, T. J., Evans, A. G.** (2002). Design of a high authority flexural actuator using an electro-strictive polymer, *Sensors and Actuators A: Physical*, vol. **99**, no. 3, pp. 290-296
- [25] **Lippman, G.** (1881), Principe de la conservation de l'électricité (in French), *Annales de chimie et de physique*, vol. **24**, page 145
- [26] **Url-4** <<http://en.wikipedia.org/wiki/Piezoelectricity>>, date retrieved 12.04.2011
- [27] **Url-5** <<http://www.piezo.com/tech4history.html>>, date retrieved 26.04.2011
- [28] **Url-6** <http://www.piceramic.com/piezo_applications_more.php?appid=3>, date retrieved 26.04.2011
- [29] **Url-7** <<http://www.tb-moeller.de/en/technology-fields/sensor-technology/intelligent-sensor/piezoelectricity.html>>, date retrieved 28.04.2011
- [30] **Xu, J., Dapino, M. J., Gallego-Perez, D., Hansford, D.** (2009). Microphone based on polyvinylidene flouride (PVDF) micro-pillars and patterned

- electrodes, *Sensors and Actuators A: Physical*, vol. **153**, no. 1, pp. 24-32
- [31] **Chuang, C., Dong, W., Lo, W.** (2008). Flexible piezoelectric tactile sensor with structural electrodes array for shape recognition system, *3rd International Conference on Sensing Technology*, pp. 504-507
- [32] **Kanda, T., Makino, A., Ono, T., Suzumori, K., Morita, T., Kurosawa, M. K.** 2006, A micro ultrasonic motor using a micro-machined cylindrical bulk PZT transducer, *Sensors and Actuators A: Physical*, vol. **127**, no. 1, pp. 131-138
- [33] **Edwards, K.** (1996). Standard handbook of machine design J. E. Shigley and C. R. Mischke McGraw-Hill, 1996 (second edition)
- [34] **Glassmaker, N. J., Himeno, T., Hui, C.-Y., & Kim, J.** (2004). Design of biomimetic fibrillar interfaces: 1. Making contact. *Journal of the Royal Society Interface the Royal Society*, vol. **1**, no. 1, pp. 23-33
- [35] **Maugis, D.** (1992). Adhesion of spheres: The JKR-DMT transition using a dugdale model. *Journal of Colloid and Interface Science*, vol. **150**, no. 1, pp. 243-269
- [36] **Url-8** < <http://en.wikipedia.org/wiki/Viscoelasticity>>, date retrieved 21.06.2011
- [37] **Url-9** <http://www.acronymchile.com/noteshtml/3rd_Materials/3rdMat06_handout.pdf>, date retrieved 15.09.2011
- [38] **Url-10** < <http://www.see.ed.ac.uk/~johnc/teaching/fluidmechanics4/2003-04/visco/index.html> >, date retrieved 15.09.2011
- [39] **Url-11** <http://www.acronymchile.com/noteshtml/3rd_Materials/3rdMat06_handout.pdf>, date retrieved 16.09.2011
- [40] **Du, P., Lin, I., Lu, H., Zhang, X.** 2010, Extension of the beam theory for polymer bio-transducers with low aspect ratios and viscoelastic characteristics, *Journal of Micromechanics and Microengineering*, vol. **20**, no. 9
- [41] **Lin, I. K., Ou, K. S., Liao, Y. M., Liu, Y., Chen, K. S., Zhang X.** Viscoelastic characterization and modeling of polymer transducers for biological applications, *Journal of Microelectromechanical Systems*, vol. **18**, no. 5, pp. 1087-1099
- [42] **Johnson, K.** 1985. Contact Mechanics. *Journal of the American Chemical Society*, vol. **37**, pp. 1-17. Cambridge University Press
- [43] **Kuo, B.** Silicone Release Coatings for the Pressure Sensitive Industry – Overview and Trends, pp.2-5

APPENDICES

APPENDIX A.1: MATLAB Code for Node Separation in Quadrant Electrode

9.1 APPENDIX A.1:

```
%Quadrant Electrode Voltage Distribution

c1=1;

c2=1;

c3=1;

c4=1;

voltage1_toplam=0;

voltage2_toplam=0;

voltage3_toplam=0;

voltage4_toplam=0;


% Plot the bottom voltage data

scatter3(x_y_voltage(:,1),x_y_voltage(:,2),x_y_voltage(:,3),'.');


%Quadrant Electrode Calculations

for i=1:233

    if ((x_y_voltage(i,1)>=0 && x_y_voltage(i,2)>=0))

        first(c1,1)= x_y_voltage(i,3);

        voltage1_toplam=voltage1_toplam+first(c1,1);

        c1=c1+1;

    end;

    if ((x_y_voltage(i,1)<0 && x_y_voltage(i,2)>=0))

        second(c2,1)=x_y_voltage(i,3);

        voltage2_toplam=voltage2_toplam+second(c2,1);

        c2=c2+1;
```

```

end;

if ((x_y_voltage(i,1)<0 && x_y_voltage(i,2)<0))

    third(c3,1)=x_y_voltage(i,3);
    voltage3_toplam=voltage3_toplam+third(c3,1);
    c3=c3+1;
end;

if ((x_y_voltage(i,1)>=0 && x_y_voltage(i,2)<0))

    fourth(c4,1)=x_y_voltage(i,3);
    voltage4_toplam=voltage4_toplam+fourth(c4,1);
    c4=c4+1;
end;

end

voltage1=voltage1_toplam/(c1-1)
voltage2=voltage2_toplam/(c2-1)
voltage3=voltage3_toplam/(c3-1)
voltage4=voltage4_toplam/(c4-1)

```


CURRICULUM VITAE



Name Surname: Emre AKÇA

Place and Date of Birth: Bakırköy, 20.01.1984

Address: Ferit Selim Paşa caddesi. Tuna sokak. No 2/10.
Bahçelievler / İSTANBUL

E-Mail: akcaemre@hotmail.com

B.Sc.: Middle East Technical University, Mechanical
Engineering (Undergraduate)

List of Publications and Patents:

PUBLICATIONS/PRESENTATIONS ON THE THESIS

- Akça E., Koç I.M., 2011: Design of a piezoelectric based tactile sensor for pressure mapping with bio-inspired micro/nano pillars. *38th Leeds-Lyon Symposium on Tribology*, September 6-9, 2011 Lyon, France.
- Akça E., Koç I.M., 2011: Design of a piezoelectric based tactile sensor for pressure mapping with bio-inspired micro/nano pillars. *Tribology International* (in revision progress)